

# Design and Fabrication of cm-scale Tesla Turbines

*Vedavalli Krishnan*



Electrical Engineering and Computer Sciences  
University of California at Berkeley

Technical Report No. UCB/Eecs-2015-161

<http://www.eecs.berkeley.edu/Pubs/TechRpts/2015/Eecs-2015-161.html>

June 1, 2015

Copyright © 2015, by the author(s).  
All rights reserved.

Permission to make digital or hard copies of all or part of this work for personal or classroom use is granted without fee provided that copies are not made or distributed for profit or commercial advantage and that copies bear this notice and the full citation on the first page. To copy otherwise, to republish, to post on servers or to redistribute to lists, requires prior specific permission.

Design and Fabrication of cm-scale Tesla Turbines

By  
Vedavalli Gomatam Krishnan

A dissertation submitted in partial satisfaction of the  
requirements for the degree of  
Doctor of Philosophy  
In  
Engineering – Electrical Engineering and Computer Sciences  
In the  
Graduate Division  
of the  
University of California, Berkeley

Committee in charge:  
Professor Michel Martin Maharbiz, Chair  
Professor Seth Sanders  
Professor Liwei Lin

Spring 2015

Copyright © 2015, by the author.  
All rights reserved.

Permission to make digital or hard copies of all or part of this work for personal or classroom use is granted without fee provided that copies are not made or distributed for profit or commercial advantage and that copies bear this notice and the full citation on the first page. To copy otherwise, to republish, to post on servers or to redistribute to lists, requires prior specific permission.

## Abstract

### Design and Fabrication of cm-scale Tesla Turbines

By

Vedavalli Gomatam Krishnan

Doctor of Philosophy in Electrical Engineering and Computer Science

University of California, Berkeley

Professor Michel Martin Maharbiz, Chair

This dissertation discusses the design and scaling characteristics of Tesla – or so-called “friction” – turbines, and offers design solutions for achieving optimum performance given the input specifications. The research covers turbines ranging from sub-watt power scavenging designs to watt-range mobile applications to kilowatt-range renewable energy applications. The characteristics of the turbine are demonstrated using micro fabrication, theoretical analysis, and ANSYS, COMSOL, and MATLAB simulations. A MATLAB GUI is provided for generating design specifications and turbine performance sensitivity.

In Tesla turbines, the fluid profile and the length of the fluid path inside the rotor control the pressure drop and momentum transfer. In this research, analyses of rotor performance for incompressible flow are developed for different fluid profiles and fluid-path lengths. First, frictional losses in the nozzle and at the rotor-turbine interface are investigated, along with other turbine losses. These losses are then classified and modeled in terms of their relationship to head loss and shaft power loss, and investigated using MATLAB and COMSOL. As the turbine scales down, this scaled performance is evaluated and a constraint list for turbine hardware and operating parameters is derived. These results are used to optimize performance for the full range of millimeter to meter sized turbines.

Tesla turbines at the scales covered in this dissertation (mm – m) are relatively easy to manufacture. The experimental mini-turbines presented in this research have two primary components, fabricated using commercially available technologies: 1) four 1 cm-diameter rotors with variation in number of disks, interdisk spacing, and effective area, and 2) a turbine enclosure with eight nozzles of varying area, angle, and shape.

Test results from different configurations of nozzles and rotors are presented, and observations made on the performance trends of the turbine. Flow through the 1 cm rotors is also simulated in ANSYS to verify the momentum equations. The performance difference between analytical solutions, simulation, and experimental results is then studied, and a mapping of experimental results onto analytical results is proposed.

In addition, various scaling-down methodologies are investigated. Disk spacing is varied as a power function of radius, and turbine performance is analyzed across the turbine range of 1 mm to 400 mm diameter. Using this approach, constant power density designs are specified that perform at better than 35% mechanical efficiency for the entire range. As the turbine is scaled down, the roughening of the disks must be increased to control the fluid profile. Power density is very sensitive to the rotor spacing and the input head, and efficiency is very sensitive to the operating parameters and turbine design. This dissertation argues that these sensitivities explain the wide discrepancies in published turbine performances.

A practical design tool is also offered, which inputs user specifications on head, flow, particulate size, and medium to generate a list of possible turbine designs along with a recommendation for four candidate designs. The sensitivities of turbine performance to the input head and input flow variations are also reported. The tool is designed to cover 20 mW to 20 kW power range and 2 mm to 500 mm rotor radius range. Current applications and potential extensions to the research are discussed in the conclusion.

# Dedication

---

To Geetha and Meera, my daughters, for my aspirations.

To Avalina, Kamari, and Chaidan, my grandchildren, for keeping me alert.

To Kanna, my husband, for his insight and support in my accomplishments.

To Singaram Anna, and Narasimhan Tambi, my brothers, and

Chingamma, Yadugiri, and Mangai, my sisters, for my confidence.

To Parthasarathy Ayya and Ranganayaki Amma, my parents, for who I am.

# Contents

---

|  |      |
|--|------|
| Dedication .....   | i    |
| List of Figures .....  | vii  |
| List of Tables .....   | xiii |
| Nomenclature .....   | xiv  |
| Acknowledgements.....  | xvii |
| 1 Introduction.....  | 1    |
| 1.1 Motivation.....  | 1    |
| 1.2 Background and Basic Operation.....  | 2    |
| 1.2.1 Driving Force in Tesla Water (hydro)-Turbine .....                           | 4    |
| 1.3 Tesla Turbine Applications in the Watt to Kilowatt Range .....                 | 4    |
| 1.3.1 Low-Head or Low-Flow River Turbines .....                                    | 4    |
| 1.3.2 Sub-Watt Mobile and Scavenger Applications.....                              | 6    |
| 1.3.3 Residential Combined Heat, Power, and Water .....                            | 7    |
| 1.4 Previous Work.....   | 9    |
| 1.5 Research Overview .....  | 11   |
| 1.5.1 Investigation of Micro-scale Tesla Turbine Fabrication and Performance ..... | 11   |
| 1.5.2 Analysis of the Dependence of Rotor Performance on Flow Profile .....        | 11   |
| 1.5.3 Turbine Loss Analysis .....  | 11   |
| 1.5.4 Mapping Experimental Results to Ideal Performance .....                      | 12   |
| 1.5.5 Design Constraints Table.....  | 12   |
| 1.5.6 Scalable Design Method and Examples .....                                    | 12   |
| 1.5.7 Practical Turbine Design Specification .....                                 | 13   |
| 1.5.8 Reconciling Performance Discrepancies in the Literature .....                | 13   |
| 1.5.9 Design Sensitivity Analysis .....  | 13   |
| 1.5.10 User Design Interface.....  | 13   |
| 1.6 Organization.....  | 14   |
| 2 Fabrication of a 1-cm Tesla Turbine, and Experimental Findings .....             | 15   |
| 2.1 Fabrication .....  | 15   |

|       |  |    |
|-------|--|----|
| 2.1.1 | Rotor Fabrication .....  | 15 |
| 2.1.2 | Nozzle Fabrication and Turbine Enclosure.....  | 17 |
| 2.2   | Turbine Experimental Setup and Operation .....   | 19 |
| 2.2.1 | Data Collection and Analysis .....   | 21 |
| 2.2.2 | Torque, Power, and Efficiency .....  | 23 |
| 2.2.3 | Observations .....   | 24 |
| 2.3   | Experimental Uncertainty .....   | 27 |
| 2.3.1 | Fabrication Uncertainty (4%) .....   | 27 |
| 2.3.2 | Test Procedure Uncertainty (5%).....   | 27 |
| 2.3.3 | Test Data Uncertainty (10%).....   | 27 |
| 2.3.4 | Conclusions .....  | 28 |
| 3     | Analytical and Computational Turbine Models.....   | 29 |
| 3.1   | Computational Rotor Model .....  | 29 |
| 3.1.1 | Disk Roughness and Flow Profile .....  | 29 |
| 3.1.2 | Rotor Equations .....  | 31 |
| 3.1.3 | Efficiency Estimate for the Ideal Rotor and Turbine.....                                 | 32 |
| 3.1.4 | Rotor Streamlines .....  | 32 |
| 3.1.5 | Effect of Flow Profile on Ideal Turbine Performance.....                                 | 34 |
| 3.1.6 | Nozzle Flow .....  | 37 |
| 3.2   | Comparison of Experimental Efficiency and Predicted Efficiency .....                     | 37 |
| 3.3   | ANSYS Verification of Flow Model Testing.....  | 38 |
| 3.3.1 | Simulation Variations and Observations.....  | 39 |
| 3.3.2 | Simulated Systems and Results.....   | 40 |
| 3.3.3 | Performance Trend Comparison.....  | 40 |
| 3.3.4 | Conclusions: .....   | 42 |
| 4     | Turbine Mechanical Losses and Mapping Test System Performance to the Ideal Turbine ..... | 43 |
| 4.1   | Loss Models and Estimation .....   | 44 |
| 4.2   | Head Loss Contributors.....  | 45 |
| 4.2.1 | Nozzle Loss .....  | 45 |
| 4.2.2 | Kinetic Energy Loss at Exhaust .....   | 47 |
| 4.2.3 | Rotor Loss Fraction .....  | 47 |

|       |   |    |
|-------|---|----|
| 4.3   | Shaft Power Loss Contributors.....  | 47 |
| 4.3.1 | Disk Friction Loss.....   | 47 |
| 4.3.1 | Rotor Turbulence Loss .....   | 50 |
| 4.3.2 | Partial Admission .....   | 50 |
| 4.4   | Other Losses.....   | 50 |
| 4.4.1 | Leakage .....   | 50 |
| 4.4.2 | Leading and Trailing Flow Losses .....  | 51 |
| 4.4.3 | Bearing Loss .....  | 51 |
| 4.5   | Mechanical Efficiency Estimate with all Losses .....                            | 52 |
| 4.6   | Estimated Turbine Performance with Losses .....                                 | 52 |
| 4.7   | Test Turbine Performance Evaluation and Mapping .....                           | 56 |
| 4.8   | Mapping Experimental Results to Ideal Performance .....                         | 58 |
| 4.8.1 | Test Rotor Performance Analysis.....  | 58 |
| 4.8.2 | Test System Model.....  | 59 |
| 4.8.3 | Analytical-to-Experimental Mapping.....   | 60 |
| 4.8.4 | Conclusion.....   | 61 |
| 5     | Design Constraints, Scaling Criteria and Sensitivity Analysis .....             | 62 |
| 5.1   | Design Approach .....   | 62 |
| 5.2   | The Optimal Rotor.....  | 62 |
| 5.2.1 | Flow Profile $n$ .....  | 62 |
| 5.2.2 | Rotor Reynolds Numbers, $RE_{rot}$ and $N_{RE}$ .....                           | 63 |
| 5.2.3 | Non-dimensional Fluid Tangential Velocity, $Vt_o$ .....                         | 63 |
| 5.2.4 | Non-dimensional Flow Rate indicator, $Vr_o$ .....                               | 63 |
| 5.2.5 | The Exhaust to Rotor Radius ratio, $\xi_i$ .....                                | 63 |
| 5.3   | Minimizing Losses .....   | 63 |
| 5.3.1 | Head Loss Minimization .....  | 64 |
| 5.3.2 | Shaft Power Loss Minimization.....  | 65 |
| 5.3.3 | Minimizing Other Losses.....  | 65 |
| 5.4   | Scaling Approach.....   | 66 |
| 5.4.1 | Scaling Rotor Hardware Parameters.....  | 66 |
| 5.5   | Design for Constant power density over the Range of 2 mW to 20 kW Turbines..... | 68 |
| 5.5.1 | Design Constraint Table .....   | 70 |

|        |   |     |
|--------|---|-----|
| 5.5.2  | Constant Power Density Design Examples.....                       | 71  |
| 5.6    | Turbine Design for a Given Head, Flow, and Particulate Size ..... | 72  |
| 5.6.1  | Methodology and Tool.....   | 72  |
| 5.7    | Sensitivity Analysis and Verification .....                       | 74  |
| 5.8    | Design Graphs and Mapping of Published Turbines.....              | 75  |
| 5.8.1  | Design Graphs .....   | 75  |
| 5.8.2  | Mapping of Published Turbines .....                               | 78  |
| 5.8.3  | Reconciliation of observed Turbine Discrepancies .....            | 79  |
| 5.8.4  | Designs Examples for Intended Applications.....                   | 80  |
| 6      | Conclusions and Future Work .....                                 | 82  |
| 6.1    | Conclusions .....   | 82  |
| 6.1.1  | The Value of the Tesla Turbine .....                              | 82  |
| 6.1.2  | Optimizing Performance .....                                      | 82  |
| 6.1.3  | The Importance of the Design Tools.....                           | 82  |
| 6.1.4  | Practical Limits for Tesla Hydro Turbines.....                    | 82  |
| 6.2    | Future Work.....  | 83  |
|        | Bibliography .....  | 84  |
|        | Appendix - A: Design Tool .....                                   | 87  |
| A.1    | Methodology.....  | 87  |
| A.2    | Design Tool Flow Chart .....                                      | 89  |
| A.3    | MATLAB Code .....   | 90  |
| A.3.1  | Design_Turbine .....  | 90  |
| A.3.2  | Evaluate_Turbine .....  | 92  |
| A.3.3  | Nozzle Loss.....  | 94  |
| A.3.4  | Gap and Tip Torque Losses .....                                   | 95  |
| A.3.5  | Rotor Flow Characterization .....                                 | 96  |
| A.3.6  | Sensitivity of Designed Turbine to Head and Flow Variations.....  | 97  |
| A.3.7  | Analyze Sensitivity for a Particular Head and Flow.....           | 98  |
| A.3.8  | Setup constants and variables for Design.....                     | 99  |
| A.3.9  | Setup Variables to Analyze Design's Sensitivity.....              | 104 |
| A.3.10 | Turbine Performance graphs .....                                  | 105 |
| A.3.11 | Turbine Specification Table Generation .....                      | 107 |

|        |   |     |
|--------|---|-----|
| A.3.12 | Plot Algorithm: Sankey.....                     | 110 |
| A.3.13 | Design Tool.....                                | 117 |
| A.3.14 | Table of Design Specification .....             | 123 |
| A.4    | GUI .....                                       | 124 |
| A.4.1  | GUI –Interface -1: Low Head and high flow ..... | 124 |
| A.4.2  | GUI -Interface -2: High Head and Low Flow ..... | 125 |

## List of Figures

---

|  |    |
|--|----|
| Figure 1-1: S.J. Williamson, B.H. Stark, J.D. Booker (2011). “Low Head Pico Hydro Turbine Selection using a Multi-Criteria Analysis.” At the low-head and low-flow region, the Tesla (cm-scale) turbine operating range is superimposed. ....  | 2  |
| Figure 1-2: Tesla turbine, basic design and operation. Fluid entering through the inlets spirals inwards between disks, transferring power to the rotor shaft. This fluid exits through holes near the center of each disk and downwards out of the turbine. ....  | 3  |
| Figure 1-3: Application concept in a river turbine. The head is 1 to 5 meters and the flow 1 to 20 liter/sec with power output 50 W to 2 kW. ....  | 5  |
| Figure 1-4: (Left) The micro turbine is rotated by evaporation-driven fluid flows in an open-loop scavenging or closed-loop cooling application. (Right) The micro turbine operates in an organic Rankine or Sterling cycle depending on the motive fluid’s phase transition temperatures and on power needs. ....   | 6  |
| Figure 1-5 : CPVT application. The Tesla turbine, using a low boiling medium in a closed loop, generates power from waste heat at about 120°C. An organic Rankine or Kalina cycle can be used for efficient recovery. The heat in the exhaust medium is used to desalinate water at about 70°C. ....   | 7  |
| Figure 1-6: Combined heat and power systems. A solar collector serves as the energy source. Here Tesla principle can be used in the expander turbine and the pump. V.P.Carey, “Assessment of Tesla Turbine Performance for small scale Rankine Combined Heat and Power Systems” [11]. ....   | 8  |
| Figure 2-1: (Top left) Three 1 cm rotors and one 2 cm rotor, fully assembled. (Top right) White light microscopy (20x) showing R1 with 125 μm spacing and post-assembly gap uniformity in the rotor stack. (Middle left) Photo-etched stainless steel disks with different exhaust patterns, end disks, spacers, and bronze square axles, and (at center) a 4 cm <sup>3</sup> turbine with four symmetric nozzles. (Middle right) R5 close-up (20 disks, 125 μm spaced, pattern 3). (Bottom row) Three exhaust patterns with 0.47, 0.51, and 0.6 effective exhaust-to-entry radius ratio (Table 2-1). .... | 16 |
| Figure 2-2: Nozzle architecture. The bottom entry face of all nozzles is circular, with a 4.04 mm diameter. The top exit face of the rotors (Left) for nozzles 1, 2, 3, 4, 6, and 8 is slit with a converging body, (Center) for nozzle 5 features five circular exits of 0.4 mm diameter with a converging body, and (Right) for nozzle 7 features a wider arc slit with a funnel-shaped body. ....   | 18 |
| Figure 2-3: (Left) An exploded CAD view of the enclosure, with the eight nozzles. The center rotor housing diameter is 1.013 cm, and nozzle-entry diameter is 4.04 mm. All except nozzle 5 are slits scanning many rotors; nozzle 5 has five circular exits. (Right) Six turbine exhaust holes are at the bottom of the enclosure, and in the center is the bearing assembly. ....   | 19 |

Figure 2-4: Test turbines. (Left and middle) Top and bottom view of the 1 cm rotor in a 1.6 cm cubic turbine with four tangential nozzles at 90 degree spacing. (Right) A 4 cm octagonal turbine with eight nozzles, used for testing the four rotors at eight nozzle configurations. .... 19

Figure 2-5: (Left) The water head drives the rotor. (Right) The gear pump draws water from a tank and drives the rotor. In all tests, nozzle inlet pressure is measured using a gauge, and rotor movement is recorded using a high-speed camera. The flow rate is controlled by the pump, which is driven for 25 seconds for each test. The camera records the rotor from rest to full speed to rest, capturing the acceleration and deceleration phases. .... 20

Figure 2-6: Free running RPM for four test systems. (Left): RPM dependence on head in meter. (Right) RPM dependence on flow rate in  $\text{cm}^3/\text{s}$ . .... 20

Figure 2-7: Rotor revolutions/sec (frequency) derived from raw video data (o), and second-order polynomial curve fits for acceleration (solid) and deceleration (dashed). Scaled slopes correspond to angular acceleration  $\alpha_1$  and angular deceleration  $\alpha_2$ . Torque ( $\tau$ ) and power output is then calculated from  $\alpha_1$  and  $\alpha_2$ . .... 22

Figure 2-8: Rotor movement details – Average fitted curve with data variations given by the double arrow lines. (Left) Rotor frequency (solid) and acceleration (dotted) at start of flow. (Right) Rotor frequency (solid) and deceleration (dotted) after flow is stopped ..... 22

Figure 2-9: Curve fit data. Curve fit results for rotor 1, nozzle 3 (R1-N3) at  $10 \text{ cm}^3/\text{s}$  flow rate. (Top) Indicates torque spread and (Bottom) indicates efficiency spread. The mean is plotted in solid line. .... 23

Figure 2-10: R3-N3 performance vs. RPM at flow rates of  $2 \text{ cm}^3/\text{sec}$  to  $10 \text{ cm}^3/\text{s}$ . (Top Left) Accelerating, decelerating, and total torque at  $10 \text{ cm}^3/\text{s}$  flow rate. Performance curves for flow rates from  $2 \text{ cm}^3/\text{s}$  to  $10 \text{ cm}^3/\text{s}$  : (Top Right) Total torque. (Bottom Left) Power output. (Bottom Right) Efficiency ..... 24

Figure 2-11: Rotor performance comparison. (Left) Rotor 1 and rotor 2 have higher power output than rotor 3. (Right) Nozzle 3 outperforms nozzle 1. The slower the flow, the higher the efficiency in all systems. .... 25

Figure 3-1: Rotor analysis block diagram ..... 30

Figure 3-2: Rotor streamlines. (Left) The number of cycles that fluid makes with a micro rotor of 1 mm radius, a big rotor of 100 mm radius, and test rotor R1 of 5mm radius. (Right) The corresponding rotor streamlines with the  $V_{r_o}$ , flow indicator value.  $V_{t_o}=1.0$ ,  $n=2$ ,  $\xi_i=0.4$  for all rotors. .... 33

Figure 3-3: For the three rotors in Figure 3-2, normalized tangential velocity along the flow path from entry to exit. (Left) Plotted along the rotor streamlines. (Right) Plotted as a function of normalized radius. Solid: 20 cm rotor ( $V_{r_o}= 0.02$ ,  $n=2$ , exit velocity= 20% of entrance); Dot: fabricated 1 cm rotor R1-N3 ( $V_{r_o} = 0.09$ ,  $n=2$ , exit velocity 40% of entrance); Dash: 2mm design rotor ( $V_{r_o} = 0.08$ ,  $n=6$ , exit velocity 30% of entrance);  $V_{t_o}=1.3$ ,  $\xi_i=0.4$  for all three. .... 34

Figure 3-4: (Top left) Flow profile in the interdisk space for  $n = 2, 4, 6,$  and  $8,$  showing the effect of profile ( $n = 2, 5, 8$ ). Rotor parameters for profiles  $n = 2, 5,$  and  $8$  at low and high flow  $V_{r_o} = 0.01, 0.1;$  (Top right) Non-dimensional tangential velocity  $V_{t_r}$  in the rotor. (Bottom left) Non-dimensional pressure drop  $P_r.$  (Bottom right) Non-dimensional torque  $T_r$ ..... 35

Figure 3-5: Profile effect on ideal rotor performance. Three sets of operation are chosen ( $\xi_i=0.4$  for all). 1) the smooth surface ( $PO=24, n=2, N_{RE}=4$ ), 2) rough surface ( $PO=36, n=3.5, N_{RE}=6$ ), and 3) even rougher surface ( $PO=48, n=5, N_{RE}=8$ ). Efficiency (top left), non-dimensional pressure (top right) and non-dimensional torque (middle left) are the same for all three sets, and are plotted for the reference set against the velocity and flow indicators. (Middle right) Power is normalized to the reference operating condition at  $V_{t_o} = 1.2, V_{r_o} = 0.02, N_{RE}=4.$  This normalization is used to compute the achievable relative power of the other two operating sets. The cubic relation of power vs.  $N_{RE}$  (RPM) and the linear relationship of torque  $V_{r_o}$  vs. flow rate combine to provide 21x the reference power at  $V_{t_o} = 1.5, V_{r_o} = 0.1, N_{RE}=6$  (bottom left) and 50x the reference power at  $V_{t_o} = 1.5, V_{r_o} = 0.1, N_{RE}=8$  (bottom right)..... 36

Figure 3-6: Nozzle drop and exit velocity profiles studied using COMSOL. (Left) Nozzle 4 pressure drop in Pascal. (Middle) Nozzle 4 flow velocity in m/s. (Right) Nozzle 7 velocity in m/s. The model design is shown in Figure 2-2. Boundary conditions are set to the following: atmospheric pressure at the exit, water flow rate of  $10 \text{ cm}^3/\text{s},$  and parabolic velocity profile at the nozzle input. Nozzle flow is laminar and nozzle walls are smooth. .... 37

Figure 3-7: Experimental efficiency vs. predicted efficiency. (Left) Experimental efficiency has a linear correlation with predicted efficiency for the rotors tested – rotors R1, R3, and R4 (rotor- disk space specified at 125, 250, 500  $\mu\text{m}$ ) with nozzle 3. (Right) Experimental efficiency also has a linear correlation with predicted efficiency for the nozzles tested – nozzles N3, N4, and N7 (nozzle-length, nozzle-width at 2.3, 3.2, 7.2  $\text{mm}^2$  area) with rotor 1..... 38

Figure 3-8: (Left) The ANSYS domain (highlighted) is bounded by a symmetry plane through the center of a gap and by a symmetry plane through the center of a disk. The disk edge forms a rotating boundary. (Right) ANSYS geometry..... 39

Figure 3-9: (Left)  $V_{t_o}$  based on velocity vector:  $V_{t_o} = \sqrt{(V_{noz}^2 - V_{r_o}^2)}.$  (Right)  $V_{t_o}$  matched to ANSYS..... 40

Figure 3-10: (Left) Efficiency vs. disk spacing. The smaller the disk spacing, the higher the efficiency. The smooth curve is the trend predicted by the integral perturbation solution, and the rotors and nozzles for the experimental and ANSYS results are indicated. (Right) Efficiency vs. nozzle area. The smaller the nozzle area, the higher the nozzle exit velocity and the higher the efficiency for the tests simulated. The trend as well as the experimental and ANSYS data are plotted. .... 41

Figure 4-1 : Turbine hardware naming convention used in this chapter to study the losses. .... 43

Figure 4-2: Turbine loss model is categorized into head loss, shaft power loss that are part of the turbine hardware and operation and other losses that are more implementation dependent. These loss estimates are applied to our turbine model, and turbine performance is evaluated for various flow profiles..... 44

Figure 4-3: (Top) Moody diagram used in this research [25]. Transitional region 2300 to 4000 (from laminar to turbulence) is undefined and is to be avoided, though in the figure a linear interpolation is used to show the transition. (Both bottom) Nozzle loss for R1-N4 at  $V_{r_o}=0.06$ ,  $V_{t_o}=1.1$ . (Bottom left) Nozzle Reynolds number 2300 at reference. (Bottom right) Non-dimensional head loss 0.17 and nozzle loss = 14.3% at reference... 46

Figure 4-4: Disk friction [26]. (Top left) Rotor and housing for disk friction measurement. (Top right) Gap friction coefficient (torque multiplier) used in this dissertation. (Bottom, both) Non-dimensional torque loss factors for R1-N4 at  $V_{r_o}=0.09$ ,  $V_{t_o}=1.5$ . (Bottom left) Tip friction loss 4% and (Bottom right) Gap friction loss 1.1% at reference. .... 49

Figure 4-5: Flow path visualization at the entry and exit of the rotor. (Left) Flow path bending around the disk edges into 125  $\mu\text{m}$  interdisk space from the 250  $\mu\text{m}$  nozzle exit (entry) at the bottom. (Right) Flow path making a 90° turn at the exit. .... 51

Figure 4-6: 2 mm turbine;  $b=35\mu\text{m}$ ,  $n=5$ ,  $NRE=8$ ,  $RPM=62500$  (Table 4-1) (Top) Sankey diagram, derived at reference point  $V_{r_o}=0.04$ ,  $V_{t_o}=1.2$ ,  $RE_{rot}=1.28$ . (Middle left) Ideal turbine efficiency. (Middle right) Lossy turbine efficiency. (Bottom left) Power density. (Bottom right) Nozzle Reynolds number. .... 53

Figure 4-7: 4 cm turbine;  $b=86\mu\text{m}$ ,  $n=3.5$ ,  $NRE=6$ ,  $RPM=7700$  (Table 4-1) (Top) Sankey diagram, derived at reference point  $V_{r_o}=0.04$ ,  $V_{t_o}=1.2$ ,  $RE_{rot}=0.96$ . (Middle left) Ideal turbine efficiency. (Middle right) Lossy turbine efficiency. (Bottom left) Power density. (Bottom right) Nozzle Reynolds number. .... 54

Figure 4-8: 30 cm turbine;  $b=157\mu\text{m}$ ,  $n=2$ ,  $NRE=4$ ,  $RPM=1930$  (Table 4-1); (Top) Sankey diagram, derived at reference point  $V_{r_o}=0.04$ ,  $V_{t_o}=1.2$ ,  $RE_{rot}=0.64$ . (Middle left) Ideal turbine efficiency. (Middle right) Lossy turbine efficiency. (Bottom left) Power density. (Bottom right) Nozzle Reynolds number. .... 55

Figure 4-9: Sankey diagram on test turbine mechanical power output using nozzle-4 structure. Here the optimum angle for nozzle-4 is used in calculating, resulting in better efficiency. .... 56

Figure 4-10: Rotor-1, Nozzle-4 performance at various nozzle exit angle and RPM. Efficiency increases as the nozzle angle is close to being tangential to the rotor. .... 57

Figure 4-11: Rotor 1 performance surface, projection of experimental and predicted efficiencies for N3, N4, and N7 onto the ideal efficiency surface of R1 with flow profile  $n=2$ ,  $V_{r_o}=0.1$ ..... 58

Figure 4-12: Test rotor 1 performance for nozzles 3, 4, and 7 vs. 30 cm reference rotor. (Top left) Normalized tangential velocity in the flow path, inside the rotor. (Top right) Normalized tangential velocity with respect to rotor radius ratio. (Bottom left) Pressure drop and (Bottom right) momentum transfer with respect to radius ratio. All test nozzle curves show higher unspent kinetic energy, higher pressure drop, and lower torque

transfer compared with the reference turbine. Nozzle 7 performance is especially poor. .... 59

Figure 4-13: R1-N3 test system efficiencies. Ideal turbine efficiency maps first to the prediction ( $\eta_{id2pr}$ ), then to the experimental efficiency ( $\eta_{id2ex}$ ). .... 60

Figure 5-1: Spiral Nozzle: Eight slit nozzles scanning the entire rotor stack located around the rotor. Length of the nozzles is small. The width of the slit nozzles are shown exaggerated. Normally the nozzle slit width for this implementation is less than  $5^\circ$ . .... 64

Figure 5-2: Effect of scaling exponent  $k$  on (Top left) interdisk space, (Top right) power density, (Middle left) RPM, (Middle right) power output, (Bottom left) head, and (Bottom right) flow rate per disk, while maintaining optimal non-dimensional operating parameters (based on a 300 mm reference turbine). .... 67

Figure 5-3: Level-1 design for 1 mm to 400 mm diameter rotors;  $k = 0.33$ ,  $Vt_o = 1.3$ , minimum interdisk spacing is  $30 \mu\text{m}$ . (Left) System efficiency (turbine with nozzle and disk friction loss) variation 0.54 to 0.73. (Center) Power density variation  $38 \text{ W/cm}^3$  to  $1.3 \text{ W/cm}^3$ . (Right) Flow control parameters. .... 68

Figure 5-4: Design graphs for 1 mm to 400 mm diameter rotors;  $k = 0.3$ ,  $NRE = 5$ ,  $Vr_o$  and  $Vt_o$  adjusted to meet the desired efficiency and power density,  $b = 32.5 \mu\text{m}$  for 1 mm rotor at scaling =1. Level-3 optimization with interdisk space linear scaling at 0.93, 1.0 (Level-2, solid line), 1.07, and 1.14. Level-2, parameter range at scaling = 1. (Left) System efficiency 0.41 to 0.75 (mostly constant over the scaling range). (Center) Power density  $2.2 \text{ W cm}^3$  to  $4.4 \text{ W cm}^3$ . (Right) Head 2 m to 180 m. .... 69

Figure 5-5: Level-3 design graphs for rotors from 1 mm to 400 mm in diameter; all parameters as in Figure 5-4. (Left) Flow rate / disk is from  $20 \text{ mm}^3 / \text{s}$  to  $160 \text{ cm}^3 / \text{s}$ . (Center) Power in watts/disk varies by approximately 300% as interdisk space scaling varies by 21%. (Right) RPM varies by 42% in the same range. .... 69

Figure 5-6: Power and power density variations for rotors in radius range from 2 mm to 150 mm at the input specifications of the (150 mm radius) reference rotor. The optimal turbine radius according to our study is 66 mm. .... 74

Figure 5-7: Head and flow sensitivity analysis of the designed turbine. (Top right) Efficiency is relatively stable ( $\pm 2\%$ ) over a wide range of input head ( $\pm 20\%$ ) and of input flow ( $\pm 10\%$ / $-20\%$ ). Values of (top right) power density, (bottom left) power, and (bottom right) RPM. .... 75

Figure 5-8: 3D slice graphs. .... 77

Figure 5-9: Four turbine designs mapped on the 3D grid: 1) triangle - test turbine R1-N4 2) star - the Razak river turbine redesign 3) circle - Ho-Yan's open falls turbine 4) square- Lawn's 30 cm reference hydro turbine. (Left)  $\log_{10}$  (power density) plot for 120 turbine designs. Density varies by five orders, and lower dust particle size and higher head both result in higher power density. (Right) Efficiency varies 10% to 70%. In the higher flow range, the inverse relationship between power (efficiency) and power density can be observed. .... 78

Figure A--1: Design Tool program flow chart. .... 89

Figure A-2: Williamson turbine input-specification is used in this Tesla turbine based redesign..... 124

Figure A-3: Ho-Yan’s turbine redesign with 126 mm radius and 1 mm interdisk space 125

## List of Tables

---

|  |     |
|--|-----|
| Table 1-1: Power/cc for reported Tesla Turbines. (Rotor volume is used in this calculation).....   | 10  |
| Table 2-1: Rotors, 1cm diameter and 2 cm diameter .....  | 17  |
| Table 2-2: Nozzle Specifications.....  | 18  |
| Table 2-3: Test system performance: R1-N4-12 best power and efficiency, and R3-N3-2 best efficiency. ....  | 26  |
| Table 3-1: Dimensions and operating points of ANSYS simulations. Rotor# and Nozzle# ID correspond to those in Table 2-1 and Table 2-2. Nozzle angles are measured from the radial direction to nozzle flow direction at the center of the nozzle. .... | 41  |
| Table 4-1: Turbine Hardware and Operating Specifications.....  | 57  |
| Table 5-1: Turbine design parameters and constraints.....  | 70  |
| Table 5-2: Possible constant power density Designs for four hydro turbines from micro to big. Here particulate size in the medium is not taken in to account. ....   | 71  |
| Table 5-3: Optimum efficiency design for hydro applications discussed in Chapter 1.3 .   | 80  |
| Table A-1: Design specification for a Tesla turbine (input spec. from Williamson’s Turgo turbine).....   | 123 |

# Nomenclature

---

## Turbine Specification related parameters

|                          |   |
|--------------------------|---|
| RPM                      | rotor revolutions/min                         |
| Head ( $p$ )             | Fluid pressure head at Turbine input (Pascal) |
| Flowrate ( $q$ )         | Volume flow rate of the fluid ( $m^3/s$ )     |
| Particulate size ( $d$ ) | Size of the particles in the fluid (m)        |
| Power out                | Nominal output power of the turbine (W)       |
| Power density            | power out / $cm^3$ ( $W/cm^3$ )               |

## Motive fluid

|        |   |
|--------|---|
| $\rho$ | density of the motive fluid ( $kg/m^3$ )                    |
| $\mu$  | dynamic viscosity of the fluid ( $kg\ s/m^2$ )              |
| $\nu$  | kinematic viscosity of the fluid = $\rho / \mu$ ( $m^2/s$ ) |

## Cylindrical coordinate system

|          |                    |
|----------|--------------------|
| $z$      | axial coordinate   |
| $r$      | radial coordinate  |
| $\theta$ | angular coordinate |

## Subscripts

|     |                         |
|-----|-------------------------|
| $o$ | (outer- at rotor entry) |
| $i$ | (inner-at rotor exit)   |
| $r$ | (at rotor radius "r")   |

## Hardware

|            |   |
|------------|---|
| $b$        | spacing between disks (m)                     |
| $r_o$      | rotor disk radius (m)                         |
| $r_i$      | rotor exhaust radius (m)                      |
| $t$        | disk thickness (m)                            |
| $N_{disk}$ | number of disks in the rotor stack            |
| $W_{noz}$  | nozzle width (m)                              |
| $H_{noz}$  | nozzle height (m)                             |
| $D_{noz}$  | hydraulic diameter of the nozzle              |
| $L_{noz}$  | nozzle length (m)                             |
| $c$        | clearance between rotor tip and enclosure (m) |
| $s$        | 'gap' between end disk and enclosure (m)      |

## Turbine Operation parameters

|                     |   |
|---------------------|---|
| $\phi(z)$           | fluid velocity profile in axial (z) direction in the rotor          |
| $\omega$            | rotor disk angular velocity = $2\pi \text{ RPM} / 60$ (/s)          |
| $V_{\text{tip}}$    | rotor tip speed used as the normalizing factor = $\omega r_o$ (m/s) |
| $V_{\text{tan}}(r)$ | tangential velocity of flow at rotor radius r (m/s)                 |
| $V_{\text{rad}}(r)$ | radial velocity of flow at rotor radius r (m/s)                     |
| $V_{\theta}(r)$     | axially averaged $V_{\text{tan}}(r)$ based on fluid profile - (m/s) |
| $V_r(r)$            | axially averaged $V_{\text{rad}}(r)$ based on fluid profile - (m/s) |
| $V_{\text{noz}}$    | fluid velocity at the nozzle exit (m/s)                             |

### Dimensionless Parameters

|                 |   |
|-----------------|---|
| $\lambda$       | roughness ratio of the nozzle   |
| $F_{\text{PO}}$ | rotor disk roughness indicator = $\text{PO} / 24$                                   |
| $n$             | fluid profile controller = $3 * F_{\text{PO}} - 1$ ; $n=2$ parabolic; $n=6$ uniform |
| $\epsilon$      | aspect ratio = disk space / rotor radius = $b / r_o$                                |
| $\xi_r$         | radius ratio = $r/r_o$ ; $\xi_i = r_i / r_o$  |
| $V_{t_r}$       | normalized average tangential velocity = $V_{\theta}(r) / V_{\text{tip}}$           |
| $W_r$           | normalized relative tangential velocity = $V_{t_r} - \xi_r$                         |
| $V_{r_r}$       | normalized average radial velocity = $V_r(r) / V_{\text{tip}}$                      |
| $V_{r_o}$       | flow rate indicator = $V_{r_r}$ at rotor entry                                      |

### Reynolds numbers related

|                   |   |
|-------------------|---|
| $N_{\text{RE}}$   | rotational Reynolds number = $\omega b^2 / \nu$   |
| $RE_{\text{gap}}$ | gap Reynolds number = $\omega r_o^2 / \nu$  |
| $RE_{\text{noz}}$ | nozzle Reynolds number =  |
| $RE_{\text{rot}}$ | Rotor Reynolds number = $4 N_{\text{RE}} V_{r_o} = 2 b q_{\text{disk}} / \pi r_o^2 \nu$ |
| $\alpha_r$        | Nendl visco-geometric number = $0.25 RE_{\text{rot}} / \xi_r^2$                         |

### Derived:

|                       |   |
|-----------------------|---|
| $J$                   | moment of inertia of the rotor ( $\text{kg.m}^2$ )  |
| $Q$                   | flow rate through rotor = $2\pi b r_o V_{\text{rad}} N_{\text{disk}} = 2\pi V_{r_o} b \omega r_o^2 N_{\text{disk}}$ ( $\text{m}^3/\text{s}$ ) |
| $Q_{\text{disk}}$     | flow rate / disk pair = $Q / N_{\text{disk}}$ ( $\text{m}^3/\text{s}$ )   |
| $\dot{m}$             | mass flow rate between a disk pair = $\rho Q_{\text{disk}}$ ( $\text{kg}/\text{s}$ )  |
| $P_t$                 | dimensionless pressure = $p / \rho (V_{\text{tip}})^2$  |
| $R_{\text{momentum}}$ | dimensionless momentum transfer   |
| $\tau$                | available rotor torque (N-m)  |
| $T$                   | dimensionless torque = $\tau / (r_o^2 b \rho (V_{\text{tip}})^2 N_{\text{disk}}) = 2\pi V_{r_o} R_{\text{momentum}}$                          |

$\dot{W}_{\text{in}}$  Input power = flow rate \* head =  $q p$  (Watt)

$\dot{W}_{\text{out}}$  Work done = torque \* angular velocity =  $\tau \omega$  (Watt)

### Dimensionless Losses

|                   |  |
|-------------------|--|
| $P_{nozLoss}$     | frictional loss in the nozzle  |
| $P_{rotLoss}$     | frictional loss in the rotor   |
| $P_{keLoss}$      | unused kinetic energy loss at the exit   |
| $P_{headLoss}$    | calculated head loss = $(P_{nozLoss} + P_{rotLoss} + P_{keLoss})$                      |
| $P_{volLoss}$     | volume leakage loss  |
| $P_{pathLoss}$    | entering, exit flow path loss  |
| $P_{otherLoss}$   | estimated head loss = $(P_{volLoss} + P_{pathLoss})$                                   |
| $T_{gapLoss}$     | torque loss due to trapped fluid between end disks and enclosure                       |
| $T_{tipLoss}$     | torque loss due to trapped fluid between disk tips and enclosure                       |
| $T_{rotLoss}$     | torque loss due to turbulence in flow near the disk exhaust                            |
| $T_{bearingLoss}$ | bearing loss   |
| $T_{diskLoss}$    | calculated torque loss = $(T_{gapLoss} + T_{tipLoss} + T_{rotLoss} + T_{bearingLoss})$ |
| $M_t$             | Output: $R_{momentum} * (1 - T_{diskLoss})$  |
| $P_t$             | Input: $R_{momentum} + P_{headLoss} + P_{otherLoss}$                                   |

### Efficiency

$$\eta \quad \text{efficiency} = M_t / (P_t) = \tau \omega / (q p) = \dot{W}_{out} / \dot{W}_{in}$$

## Acknowledgements

---

I am deeply indebted to my advisor Professor Michel Maharbiz for giving me this opportunity to do research under him and for his insights and encouragement throughout. My special thanks to my committee professors Seth Sanders, Liwei Lin and Alexandra von Meier for their input on organizing this dissertation.

I also like to thank Vincent Romanin and Matthew Ritchie for their review of my dissertation, Sisi Chen, Daniel Cohen, Hirotaka Sato, and Gabriel Lavella for various discussions and advice on fabrication, Joseph Gavazza of Electrical machine shop for his assistance during the fabrication of the rotor and Zohoro Iqbal, Frederick Dopfel, and Loqi Tamaroon for their help in the experiments.

My time in school was enriched by the invigorating classes especially in MEMs by Clark Nguyen and by Ali Javey, in image processing by Avidah Zakhor, in Optical imaging by Laura Waller, in Power engineering by Kameshwar Poola, and in Renewable energy by Daniel Kammen.

I am grateful for the GSI mentorship from professors Vivek Subramanian, Babak Ayazifar, and Stephen Derenzo, for the counsel from graduate advisors Shirley Salanio, and Ruth Gjerde, for the encouragements from professors Debbie Senesky, Ming Wu, and Anant Sahai, for the lab support from Ming Wong, for the software support from Computer user support group, for the endorsements from colleagues Karl Nordling, Fred Schuckert, and Rajeev Agrawal, and for the support from family Narasimhan R.A. and Matthew Ronfeldt.

Finally, I express my thanks for the early funding from the Army MAST program during micro fabrication of the turbine, for the support from BSAC in advancing the research, and for the GSI appointments from the EECS department.

# Chapter 1

## 1 Introduction

---

### 1.1 Motivation

There is undoubtedly a need for low-cost, low-maintenance, reliable power generators in the  $< 10$  kW range. This range covers three distinct groups of applications: residential and remote renewable energy projects range from about 50 W to 10 kW, small mobile and unmanned aerial vehicle (UAV) applications need power in the W to 100 W range, and power scavenger applications use  $\mu$ W to W. Tesla turbines are well-suited for these applications.

Prior theoretical work has claimed greater than 80% efficiency ([1], [2]), but experimental turbines have also reported less than 30% efficiency ([3], [4], [5], [6]). Current publications do not adequately address the practical design methodology and effect on performance of the turbines' input specifications, proposed hardware, and operating parameters. To date, no comprehensive work covers scaling constraints and performance trade-offs when attempting to engineer small ( $\sim 2$  cm<sup>3</sup>) Tesla friction turbines. The motivation behind the present research is therefore to fill this gap, which it does in two ways: 1) by recommending design guidelines and scaling methodologies for micro to small scale Tesla turbines with power output in the range of 1 mW to 10 kW, and 2) by providing tools to generate a set of turbine design specifications and performance sensitivities for a given range of inputs. With such design methodologies in place, Tesla turbines can become ideal power generators for renewable and mobile power applications.

At present, Tesla turbines have limited use outside the watt to kilowatt power range due to the availability of stronger competing technologies; in particular, because of advancing photovoltaic technology there is less interest in sub-watt turbine technologies, and mature inertial turbines are available in the range greater than 10 kW. Conversely, the design concepts and tools presented here place no restrictions on turbine power and size. With the aid of design tools and with experience in practical implementation, Tesla turbines are capable of competing across a full range of applications.

Low-power applications target residential users and remote-village users, for whom capital and maintenance costs are the deciding factors. Tesla turbines can be locally

manufactured due to their simple structure and affordability, and because they do not have vanes in the fluid path they are more suitable for mixed flows and particulate mediums. Modularization is also straightforward, which is an important consideration in remote areas where the flow rate changes drastically throughout the year and from place to place. Further, unloaded Tesla rotors cannot exceed a maximum speed due to centrifugal force, and are therefore safer.

Williamson, Shark, and Booker [7] map the working range of the various types of turbine. The recommended operating range for Tesla turbines is shown in Figure 1-1.

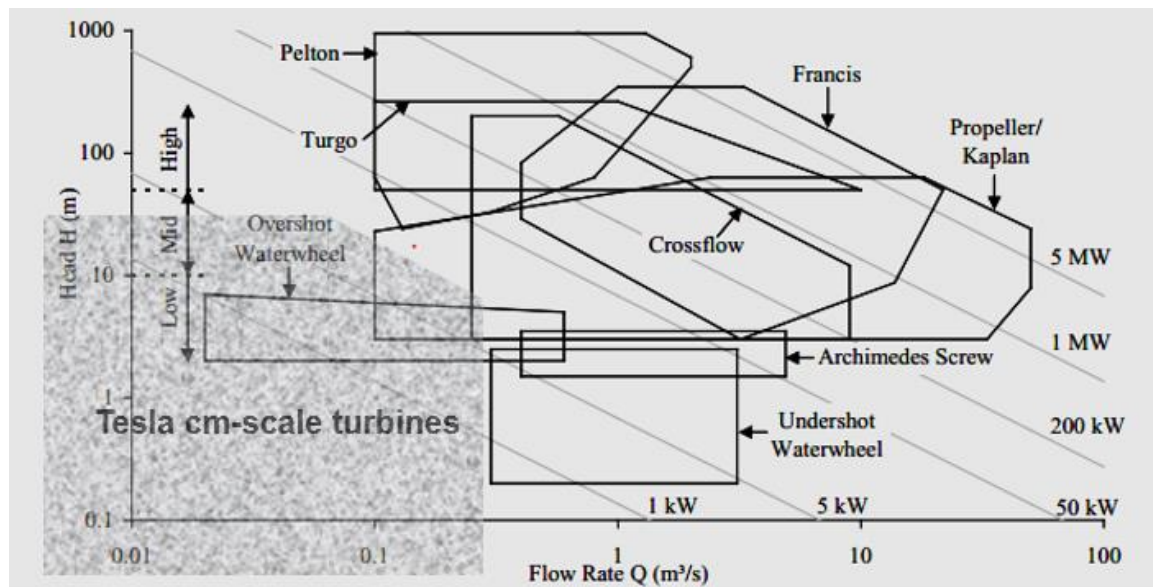


Figure 1-1: S.J. Williamson, B.H. Stark, J.D. Booker (2011). “Low Head Pico Hydro Turbine Selection using a Multi-Criteria Analysis.” At the low-head and low-flow region, the Tesla (cm-scale) turbine operating range is superimposed.

## 1.2 Background and Basic Operation

The “Tesla” turbine was first proposed in 1906 by Nikola Tesla [8], and the Allis-Chalmers manufacturing company produced one of the largest (1.5 meter diameter) Tesla steam turbines in 1911. This 500 kW turbine operated at 3600 RPM, with 38% mechanical efficiency. However, it could not compete against the inertial turbines of the time due to warping of the disks after prolonged usage. In the modern age – with the advent of mobile, residential, and remote renewable power applications – demand for low-power generators is growing, and it is a well-known problem that inertial turbines suffer heavy losses as they scale down. When turbine power and size are reduced, surface area-to-volume ratio increases: surface tension, adhesion, and

cohesion forces begin to dominate inertial forces, lowering the efficiency of such turbines. In contrast, Tesla rotors use kinematic viscosity and surface effects (rather than inertia) to convert flow energy into rotational motion. As such, Tesla turbines are excellent candidates for micro-scale power generation machinery.

In Tesla turbines, the adhesion and viscosity of a moving medium are used to propel closely-spaced disks into rotation (Figure 1-2). The fluid enters the inner space between the disks from the periphery and exits through central holes near the axle (as indicated by the dotted lines). There are no constraints or obstacles to couple inertial forces (i.e., vanes) as in traditional turbines. The fluid enters tangentially at the periphery and makes several revolutions while spiraling toward the central exhaust (again, the dotted lines). During this process, the fluid transfers momentum to the disks.

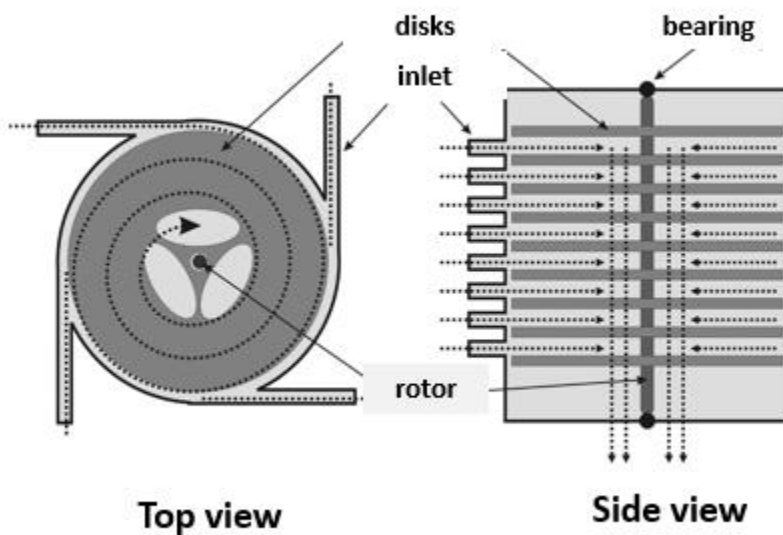


Figure 1-2: Tesla turbine, basic design and operation. Fluid entering through the inlets spirals inwards between disks, transferring power to the rotor shaft. This fluid exits through holes near the center of each disk and downwards out of the turbine.

### 1.2.1 Driving Force in Tesla Water (hydro)-Turbine

In a turbine the torque  $\tau$ , imparted onto the shaft of a rotor is equal to the momentum change of the fluid from entry to exit. The shaft power  $P_{out}$  is derived multiplying torque by  $\omega$ , the angular velocity of the rotor. This is the basis of Euler's equation. This can be rewritten in terms of changes in kinetic energy, centrifugal force, and the relative head of the fluid between entry and exit, (Eq. 1-1, and 1-2, [9]). It can be shown that the Tesla rotor is driven by both impulse and reaction forces.

$$P_{out} = \tau \omega = \dot{m} \omega (r_o v_{tan,o} - r_i v_{tan,i}) \quad 1-1$$

$$P_{out} = 0.5 * m \{ (v_o^2 - v_i^2) + \omega^2 (r_o^2 - r_i^2) + (v_{rel,i}^2 - v_{rel,o}^2) \} \quad 1-2$$

A change in kinetic energy corresponds to the impulse force, while a change in the head due to the centrifugal force and relative velocity corresponds to the reaction force. By design, the rotor flow entry velocity  $v_o$  is between 1.05 and 1.5 times the rotor tip velocity  $\omega r_o$ , and the relative flow velocity  $v_{rel}$  is less than half of the tip velocity. Thus, the reaction contribution to shaft power is between 25% and 50% of total power.

## 1.3 Tesla Turbine Applications in the Watt to Kilowatt Range

Although the experimental work in this dissertation focuses on open-loop water (hydro) turbines, the applications for the Tesla turbine are not limited to this. Five additional applications are discussed here, with the corresponding hydro turbine design specifications reported in Table 5-3

### 1.3.1 Low-Head or Low-Flow River Turbines

River turbines operate at low head with a medium to high flow that contains microorganisms and dust particles. The components of a standard river turbine are shown in Figure 1-3. Small dams (weir) are installed along the river to collect water and the water is supplied to the turbine through a penstock after filtering river particulates. The water at turbine exhaust is rerouted to the river downstream.

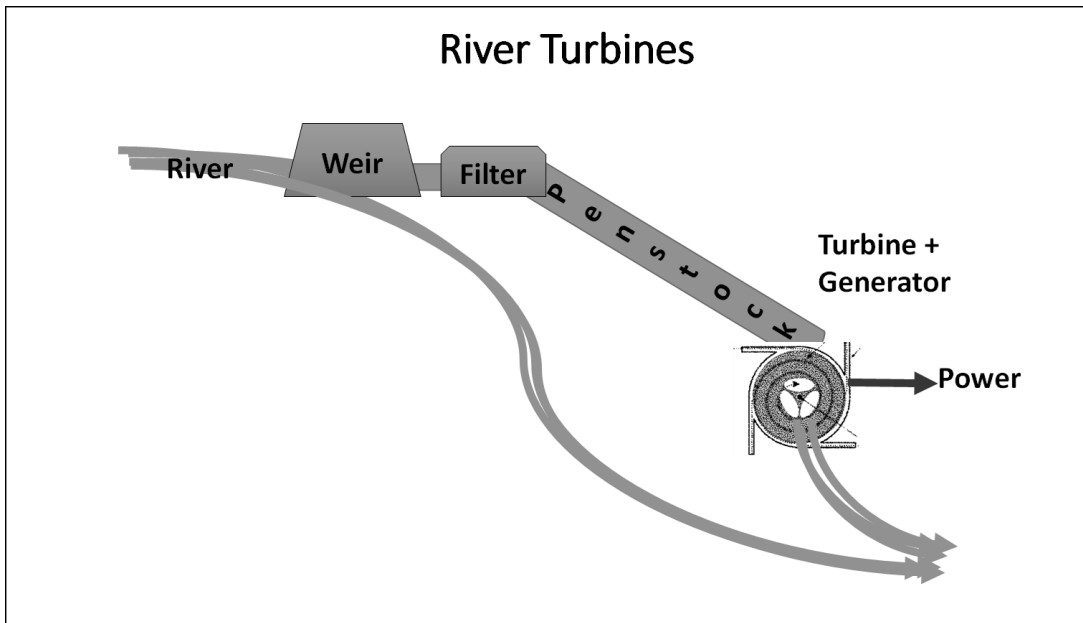


Figure 1-3: Application concept in a river turbine. The head is 1 to 5 meters and the flow 1 to 20 liter/sec with power output 50 W to 2 kW.

Razak et al. [10] built a 100 W low-head 12 kPa cross-flow turbine with a diameter of 0.5 meters. Williamson [7] tested a 1.3 kW low-head (36 kPa) jet Turgo turbine with a 0.5 meter diameter. From the given dimensions, power density estimate for these turbines is  $\sim 10 \text{ mW /cm}^3$ . In contrast, Tesla turbine arrays can be designed for low head or low flow in the 50 W to 2 kW range with good power densities from  $\text{mW /cm}^3$  to  $\text{W /cm}^3$  depending on the particulate size in the medium. As a replacement for a Razak cross-flow turbine or for Williamson's Turgo turbine, Tesla turbines can be designed to operate at 3x to 9x power density with 500  $\mu\text{m}$  interdisk spacing (to accommodate river particulates); the resultant smaller turbines also have better portability.

Another feature of this turbine is its simplicity. Once an optimum design is created for a specific head and particulate size, turbines with a specified number of disks can be manufactured or an array of turbines installed based on the available flow rate. This makes the design modular, affordable, and reliable, and allows smaller back-up turbines to be kept on-hand in case of failure. To illustrate this point, two designs are proposed in 5.8.4, for replacing Williamson's Turgo turbine – one providing 1.5 kW and another 300 W, both with similar flow/disk and power/disk.

### 1.3.2 Sub-Watt Mobile and Scavenger Applications

This research also addresses sub-watt power applications, and investigates a transpiration-based energy scavenger application in the mW power range. For mobile and UAV applications where higher energy density is needed, a fuel-based micro turbine in the watt range is also proposed (Figure 1-4).

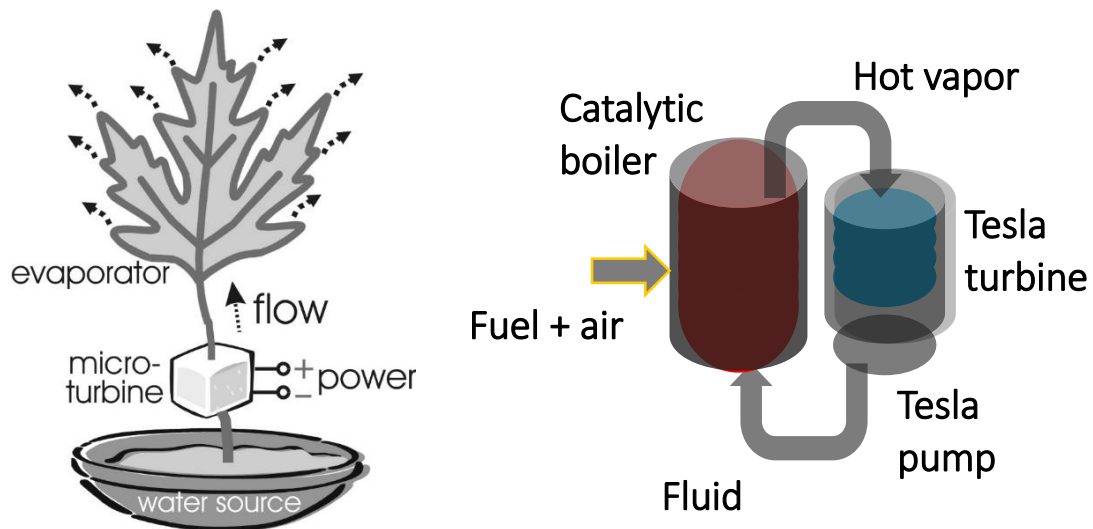


Figure 1-4: (Left) The micro turbine is rotated by evaporation-driven fluid flows in an open-loop scavenging or closed-loop cooling application. (Right) The micro turbine operates in an organic Rankine or Sterling cycle depending on the motive fluid's phase transition temperatures and on power needs.

### 1.3.3 Residential Combined Heat, Power, and Water

In small-scale residential applications, a Tesla turbine can be used to generate power from solar, geothermal, or fuel sources and to deliver the exhaust heat for different applications such as water desalination and heating potable water. The turbine can itself be a primary power generator, or a secondary generator that uses waste heat from the primary.

In concentrated photovoltaic thermal systems (CPVT, Figure 1-5), the turbine works as a secondary generator and its lower exhaust heat is used for desalination. The high concentration of solar power necessitates cooling the multi-junction photo cells to deliver 40% efficiency. Maintaining a higher temperature of about 120°C at 35% efficiency, a turbine with 50°C differential can be used to regain about 10% efficiency and the lower-temperature heat at 70°C can be used for desalination, thus creating precious drinking water while converting 45% of solar energy into electrical energy [12].

#### Solar CPVT → Power and Desalinated Water from Wasted Heat

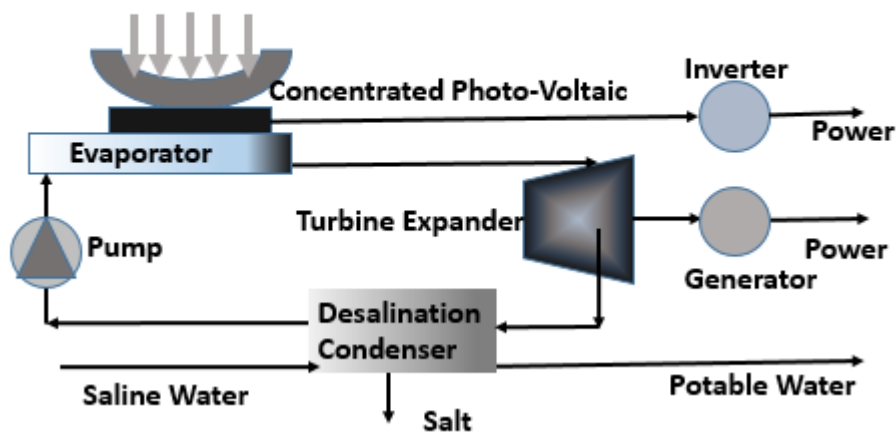


Figure 1-5 : CPVT application. The Tesla turbine, using a low boiling medium in a closed loop, generates power from waste heat at about 120°C. An organic Rankine or Kalina cycle can be used for efficient recovery. The heat in the exhaust medium is used to desalinate water at about 70°C.

In a concentrated solar power (CSP-solar heat) applications, the turbine acts as the main generator and its exhaust heat is used to provide hot water. Van Carey's [11] work employs a closed-loop system with water as the medium. The water Rankine cycle (Figure 1-6) collects solar energy through its concentrating collectors at a peak temperature of 165°C, a design that trades efficiency to deliver waste heat to potable water at a temperature of 90°C.

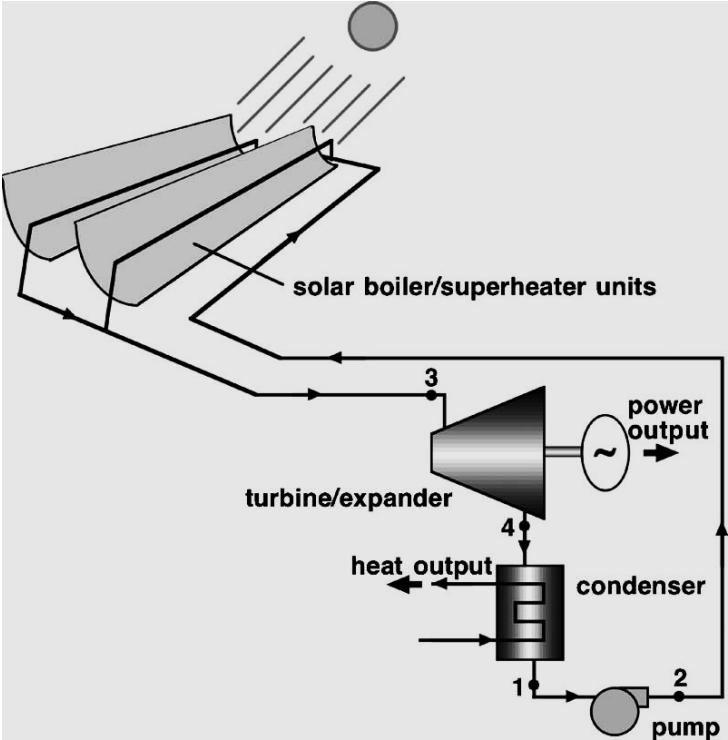


Figure 1-6: Combined heat and power systems. A solar collector serves as the energy source. Here Tesla principle can be used in the expander turbine and the pump. V.P.Carey, "Assessment of Tesla Turbine Performance for small scale Rankine Combined Heat and Power Systems" [11].

## 1.4 Previous Work

Naturally, the performance of Tesla turbines has already been characterized by a number of researchers. Rice's analysis [13] was among the first, and claims that turbines can be made up to 90% efficient. Designs by Ho-Yan [1] and Lawn [2] claim over 70% efficiency. Deam et al. [14] argued that at small scales (sub-cm diameters) viscous turbines outperform conventional bladed turbines and can provide ~40% efficiency. Hoya, Guha, and Smiley ([3], [15]) analyzed medium to large Tesla turbines with computational models, experimentation, and analysis, claiming 25% efficiencies but demonstrating nozzle designs that could improve this. Though derived for meso-scale and macro-scale turbines, this prior research provides an excellent basis for verification of micro turbine designs.

A large body of literature does exist on micro-scale *inertial* turbines and similar power-generating microelectromechanical systems (MEMS); Epstein, Herrault, Jan Peirs, and Camacho reported systems that operate between 100 k and 1 M rpm at power densities a full order higher compared with larger versions of the same ([16], [17], [18], [9]).

There have been many attempts to employ various motive mediums in Tesla turbines. Designs with power densities ranging from 5 mW/cm<sup>3</sup> to 30 W/cm<sup>3</sup> have been offered by various researchers, including the author ([19], [4], [5], [1]). In general, the reasons behind such a wide variation in power density are not well explained, and the efficiency discrepancy between theory and practice has not been adequately quantified. One of the goals of this study is to reconcile these discrepancies so that a unified design approach can be specified. Table 1-1 lists a set of published turbines.

As turbine structures become smaller, frictional forces increase and new methods to accurately estimate friction are necessary. Kandlikar et al. [20] modified the traditional Moody diagram to account for surfaces with a relative roughness higher than 0.05, arguing that above this value flow constriction becomes important. Croce, Agaro, and Nonino [21] used a computational approach to model conical roughness elements and their effect on flow through microchannel. Like Kandlikar, he also reported a shift in the friction factor due to surface roughness, and compared the results of his computational analysis to the equations proposed by several other researchers for the constricted hydraulic diameter of two different roughness periodicities. Gamrat [22] provides a detailed summary of previous studies reporting that Poiseuille number increases with surface roughness. The primary motivation for almost all of this previous research has been to analyze frictional loss; however, this substantial body of work also raises the possibility of performance enhancement for the Tesla rotor, which is moved by shear force.

Table 1-1: Power/cc for reported Tesla Turbines. (Rotor volume is used in this calculation)

| Reports (Gas)             | Radius<br>r (mm) | Spacing<br>b (μm) | Power<br>Watt | Volume<br>Liter | Power density<br>W / cm <sup>3</sup> |
|---------------------------|------------------|-------------------|---------------|-----------------|--------------------------------------|
| Luther cox-air [5]        | 50               | 1588              | 35            | 0.24            | 0.141                                |
| Leaman-air [5]            | 64               | 2007              | 83            | 0.20            | 0.406                                |
| Bean-air [5]              | 76               | 508               | 1800          | 0.46            | 3.885                                |
| Hoya-air [3]              | 46               | 200               | 140           | 0.01            | 13.163                               |
| Tesla-steam [5]           | 102              | 3175              | 22500         | 1.65            | 13.658                               |
| Tesla-air [5]             | 76               | 2381              | 22500         | 0.69            | 32.374                               |
|                           |                  |                   |               |                 |                                      |
| Reports (Fluid)           |                  |                   |               |                 |                                      |
| Ho-Yan-water [1]          | 250              | 5000              | 300           | 58.90           | 0.005                                |
| Lawn-Glycerine [23]       | 584              | 2489              | 27825         | 1083.57         | 0.026                                |
| Krishnan-water [19]       | 5                | 125               | 0.025         | 0.0004          | 0.115                                |
| Lawn-liquid hydrogen [23] | 584              | 104               | 29565         | 223.76          | 0.132                                |
| Lawn-Glycerine [23]       | 584              | 1760              | 210750        | 1030.46         | 0.205                                |
| Lawn-liquid sodium [23]   | 584              | 163               | 134093        | 374.04          | 0.358                                |
| Lawn-water [2]            | 152              | 211               | 9000          | 14.71           | 0.612                                |
| Lawn –Glycerine [23]      | 25               | 368               | 240           | 0.05            | 4.728                                |

## 1.5 Research Overview

The present work is grouped into four major topics. The first three cover turbine performance characterization, design constraints and scaling properties, while the fourth provides a consolidated approach to practical design and reconciles some of the open questions about discrepancies among the published turbines.

### 1.5.1 *Investigation of Micro-scale Tesla Turbine Fabrication and Performance*

An initial design for a 1 cm micro turbine was derived from design graphs for macro-scale turbines presented by Lawn [2]. Turbines were fabricated and performance was investigated by varying the nozzles and rotors [19].

### 1.5.2 *Analysis of the Dependence of Rotor Performance on Flow Profile*

The present research is the first to derive Tesla turbine performance for incompressible flow at rotor flow profiles ranging from parabolic to uniform. This work quantifies how a uniform flow profile increases power transfer and efficiency over parabolic flow. This is particularly useful where the fluid leaves the rotor without transferring its momentum, such as when the fluid path is short inside the rotor (as with micro rotors), and when inter-disk space is very large to accommodate occasional big particles (as in river turbines).

The rotor flow model is based on the integral perturbation model posed by Romanin [24] for rotor momentum and pressure drop. The ideal rotor momentum transfer and the pressure drop are first derived by modifying the analysis to allow for incompressible flow. The rotor equations are also verified using MATLAB simulation of the 30 cm rotor as reported by Lawn [2]. The resulting rotor momentum equation was verified using ANSYS simulation of 1 cm rotor disks and reported by Romanin and Krishnan [25].

### 1.5.3 *Turbine Loss Analysis*

Actual turbine performance is calculated by adding losses incurred across the turbine. Losses due to nozzle path friction and enclosure interface disk friction dominate performance loss in regions of low laminar flow, while volume loss, exit kinetic energy loss, exit path loss, and bearing loss increase in high-flow, high rotor speed regions. There is also impact loss in slot nozzles at the nozzle-rotor interface. These losses are a function of the turbine hardware and operating parameters, and performance drops as the system scales down to the millimeter level. This leads to different optimum operating regions for macro and the micro turbines. The two major losses at the nozzle

[26] and disk interfaces with the enclosure [27] are modeled, and other losses are estimated based on previously published results [28].

#### *1.5.4 Mapping Experimental Results to Ideal Performance*

As a case study, loss analysis is applied to the 1 cm micro turbines, and theoretical and predicted results are compared with the experimental results. All losses in the turbine are categorized into one of two types: either a head loss as a cubic function in flow rate, or a torque loss as a linear function of momentum transfer. A novel mapping methodology for the losses is derived and used to map the experimental results to ANSYS-verified momentum prediction results and to theory based on ideal and lossy turbine results.

#### *1.5.5 Design Constraints Table*

The present work links various losses in the Tesla turbine to the design and operating parameters of the turbine, and recommends a set of design constraints to jointly optimize both power and efficiency. It also investigates the scaling effect – the varying effect of main turbine parameters (rotor radius, interdisk space, rotor thickness, number of disks, tip clearance, rotor-enclosure gap, nozzle width, nozzle height, nozzle angle, and the ratio of exhaust to entry radius) on performance as the turbine scales down.

#### *1.5.6 Scalable Design Method and Examples*

The behavior of a Tesla turbine is very sensitive to the rotor and nozzle dimensions [29]. Stable, and reliable performance demands high accuracy and precision in fabrication, which becomes increasingly difficult as the turbine scales down. With this in mind, different scaling techniques are investigated, and recommendations made for the micro turbine design. In particular, a new design methodology is disclosed for a wide range of turbines (1 mm to 500 mm rotors) with the goal of maintaining a constant power density while keeping mechanical efficiency above 35% for the entire range.

A three-level optimization method is derived to scale a 9 kW, 300 mm reference turbine [2] with 80% efficiency and  $0.5 \text{ W/cm}^3$  power density to turbines ranging from 1 mm to 400 mm in diameter. A constant power density is maintained using a power scaling relationship between rotor radius and interdisk spacing. No minimum requirement is imposed on the interdisk space in this analysis. In the first two levels, with the aid of the design constraint table, the operating parametric regions of the turbines are modified across the full range to satisfy the power density and efficiency requirements. In the final level, power density is fine-tuned through small linear scaling adjustments to the interdisk space – a 7% decrease in spacing doubles the power. Based on this design methodology, four turbines with 2 mm, 4 mm, 58 mm, and 236 mm diameter are

designed for 1.5 W/cm<sup>3</sup> power density with 48%, 46%, 65%, and 70% projected efficiency respectively (Table 5-2).

### *1.5.7 Practical Turbine Design Specification*

The turbine design specification is derived from the input head, flow rate, and particulate-size specification, with particulate size determining the lower limit for interdisk space. This dissertation offers a two-level optimization program according to these factors. At the first level, operating parameters are varied at a given radius to select four configurations, corresponding to maximum power, maximum power density, closest to head, and good aspect ratio between 0.5 and 5. At the second level, the four best configurations across 2 mm to 500 mm diameter turbines are selected, one from each of the four sets of configurations. The process sorts and limits the number of turbines based on efficiency and power density, and recommends a turbine design specification in each configuration set.

### *1.5.8 Reconciling Performance Discrepancies in the Literature*

This design tool is used to derive turbine specifications over the application range, with variations in head, flow, and particulate size producing over 300 different turbines. The efficiency, power, power density, and RPM of the designed turbines are then studied using 3D visualization tools. The published turbines are then mapped onto this graph and analyzed to account for performance discrepancies in the published literature.

### *1.5.9 Design Sensitivity Analysis*

In a practical system, input conditions such as head and flow as well as output load and RPM can vary; as such, stability of performance is an important criterion in selecting the optimum turbine. The selected turbine's performance is studied for +/- 20% variation in input head and input flow, and up to 60% variation in power density is observed with only 9% variation in efficiency.

### *1.5.10 User Design Interface*

A graphical user interface is provided that offers multiple turbine designs for a given user input of head, flow, particulate size, and medium. The sensitivity graphs are also available at this user interface for the designed turbines. A set of example turbine designs for micro to large applications is also included.

## 1.6 Organization

Chapter 2: Fabrication of 1 cm turbine, experimental methodology and observations.

Chapter 3: Theoretical and computational study of rotor performance at different fluid profiles and ideal turbine performance. Verification of analytical rotor flow using ANSYS simulation, and correlation between theory, simulation, and experiment. Verification of performance trends in Tesla turbine.

Chapter 4: Turbine loss models and turbine performance over a wide power range, with emphasis on the following topics: 1) performance with nozzle losses, 2) performance with disk friction losses, 3) the effect of other losses, and 4) system performance with all losses. Methodology for mapping the experimental results to an ideal turbine.

Chapter 5: Design and scaling-down considerations from 2 mW to 20 kW turbines. Design specification and sensitivity analysis for a given user input specification through the graphical user interface. Practical examples of low-head high-flow river turbines, high-head low-flow mobile applications, low-head low-flow power scavengers, and high-head high-flow hydraulic power turbines.

Chapter 6: Conclusions from this research and discussion of potential future study.

Appendix A: GUI design Tool and MATLAB code.

# Chapter 2

## 2 Fabrication of a 1-cm Tesla Turbine, and Experimental Findings

---

### 2.1 Fabrication

This chapter details the fabrication of a cm-scale Tesla turbine. The performance of this turbine is then investigated using different nozzles and rotors, and the impact of effective transfer area, interdisk spacing, nozzle position, type, and size is observed. Initial test results were reported by Krishnan et al. [19]. Additional test results are included here and the turbine's general performance trends are identified.

#### 2.1.1 Rotor Fabrication

Disks of 1 cm and 2 cm diameter, with three different hole patterns for center exhaust and with spacers for the rotors, were fabricated from 125  $\mu\text{m}$  thick, 300-series full hard stainless steel sheets using commercial photo-etching technology (Figure 2-1, Microphoto, Inc., Roseville, MI). Rotors were assembled manually, and square axles with rounded ends were used to enable automatic alignment of the disks.

Five rotors (R1-R5) were fabricated to fit into the same turbine enclosure. Rotors R1, R2, R5 use different exhaust patterns disks. Rotors (R1, R2, and R5), R3, and R4 were assembled with interdisk spacing of 125  $\mu\text{m}$ , 250  $\mu\text{m}$ , and 500  $\mu\text{m}$ , with 20, 13, and 8 disks (respectively). Rotor stack height was 5.375 mm in all cases (Table 2-1).

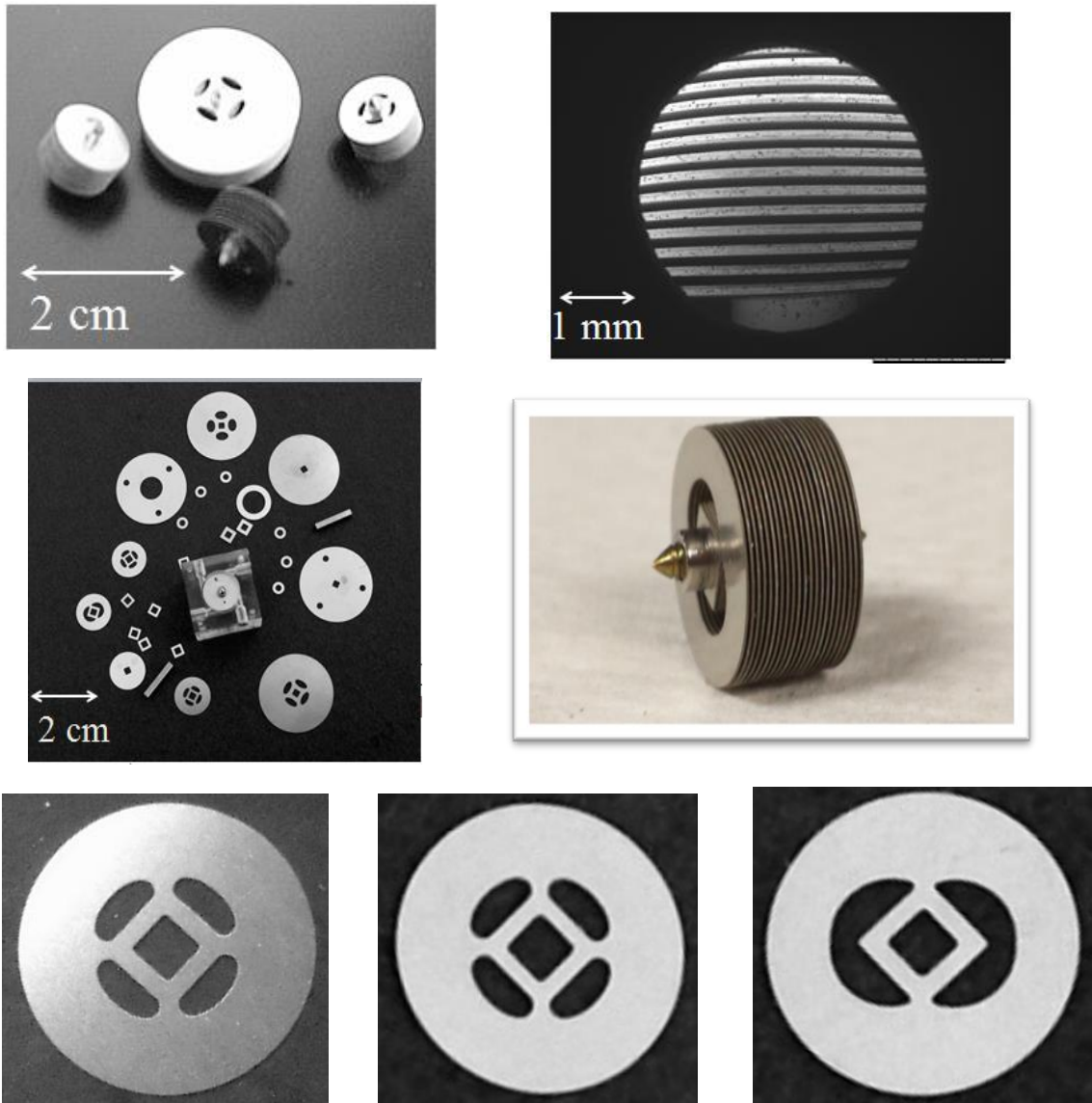


Figure 2-1: (Top left) Three 1 cm rotors and one 2 cm rotor, fully assembled. (Top right) White light microscopy (20x) showing R1 with 125  $\mu\text{m}$  spacing and post-assembly gap uniformity in the rotor stack. (Middle left) Photo-etched stainless steel disks with different exhaust patterns, end disks, spacers, and bronze square axles, and (at center) a 4  $\text{cm}^3$  turbine with four symmetric nozzles. (Middle right) R5 close-up (20 disks, 125  $\mu\text{m}$  spaced, pattern 3). (Bottom row) Three exhaust patterns with 0.47, 0.51, and 0.6 effective exhaust-to-entry radius ratio (Table 2-1).

Table 2-1: Rotors, 1cm diameter and 2 cm diameter

| ID | Diameter (cm) | Disks | Gap ( $\mu\text{m}$ ) | $r_i / r_o$<br>inner/outer radius ratio | exhaust/entry<br>area ratio |
|----|---------------|-------|-----------------------|---|-----------------------------|
| R1 | 1             | 20    | 125                   | 0.47 ( pattern 1)                       | 0.105                       |
| R2 | 1             | 20    | 125                   | 0.51 (pattern 2)                        | 0.143                       |
| R3 | 1             | 13    | 250                   | 0.47 (pattern 1)                        | 0.105                       |
| R4 | 1             | 8     | 500                   | 0.47 ( pattern 1)                       | 0.105                       |
| R5 | 1             | 20    | 125                   | 0.6 (pattern 3)                         | 0.2                         |
| R6 | 2             | 20    | 125                   | 0.32 (pattern 4)                        | 0.105                       |

### 2.1.2 Nozzle Fabrication and Turbine Enclosure

Nozzle design plays a critical role in turbine performance ([15], [30]). To explore the nozzle parameter space, 3D plastic rapid prototyping (ProtoTherm 12120 polymer, 50  $\mu\text{m}$  layer thickness, high-resolution stereo lithography-3, FineLine Prototyping, Inc., Raleigh, NC) enables turbine enclosure and nozzle designs that would otherwise be un-machinable. Eight nozzles (N1-N8) were designed using three different shapes, three different exit areas, and four different angles of entry. Nozzles 1-4, 6, and 8 are circular at the nozzle entry (upstream) and slit or oblong at the nozzle exit (downstream, feeding into the rotor). Nozzle 5 is also circular at the nozzle entry but then splits into five small nozzles. Nozzle 7 is similar to Nozzle 1 but has a funnel shape, first decreasing in width and then increasing slightly to cover a wider exit arc. COMSOL models of the nozzles are shown in Figure 2-2, with these details and the arc-wise span of the nozzle exits tabulated in Table 2-2. Spring-loaded Ruby Vee bearings (1.25 mm OD, Bird Precision, Waltham, MA), which perform well at < 10000 RPM, connect the rotor shaft to the housing. Adjusting the bearings' position with a spring screw, the rotors were then located with respect to the nozzles. An exploded CAD enclosure view and exhaust view are shown in Figure 2-3. Two turbine enclosures were made: 1) a cubic turbine with four nozzles equally spaced around the rotor (Figure 2-4, left, center); 2) an octagonal cross section turbine with the eight nozzles (Figure 2-4, right)

Table 2-2: Nozzle Specifications

| ID | Type  | Area<br>mm <sup>2</sup> | Length<br>mm | Width<br>mm | Width<br>arc ° | Angle        |    |
|----|---|-------------------------|--------------|-------------|----------------|--------------|----|
|    |   |                         |              |             |                | to tangent ° |    |
| N1 | Slit  | 3.28                    | 3.5          | 1           | 19.3           | 37.3         | 15 |
| N2 | Slit  | 3.28                    | 3.5          | 1           | 15.9           | 45.8         | 25 |
| N3 | Slit  | 2.28                    | 2.5          | 1           | 37.3           | 26.5         | 0  |
| N4 | Slit  | 3.28                    | 3.5          | 1           | 37.3           | 26.5         | 0  |
| N5 | 5Array  | 0.69                    | 0.4          | 0.4         | 7.5            | 37.3         | 15 |
| N6 | Slit  | 3.28                    | 3.5          | 1           | 14             | 53.2         | 35 |
| N7 | Slit  | 7.14                    | 4.0          | 2           | 53.2           | 37.3         | 15 |
| N8 | Same as N4 in dimensions, located 180 degrees around the rotor. |                         |              |             |                |              |    |

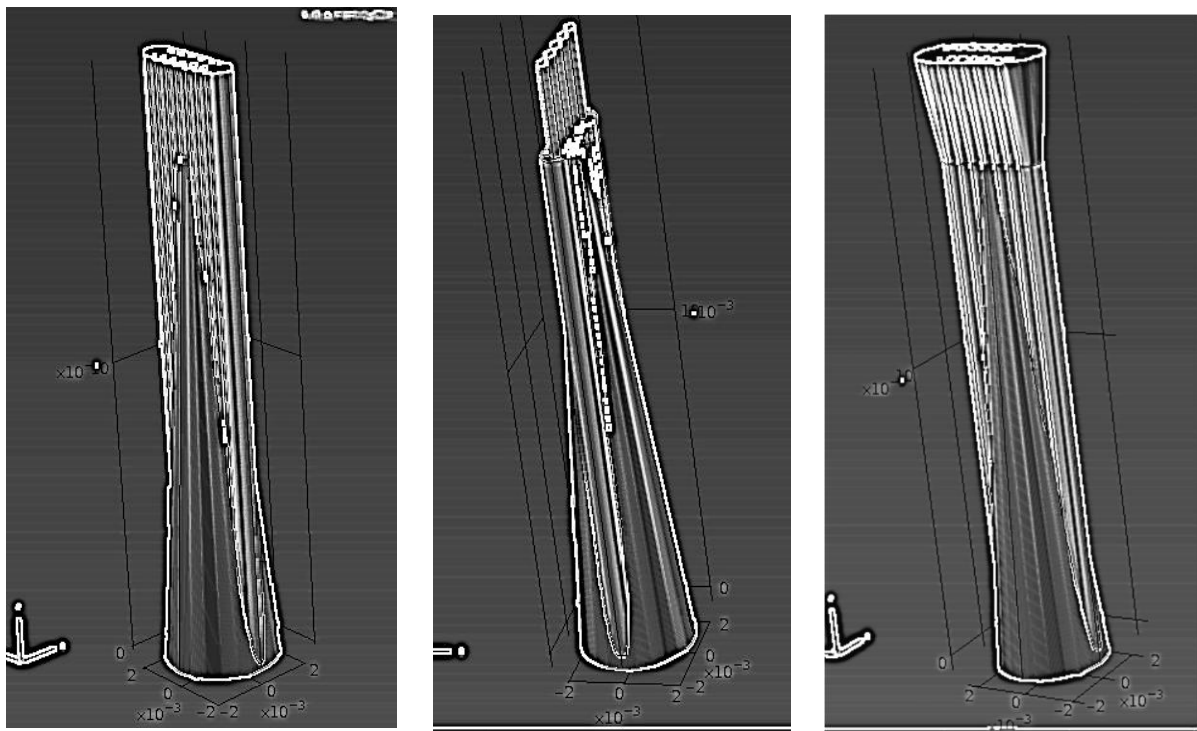


Figure 2-2: Nozzle architecture. The bottom entry face of all nozzles is circular, with a 4.04 mm diameter. The top exit face of the rotors (Left) for nozzles 1, 2, 3, 4, 6, and 8 is slit with a converging body, (Center) for nozzle 5 features five circular exits of 0.4 mm diameter with a converging body, and (Right) for nozzle 7 features a wider arc slit with a funnel-shaped body.

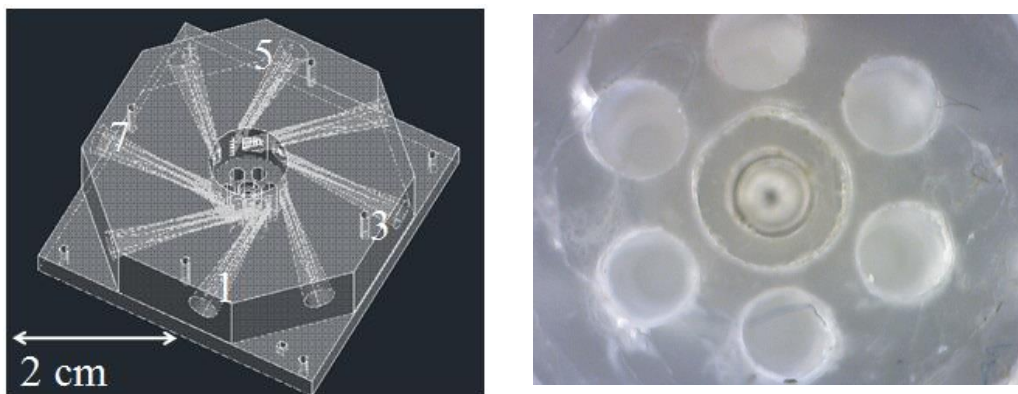


Figure 2-3: (Left) An exploded CAD view of the enclosure, with the eight nozzles. The center rotor housing diameter is 1.013 cm, and nozzle-entry diameter is 4.04 mm. All except nozzle 5 are slits scanning many rotors; nozzle 5 has five circular exits. (Right) Six turbine exhaust holes are at the bottom of the enclosure, and in the center is the bearing assembly.

## 2.2 Turbine Experimental Setup and Operation

Two experimental setups were used. Figure 2-5 (left) shows a low-head gravity feed system with maximum head of 1 m and maximum flow rate of 3 cm<sup>3</sup>/s which was used for testing a mini 4 cm<sup>3</sup> turbine. Figure 2-5 (right) shows a gear pump system capable of driving flow to a maximum of 20 cm<sup>3</sup>/s flow rate at 10 m (1 bar) head, which was used to test an eight-nozzle small turbine of 17 cm<sup>3</sup> size. The gravity setup employed a small tank mounted at different heights above the turbine, while the pump setup used a gear pump (EW-74014-40, Cole-Parmer) to induce flow. Both test systems otherwise employed the same methodology.



Figure 2-4: Test turbines. (Left and middle) Top and bottom view of the 1 cm rotor in a 1.6 cm cubic turbine with four tangential nozzles at 90 degree spacing. (Right) A 4 cm octagonal turbine with eight nozzles, used for testing the four rotors at eight nozzle configurations.

A differential pressure gauge (DPG8000-100, Omega Engineering) was installed at the nozzle inlet, and the flow rate measured at the exhaust. During operation, the rotation

of the turbine was recorded using a high-speed video camera (FASTCAM-X 1024PCI, Photron). Thermocouples at the top and bottom of the enclosure (5SC-TT-K-40-36, Omega Engineering) monitored turbine temperature (Figure 2-5)

Eight systems with various nozzles and rotors were tested, and measurements of pressure  $p_{\text{expt}}$  versus flow rate  $q_{\text{expt}}$  recorded for each. The rotational Reynolds number  $N_{\text{RE}} = \omega b^2 / \nu$  was also monitored to ensure that it remained in the desired region of  $< 15$  for the 20-disk stacks at flow rates from  $1 \text{ cm}^3/\text{s}$  to  $20 \text{ cm}^3/\text{s}$ , where  $\nu$  is fluid kinematic viscosity and  $\omega$  is rotor angular velocity.

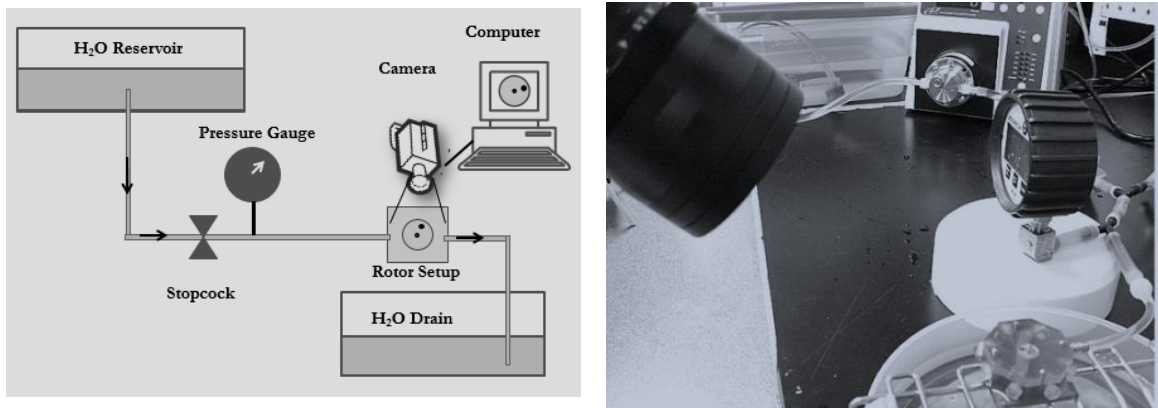


Figure 2-5: (Left) The water head drives the rotor. (Right) The gear pump draws water from a tank and drives the rotor. In all tests, nozzle inlet pressure is measured using a gauge, and rotor movement is recorded using a high-speed camera. The flow rate is controlled by the pump, which is driven for 25 seconds for each test. The camera records the rotor from rest to full speed to rest, capturing the acceleration and deceleration phases.

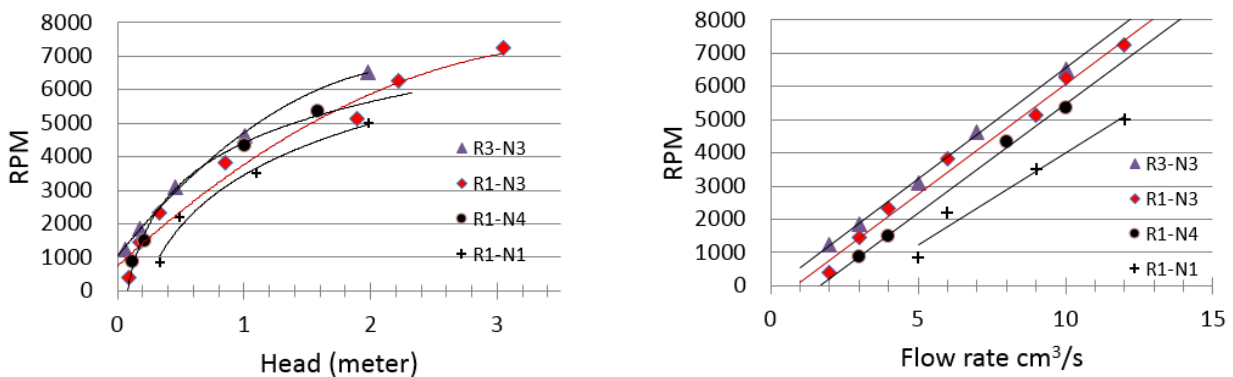


Figure 2-6: Free running RPM for four test systems. (Left): RPM dependence on head in meter. (Right) RPM dependence on flow rate in  $\text{cm}^3/\text{s}$ .

Experimental data was verified against the design before analysis. This assured the accuracy of data collection. Free running rotor speed is one of the verification criteria. Relationship between the RPM of the free running rotor with respect to head and flow are shown for four test systems in Figure 2-6. RPM is proportional to the flow rate and has major dependence on the nozzle angle and nozzle area and minor dependence on the interdisk space of the rotors.

- Higher the nozzle angle from the tangent (R1-N1 vs. R1-N4) lower the RPM for the same nozzle. As nozzle angle deviate from tangent, the radial velocity increases and the fluid exits the rotor faster transferring less energy.
- Lower the nozzle area (R1-N3 vs. R1-N4), higher the RPM for a given flow rate. This is because of the higher fluid kinetic energy (out of the lower area nozzle) entering the rotor.
- Higher the interdisk spacing (R3-N3 vs. R1-N3), higher the RPM, due to the lower mass of R3 compared to R1.

The nonlinear behavior of RPM to head is due to the square root relationship of flowrate to head for a given nozzle.

### 2.2.1 Data Collection and Analysis

In this experiment, shaft torque, power, and hydraulic-to-mechanical efficiency were derived through data analysis. Data collection began with the turbine at rest, and flow was then initiated. After rotor speed had been stable for about 20 seconds, flow was halted; data collection continued until the turbine returned to rest. Angular acceleration and deceleration were computed from video data by performing polynomial curve fit on the frequency versus time data and extracting the slopes of the fitted curve at multiple frequencies (Figure 2-7). At any RPM, the acceleration of the turbine multiplied by the polar moment of inertia,  $J$ , of the rotor represents the torque exerted by the fluid on the rotor minus the torque loss caused by the resistive forces of the rotor mechanism. The deceleration of the rotor multiplied by  $J$  gives the torque lost to bearing friction in the rotor hardware. Assuming that this loss is recoverable with better bearing hardware, the sum of the magnitudes of torques ( $\tau$ ) was applied to calculate the unloaded torque (although the actual unloaded torque is higher when all recoverable losses are accounted for and added to the above). The total work was derived by multiplying torque  $\tau$  with the angular velocity  $\omega$  of the rotor, and the lower limit of experimental mechanical efficiency derived from this (Eq. 2-1). A similar method was applied by Hoya to calculate the unloaded torque and work done [3].

$$\eta_{\text{expt}} = J (\text{acceleration} + |\text{deceleration}|) \omega / (q_{\text{expt}} p_{\text{expt}}) \quad 2-1$$

The transition areas used for the primary up and down torque calculations are less than 0.5 seconds in length (). To achieve an accurate prediction, 27 pairs of curve fits were used between the two transitional regions, and the optimum performing curve based on goodness of fit, power output, and RPM range was chosen (Figure 2-9).

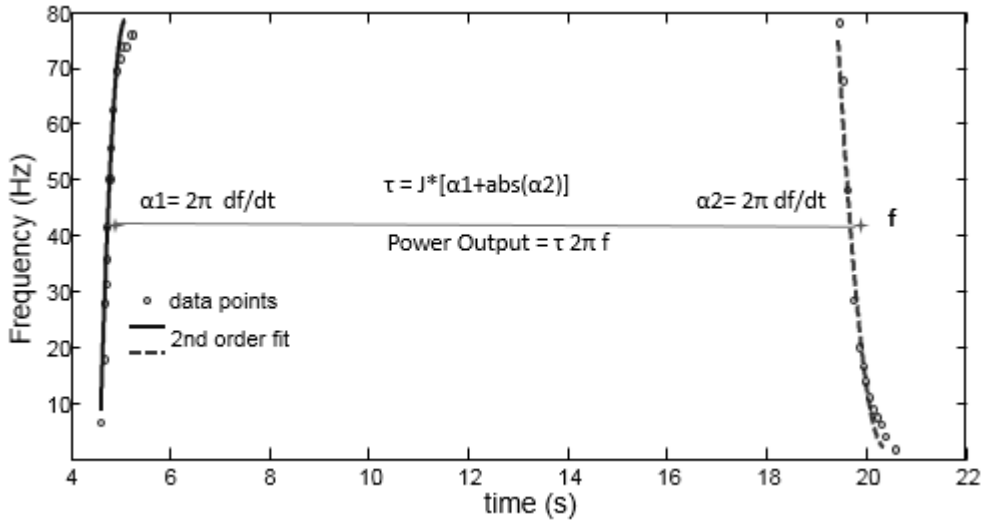


Figure 2-7: Rotor revolutions/sec (frequency) derived from raw video data (o), and second-order polynomial curve fits for acceleration (solid) and deceleration (dashed). Scaled slopes correspond to angular acceleration  $\alpha_1$  and angular deceleration  $\alpha_2$ . Torque ( $\tau$ ) and power output is then calculated from  $\alpha_1$  and  $\alpha_2$ .

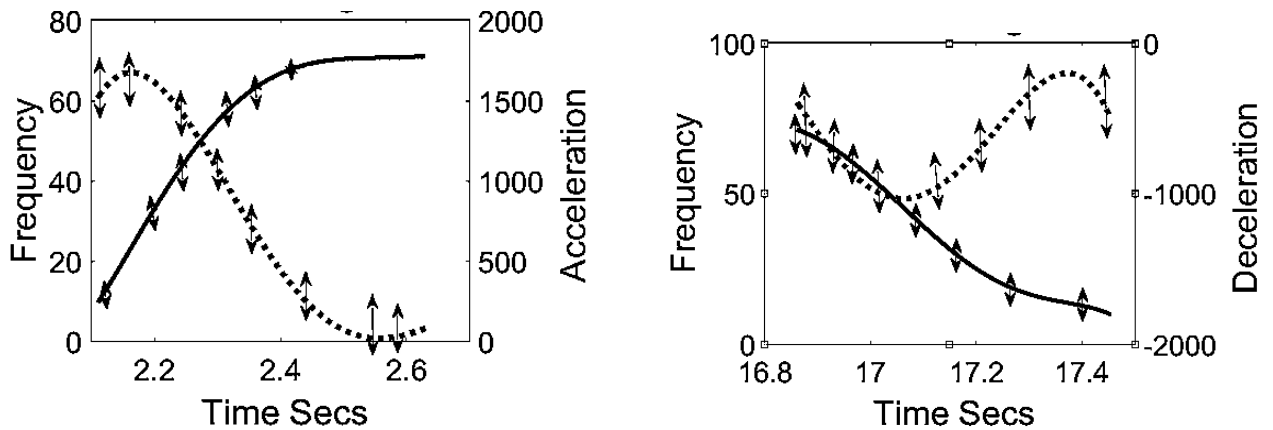


Figure 2-8: Rotor movement details – Average fitted curve with data variations given by the double arrow lines. (Left) Rotor frequency (solid) and acceleration (dotted) at start of flow. (Right) Rotor frequency (solid) and deceleration (dotted) after flow is stopped

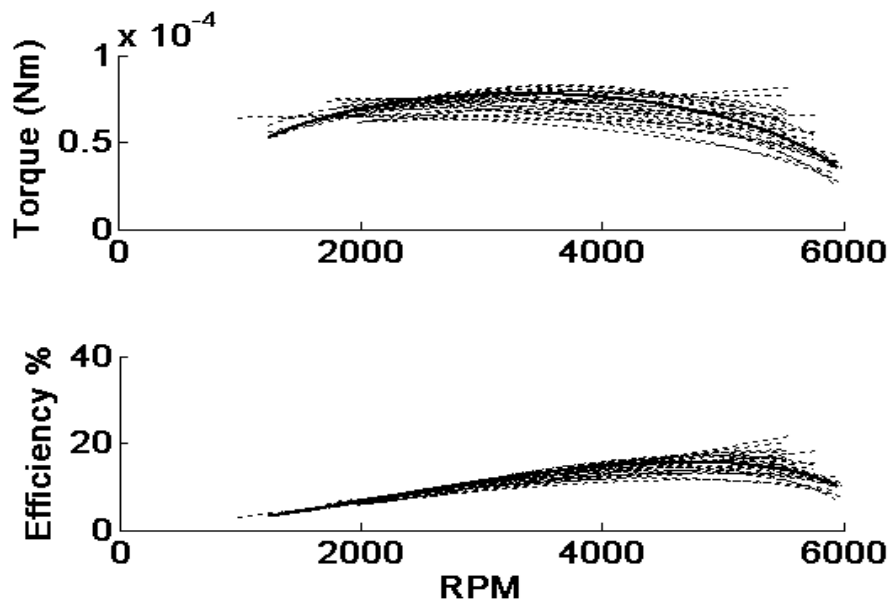


Figure 2-9: Curve fit data. Curve fit results for rotor 1, nozzle 3 (R1-N3) at 10 cm<sup>3</sup>/s flow rate. (Top) Indicates torque spread and (Bottom) indicates efficiency spread. The mean is plotted in solid line.

### 2.2.2 Torque, Power, and Efficiency

When the rotor is either free-running or at rest, torque transfer and work done is zero. Somewhere in the middle, maximum power transfer occurs [4]. Though our experimental calculations do not account for all recoverable losses in the system, they nonetheless demonstrate that maximum power occurs between resting and free running. Table 2-3 offers a summary of these test results.

The acceleration, deceleration, and total torque curves for nozzle 3 and rotor 3 at 10 cm<sup>3</sup>/s flow rate are shown at different rotor RPMs in Figure 2-10. The graphs for torque, power, and efficiency are also plotted across rotor speed for four different flow rates from 2 cm<sup>3</sup>/s to 10 cm<sup>3</sup>/s.

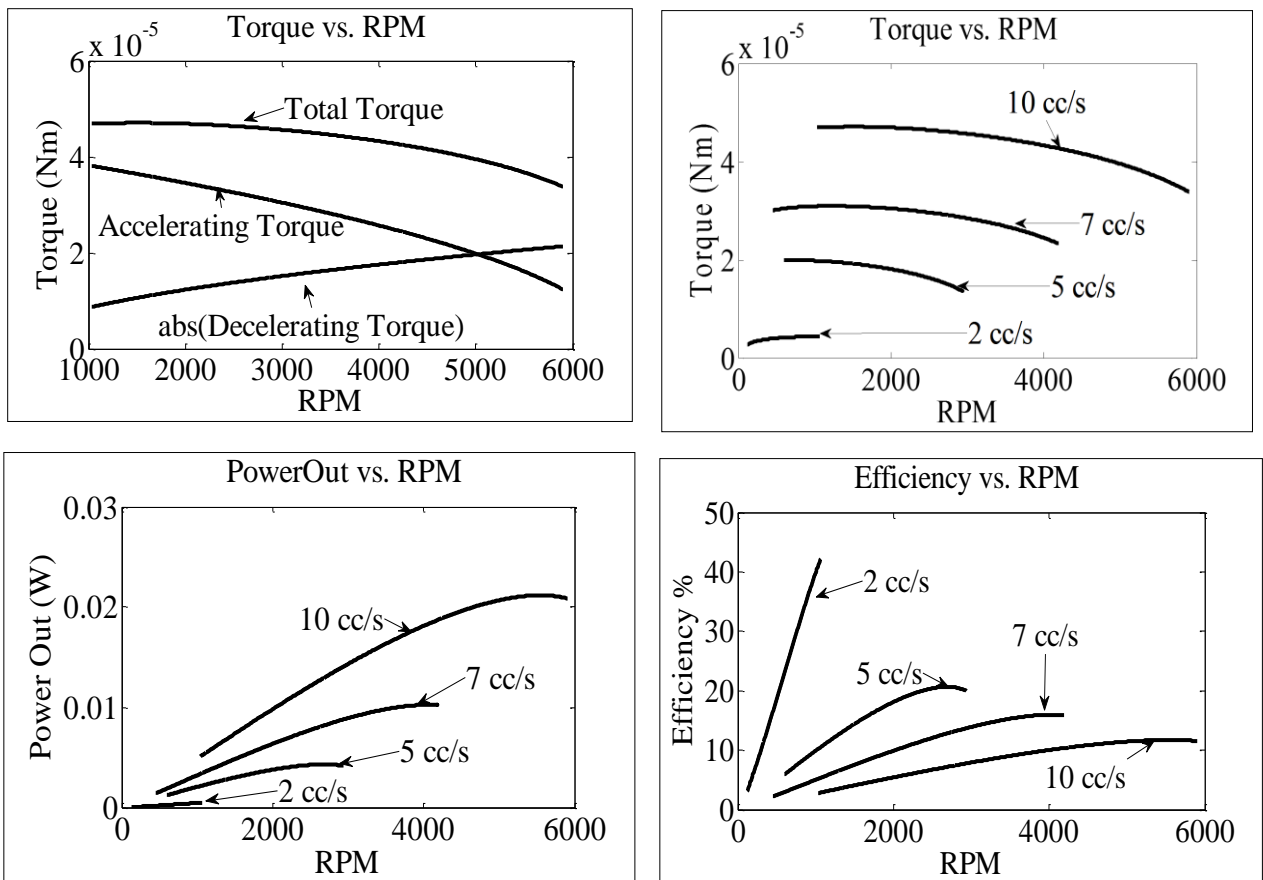


Figure 2-10: R3-N3 performance vs. RPM at flow rates of 2 cm<sup>3</sup>/sec to 10 cm<sup>3</sup>/s. (Top Left) Accelerating, decelerating, and total torque at 10 cm<sup>3</sup>/s flow rate. Performance curves for flow rates from 2 cm<sup>3</sup>/s to 10 cm<sup>3</sup>/s : (Top Right) Total torque. (Bottom Left) Power output. (Bottom Right) Efficiency .

### 2.2.3 Observations

In our tests, efficiency variation from 7% to 36% is observed (Figure 2-11, Table 2-3). As flow rate is reduced, efficiency increases. For example, in R3-N3 tests at 10 cc/s flow (R3-N3-10) efficiency is 9.3%, and at 2 cc/s flow (R3-N3-2) efficiency is 36%. This is typical of Tesla turbines, and is discussed in detail in later chapters.

The percentage of power gain from flow rate increase is one or two orders higher than percentage efficiency loss. This is evident when comparing power and efficiency at low and high flow rates for any system (R2-N3-2 vs. R2-N3-10).

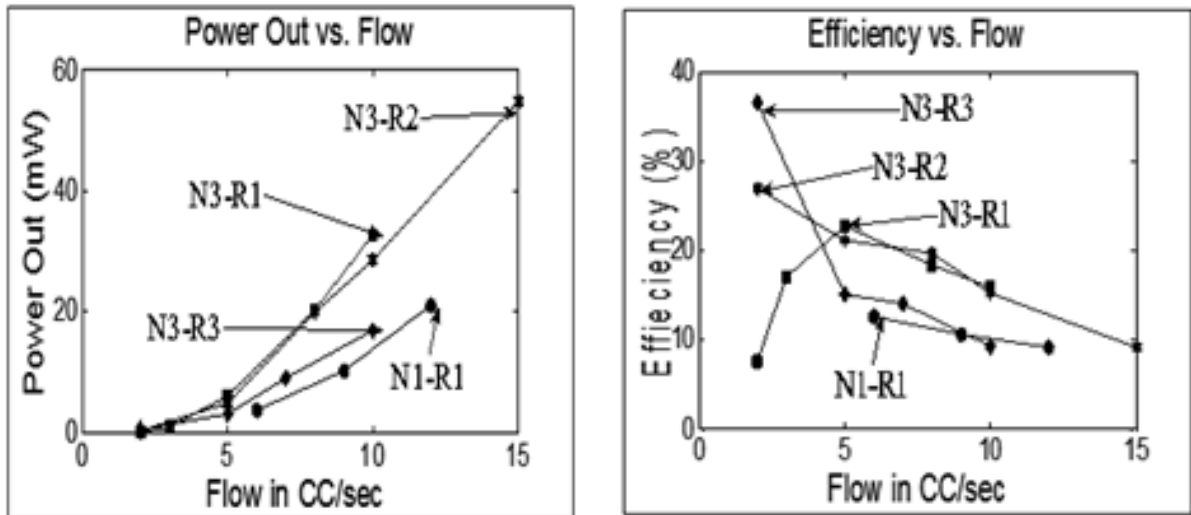


Figure 2-11: Rotor performance comparison. (Left) Rotor 1 and rotor 2 have higher power output than rotor 3. (Right) Nozzle 3 outperforms nozzle 1. The slower the flow, the higher the efficiency in all systems.

Power transfer and efficiency increased as nozzle area decreased, but only up to a certain point. Peak efficiency is observed with nozzles 3 and 4. Nozzle 7's greater exit area (9% of the rotor inlet area) and nozzle 5's lower exit area (0.8%) resulted in approximately 50% lower efficiency than the peak efficiency of nozzle 4 (4%).

Increasing interdisk space (R1 to R3) or increasing inner to outer radius ratio (R1 to R2) moved the efficiency peak to lower flow rates (with respect to R1). The higher aspect ratio of R3 and lower active area of R2 both require slower flow to ensure momentum transfer efficiency similar to R1 (Figure 2-11).

Nozzle 4 (with entry angle tangential to the rotor stack and an exit area of 4% of the rotor inlet area) with rotor 1 delivered the optimum power of 45 mW, with 17% efficiency at 12 cm<sup>3</sup>/s flow rate (R1-N4-12).

In limited tests, two nozzles placed 180 degrees from each other (using nozzles 4 and 8, R1-N4&8-14) resulted in lower performance compared with only nozzle 4 (R1-N4-12) at a similar mass flow rate. This is consistent with the initial observation that efficiency decreases as flow rate increases.

The fabricated rotor does not rotate below 1.5cm<sup>3</sup>/sec flow rate, demonstrating the opposing effects of centrifugal force and frictional forces.

Table 2-3: Test system performance: R1-N4-12 best power and efficiency, and R3-N3-2 best efficiency.

| Test ID<br>R#-N#- flow(cm <sup>3</sup> /s) | P<br>(bar) | RPM  | NRE | Power<br>(mW) | eta<br>(%)  |
|--|------------|------|-----|---------------|-------------|
| R2-N3-2                                    | 0.006      | 689  | 1.1 | 0.32          | 27.0        |
| <b>R3-N3-2</b>                             | 0.005      | 1243 | 8.1 | <b>0.4</b>    | <b>36.6</b> |
| R1-N3-5                                    | 0.06       | 3488 | 5.7 | 6.6           | 22.0        |
| R1-N1-6                                    | 0.05       | 2190 | 3.6 | 3.6           | 12.5        |
| R1-N5-6                                    | 0.29       | 4652 | 7.6 | 13.0          | 8.1         |
| R1-N4-8                                    | 0.098      | 4317 | 5.1 | 14.3          | 18.3        |
| R1-N3-8                                    | 0.15       | 5590 | 9.3 | 20.3          | 18.4        |
| R2-N3-8                                    | 0.13       | 5264 | 8.6 | 19.8          | 19.7        |
| R1-N1-9                                    | 0.11       | 3499 | 5.7 | 10.1          | 10.5        |
| R3-N3-10                                   | 0.19       | 6522 | 43  | 16.9          | 9.3         |
| <b>R1-N4-12</b>                            | 0.23       | 7247 | 12  | <b>45.0</b>   | <b>17.3</b> |
| R1-N4,8-14                                 | 0.19       | 6977 | 11  | 29.0          | 10.9        |
| R2-N3-15                                   | 0.43       | 9678 | 16  | 54.8          | 9.2         |
| R1-N7-12                                   | 0.17       | 5454 | 9.5 | 23.2          | 11.9        |

## 2.3 Experimental Uncertainty

The broad array of turbine parameters in this experiment allowed a relatively detailed exploration of performance trends. Turbine design and fabrication as well as test set-up were designed for rapid iteration and simplicity, with the goal of identifying problems in micro turbine design and deriving optimum design parameters. Fabrication, test procedure, and test data analysis contributed an uncertainty of 4%, 5%, and 10% (respectively), all of which are treated as independent random processes for estimating the overall uncertainty of 12%. Each of these are discussed below.

### 2.3.1 *Fabrication Uncertainty (4%)*

Fabrication uncertainty remained roughly consistent in the rotors and the nozzles. It affects comparisons between the predicted and the experimental results, as the predicted result is based on the design. The enclosure and the nozzles are fabricated using 3D prototyping with 50  $\mu\text{m}$  resolution, with nozzle dimensions in mm. For a fixed RPM and flow rate, a 1% dimensional uncertainty results in  $\sim 2\%$  velocity and 4% shaft power uncertainty. It also results in  $\sim 7\%$  nozzle drop uncertainty (nozzle drop is dependent on nozzle volume and square of velocity). The effect of this on turbine performance is about 4% in the tested flow range.

### 2.3.2 *Test Procedure Uncertainty (5%)*

Rotors were placed into the enclosure manually, with a position uncertainty on the order of 100  $\mu\text{m}$ . Rotors also demonstrated mild warping as tests progressed. Because a single enclosure was used for testing all rotors, a 5% uncertainty in shaft power is estimated.

### 2.3.3 *Test Data Uncertainty (10%)*

The moment of inertia of a rotor is calculated based on components in the rotor assembly and on approximations of rotor exhaust patterns; however, it is not verified through simulation. The frame rate of the recording and the markings on the rotor top disk dictate the accuracy in the estimation of acceleration and deceleration rates. Though the steady-state RPM is averaged over many revolutions and is accurate to 1%, because of the fewer points in the transitional areas the calculated peak-to-peak efficiency variation is about 30%, and the standard deviation about 10% (Figure 2-9). This constitutes the majority of overall experimental uncertainty.

### 2.3.4 *Conclusions*

We conclude, that it is possible to fabricate micro turbines using commercially available technology. Our test turbine efficiency is lower than 20% in the tested power density range of 10 mW/cm<sup>3</sup> to 50mW /cm<sup>3</sup>. In the next chapter, the rotor flow model is discussed and methods for improving the efficiency and the power density of the rotor are explored.

# Chapter 3

## 3 Analytical and Computational Turbine Models

---

Our turbine model is based on the integral perturbation method presented by Romanin [24]. The model derives rotor flow momentum and rotor pressure drop based on the flow profile, normalized flow, and normalized rotor dimensions and rotor Reynolds number. The performance characteristic of the ideal turbine is verified using published articles [2]. The flow momentum is also computed using an analytical model, and verified using ANSYS simulation.

### 3.1 Computational Rotor Model

Rotor characterization is generally based on continuity of mass, conservation of angular momentum, and conservation of energy. However, the rotor equations in this research incorporate two additional features: disk roughness (given as a function of flow profile), and the effect of large aspect ratio ( $b/r_o$ ) on rotor drop and flow velocity. Additionally, the following assumptions are made in order to simplify the equations:

- Flow is incompressible, steady, and laminar.
- Flow is two-dimensional (flow axial velocity = 0).
- The flow field is radially symmetric, such that all angular derivatives of the flow field are zero (including at the outer periphery of the rotor). Though this assumption is not true for a single-nozzle entry, our ANSYS flow simulations of the 1 cm rotor [25] showed that flow is symmetric within 10% of the entry.
- Entrance and exit effects are not considered here – only flow between adjacent rotating disks is modeled.
- The ratio of interdisk spacing to disk radius (aspect ratio)  $b/r_o$  is less than 1:20. Based on this assumption, higher-order aspect ratio terms are dropped from the rotor equation. This is acceptable because the rotors considered in this research all conform to this specification.

#### 3.1.1 Disk Roughness and Flow Profile

In this model, the fluid profile  $\phi(z)$  in the rotor interdisk space is given in terms of a profile number  $n$  ( Eq. 3-1), in which  $n=2$  corresponds to the parabolic profile of fluid flowing through smooth disks and  $n=8$  corresponds to the uniform profile that results from the flow between roughened disks (Figure 3-4).

Tangential shear force on the disks can be derived by assuming that the flow in the interdisk space is equivalent to laminar Poiseuille flow between parallel plates. It can also be derived from the gradient of the fluid profile and dynamic viscosity of the fluid. Using following steps, it can be shown that the profile number and the roughness factor are linearly related as  $8*(n+1) = F_{PO} * PO$ .

- 1) Expressing roughness as a scale of Poiseuille number PO, where PO=24 for smooth disks and scale=1-3,
- 2) Postulating that the tangential shear interaction of the flow with the disk surface is equivalent to that for laminar Poiseuille flow between parallel plates,
- 3) Deriving the tangential disk shear in terms of relative tangential velocity,
- 4) Expressing the relative tangential velocity of the fluid in terms of the profile, and
- 5) Equating the shear forces in (2) and (3), and solving.

$F_{PO}$  is the scale factor that varies from 1 to 3 to cover the flow profile range from parabolic ( $n=2 \Rightarrow F_{PO} =1$ ) and trapezoidal ( $n=5 \Rightarrow F_{PO} =2$ ) to uniform ( $n=8 \Rightarrow F_{PO} =3$ ). Kandlikar reported the feasibility of changing PO by a factor of 3.5 using micro structures [20]. However, enhancing friction using micro structuring is beyond the scope of this dissertation. Instead, the focus here is on how to use this feature to enhance the performance of the rotor, with findings presented using the profile number. The rotor analysis block diagram is shown in Figure 3-1.

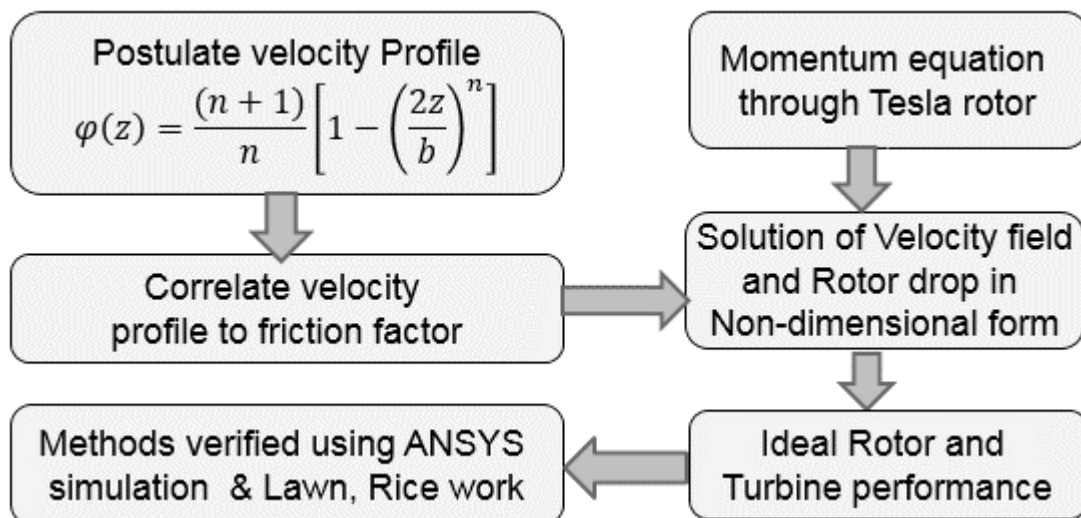


Figure 3-1: Rotor analysis block diagram

### 3.1.2 Rotor Equations

Fluid relative velocity profile in between the disks is defined as  $\phi(z)$  and is given in terms of a profile number as in Eq. 3-1. The axially averaged tangential velocity  $v_{tan}$  and axially averaged radial velocity  $v_{rad}$  of flow are calculated from the fluid tangential  $v_t$  and radial  $v_r$  velocities (Eq. 3-2). Fluid velocities are expressed in terms of the average velocities, the relative fluid profile and the rotor speed  $\omega r$  as shown in Eq. 3-3 .

$$\phi(z) = (n + 1)/n [1 - (2z/b)^n] \quad 3-1$$

$$v_{rad} = \frac{1}{b} \int_{-b/2}^{b/2} v_r dz, \quad v_{tan} = \frac{1}{b} \int_{-b/2}^{b/2} v_t dz \quad 3-2$$

$$v_r = v_{rad} \phi(z), \quad v_t = (v_{tan} - \omega r) \phi(z) + \omega r \quad 3-3$$

The analysis henceforth uses non-dimensional parameters, derived as follows: 1) size parameters are normalized by rotor radius  $r_o$ , 2) velocity parameters are normalized by rotor tip velocity  $v_{tip}$ , and 3) head and kinetic energy parameters are normalized by  $\rho v_{tip}^2$  where  $\rho$  is fluid density.

$$\xi_r = r/r_o, \quad v_{tip} = \omega r_o, \quad q_{disk} = 2 \pi r_o b v_{rad} \quad 3-4$$

$$Vt_r = v_{tan}/v_{tip}, \quad Vr_r = v_{rad}/v_{tip}, \quad W_r = Vt_r - \xi_r \quad 3-5$$

$$N_{RE} = b^2 \omega / \nu, \quad RE_{rot} = 2 b q_{disk} / \pi r_o^2 \nu = 4 Vr_o N_{RE} \quad 3-6$$

$$P_r = p_r / 2\rho v_{tip}^2 \quad 3-7$$

At any rotor normalized radius  $\xi_r$ , the rotor pressure gradient  $\delta P_r$  and the fluid tangential (normalized relative) velocity gradient  $\delta W_r$  are derived from five parameters: fluid profile  $n$ , normalized radius  $\xi_r$ , rotor Reynolds number  $RE_{rot}$ , radial velocity at rotor entry  $Vr_o$ , and relative tangential velocity  $W_r$ . The total rotor drop  $P_i$  and relative tangential exit velocity  $W_i$  are derived at the rotor exhaust by integrating iteratively on  $\xi_r = [1 \xi_i]$ . Figure 3-4 shows the effect of  $n$  on fluid profile, rotor pressure drop, normalized tangential velocity, and torque transfer along the rotor path.

$$\delta P_r = (4(n + 1)/(2n + 1))(Vr_o^2 + W_r^2 \xi_r^2) / \xi_r^3 + 4 W_r + 2 \xi_r + 32 (n + 1) Vr_o^2 / RE_{rot} \xi_r \quad 3-8$$

$$\delta W_r = -2n + 1/n + 1 - W_r / \xi_r + 8(2n + 1) \xi_r W_r / RE_{rot} \quad 3-9$$

$$\text{Initial conditions : } W_r = W_o ; P_o = 0 \text{ at } \xi_o = 1; \quad 3-10$$

$$\text{Integration range : active rotor ring : } 1 \geq \xi_r \geq \xi_i \quad 3-11$$

$$\text{Output : relative tangential velocity } W_i ; \text{ rotor drop } P_i \text{ at } \xi_i; \quad 3-12$$

### 3.1.3 Efficiency Estimate for the Ideal Rotor and Turbine

The mechanical efficiency of the rotor  $\eta_{rm}$  is derived from the utilized fluid momentum  $R_{\text{momentum}}$  (Eq. 3-13, 3-14). The ideal (simple analytical) turbine head  $P_{\text{ideal}}$  is calculated by adding the reversible kinetic energy  $KE_{\text{in}}$  at the rotor entry to the normalized head drop  $P_i$  in the rotor (Eq. 3-16), and the ideal turbine efficiency  $\eta_{\text{ideal}}$  is calculated using this turbine head. Estimated turbine efficiency  $\eta_{\text{pred}}$  is calculated using the experiment head  $P_{\text{expt}}$  in place of the ideal head as shown in Eqs. 3-18, and 3-19.

$$R_{\text{momentum}} = (W_o + 1) - (W_i + \xi_i)\xi_i \quad 3-13$$

$$\eta_{rm} = 1 - (W_i + \xi_i)\xi_i / (W_o + 1) \quad 3-14$$

$$KE_{\text{in}} = 0.5 (V_{t_o}^2 + V_{r_o}^2) \quad 3-15$$

$$P_{\text{ideal}} = 0.5 |P_i| + KE_{\text{in}} \quad 3-16$$

$$T_i = (2 \pi V_{r_o}) R_{\text{momentum}} \quad 3-17$$

$$\eta_{\text{ideal}} = (W_o + 1) - (W_i + \xi_i)\xi_i / P_{\text{ideal}} \quad 3-18$$

$$\eta_{\text{pred}} = (W_o + 1) - (W_i + \xi_i)\xi_i / P_{\text{expt}} \quad 3-19$$

### 3.1.4 Rotor Streamlines

The lower the flow rate is, the more slowly fluid travels through the rotor and the longer its path inside the rotor; however, the higher the RPM the greater the opposing centrifugal force and the longer the flow path. The flow path is computed in cycle lengths for different flow and speed conditions and plotted against the corresponding non-dimensional flow indicator  $V_{r_o}$  and the rotational Reynolds number  $N_{RE}$  (Eqs. 3-5, 3-6). All other parameters remain constant: normalized tangential entry velocity  $V_{t_o} = 1$ , fluid profile  $n = 2$ , and exhaust radius ratio  $\xi_i = 0.4$ . Three rotor operating points are selected and the corresponding cycle number and the streamlines inside the rotor are shown in Figure 3-2.

Momentum transfer can be maximized by operating at lower flow rates and higher RPM. However, another method for maximizing momentum transfer is to increase adhesion – the higher the rotor surface roughness the greater the friction factor, and so the faster the tangential velocity drops and therefore the greater the momentum transfer. To accomplish this, micro structuring to increase adhesion while maintaining laminar flow is necessary. To illustrate this, Figure 3-3 shows the normalized tangential velocity for three rotors for three sets of roughness and flow rate conditions ( $n, Vr_o$ ). The 20 cm design rotor is operated at (2, 0.02), the 2 mm design rotor at (8, 0.08) and the 1 cm test rotor R1N3 at (2, 0.09). The smaller the flow rate indicator, the shorter the flow path length inside the rotor. The flow path also increases slightly with  $N_{RE}$ , which is proportional to rotor speed.

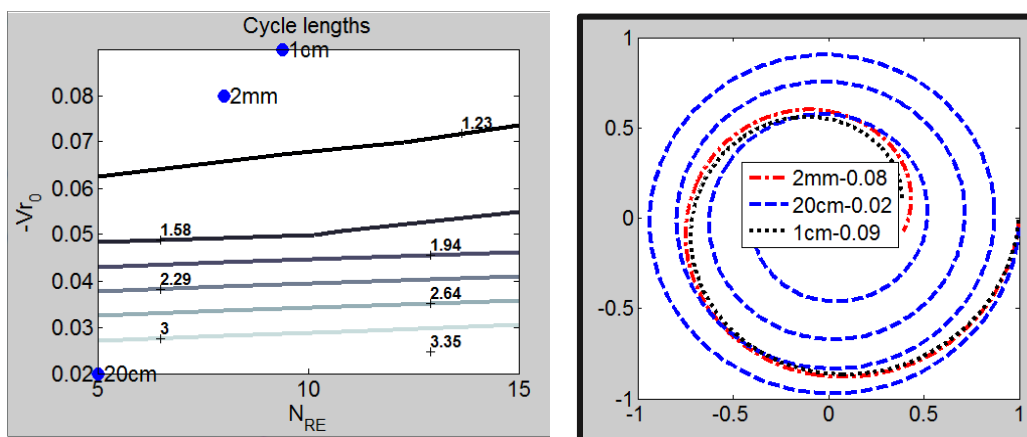


Figure 3-2: Rotor streamlines. (Left) The number of cycles that fluid makes with a micro rotor of 1 mm radius, a big rotor of 100 mm radius, and test rotor R1 of 5mm radius. (Right) The corresponding rotor streamlines with the  $Vr_o$ , flow indicator value.  $Vt_o=1.0$ ,  $n=2$ ,  $\xi_i=0.4$  for all rotors.

The tangential velocity along the flow path is shown on the left in interdisk space and on the right as a plot against the rotor radius. The lower the exit velocity of the fluid, the higher the momentum transfer and efficiency. The 20 cm rotor expends 80% of the fluid velocity inside the rotor, while the 1 cm test rotor expends only 40%. Though the 2 mm and 1 cm rotors operate at about the same flow rate, the 2 mm rotor performs much better – expending about 60% of the fluid velocity in the rotor as it is designed to operate with a uniform profile ( $n=8$ ).

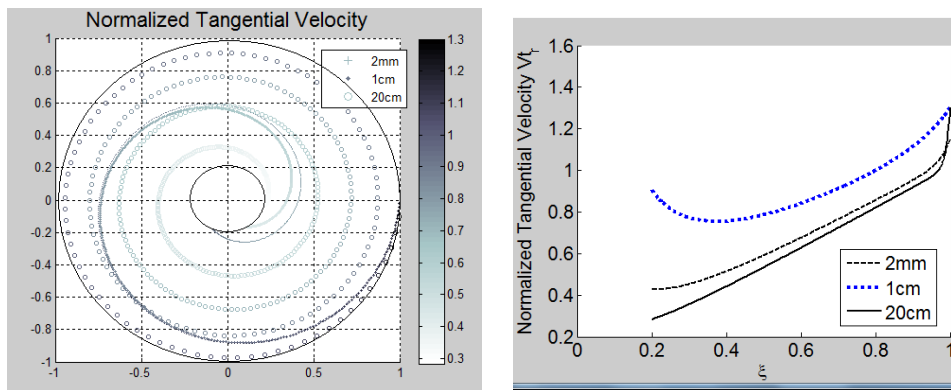


Figure 3-3: For the three rotors in Figure 3-2, normalized tangential velocity along the flow path from entry to exit. (Left) Plotted along the rotor streamlines. (Right) Plotted as a function of normalized radius. Solid: 20 cm rotor ( $V_{r_o} = 0.02$ ,  $n=2$ , exit velocity= 20% of entrance); Dot: fabricated 1 cm rotor R1-N3 ( $V_{r_o} = 0.09$ ,  $n=2$ , exit velocity 40% of entrance); Dash: 2mm design rotor ( $V_{r_o} = 0.08$ ,  $n=6$ , exit velocity 30% of entrance);  $V_{t_o}=1.3$ ,  $\xi_i=0.4$  for all three.

### 3.1.5 Effect of Flow Profile on Ideal Turbine Performance

Operating at a higher flow profile enhances performance in two ways.

First, it improves rotor efficiency by increasing momentum transfer while decreasing rotor pressure drop (Figure 3-4). Rotor parameters are calculated as the fluid travels through the interdisk space for three profiles  $n = 2, 5$ , and  $8$  at high and low flow  $V_{r_o} = 0.1$  and  $0.01$ ; when flow indicator  $V_{r_o}=0.1$ , higher the flow profile  $n$ , lower the velocity at the exit, lower the pressure drop and higher the torque. In here, efficiency increases by about 30%; when flow indicator  $V_{r_o}=0.01$ , performance improvement is small, about 1%.

Second, it enables higher power operation at the same efficiency (Figure 3-5). In our simulations, it was observed that a linear relationship between the flow profile and rotational Reynolds number results in similar rotor performance. This can also be inferred from Eq. 3-8. Rotor performance graphs are derived by varying the normalized tangential velocity  $V_{t_o}$  and the normalized radial velocity  $V_{r_o}$ , for three pairs of profile and rotational Reynolds number:  $(n, N_{RE}) = (2, 4)$ ,  $(3.5, 6)$ , and  $(5, 8)$ .

Three non-dimensional performance parameters deviated by less than 1% between the three runs: ideal turbine efficiency  $\eta_{turbine}$ , non-dimensional pressure  $P_t$ , and non-dimensional torque  $T_1$ . Because normalized power is a cubic function of RPM ( $N_{RE}$ ), all power graphs are normalized to the operating conditions of  $(2, 4)$ , which corresponds to the 30 cm reference turbine with smooth disks [2]. By changing the profile number from 2 to 5 and increasing RPM by a factor of two, power can be increased by eight

times under the same non-dimensional operating conditions. Increasing flow rate results in both non-dimensional velocities increasing at the same rate, resulting in a quadratic increase in non-dimensional torque. The graphs in Figure 3-5 show how power (and power density) can be increased by adding roughness to the disk and increasing flow rate.

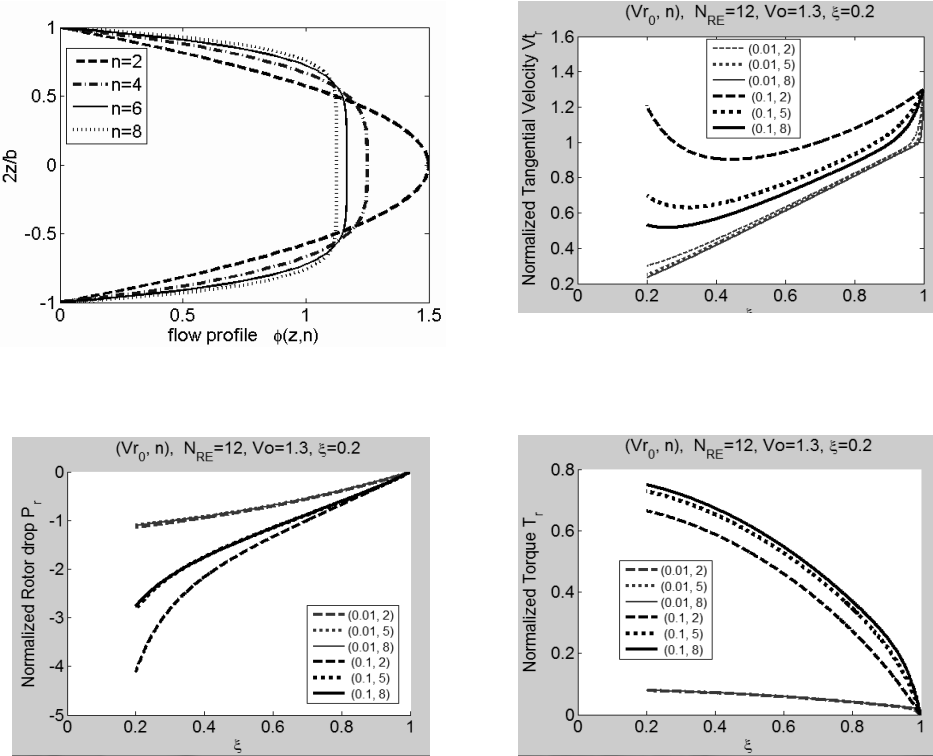


Figure 3-4: (Top left) Flow profile in the interdisk space for  $n = 2, 4, 6,$  and  $8,$  showing the effect of profile ( $n = 2, 5, 8$ ). Rotor parameters for profiles  $n = 2, 5,$  and  $8$  at low and high flow  $Vr_0 = 0.01, 0.1;$  (Top right) Non-dimensional tangential velocity  $V_t$  in the rotor. (Bottom left) Non-dimensional pressure drop  $P_r$ . (Bottom right) Non-dimensional torque  $T_r$ .

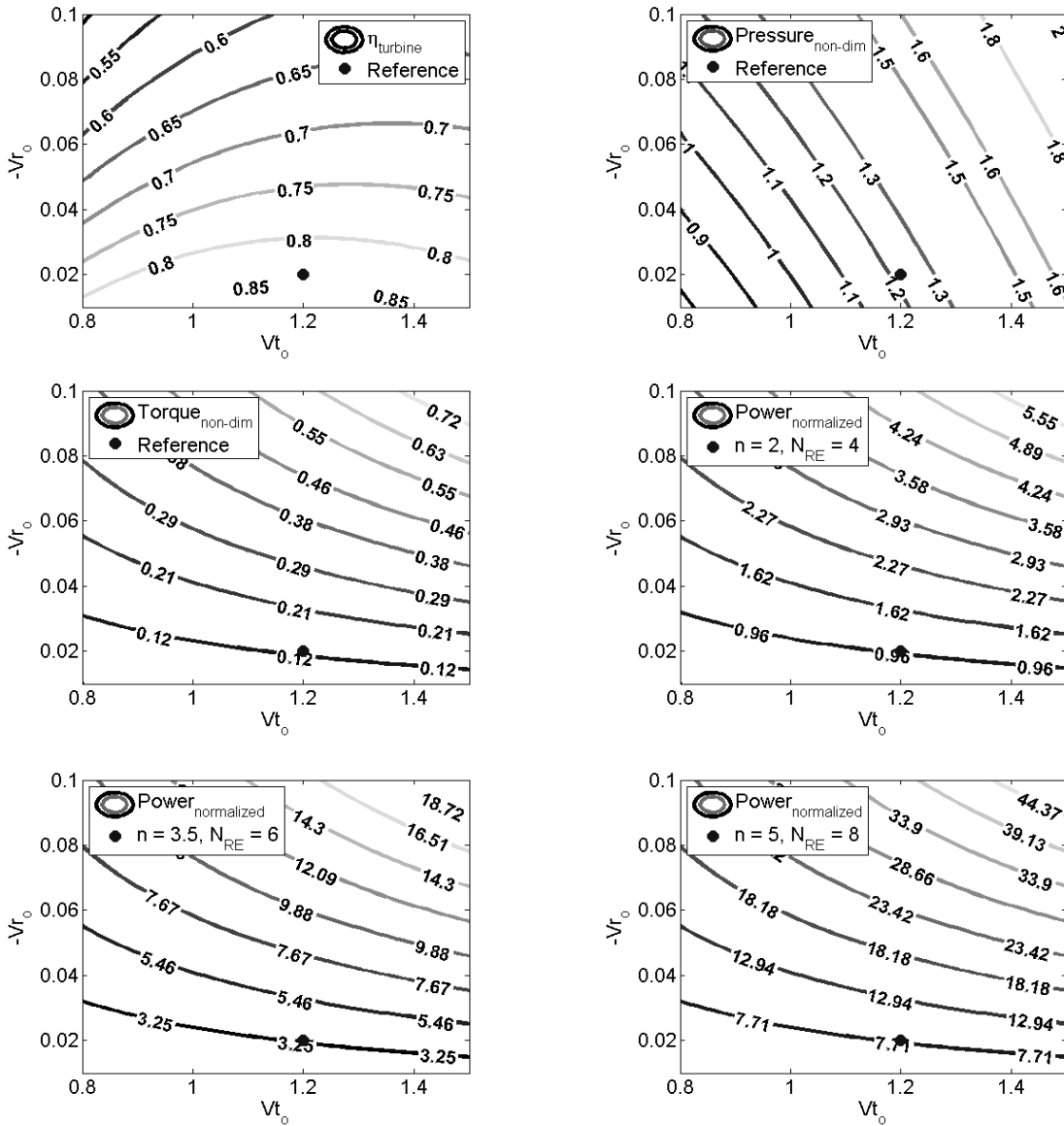


Figure 3-5: Profile effect on ideal rotor performance. Three sets of operation are chosen ( $\xi_i=0.4$  for all). 1) the smooth surface ( $PO=24, n=2, N_{RE}=4$ ), 2) rough surface ( $PO=36, n=3.5, N_{RE}=6$ ), and 3) even rougher surface ( $PO=48, n=5, N_{RE}=8$ ). Efficiency (top left), non-dimensional pressure (top right) and non-dimensional torque (middle left) are the same for all three sets, and are plotted for the reference set against the velocity and flow indicators. (Middle right) Power is normalized to the reference operating condition at  $Vt_o = 1.2, Vr_o = 0.02, N_{RE}=4$ . This normalization is used to compute the achievable relative power of the other two operating sets. The cubic relation of power vs.  $N_{RE}$  (RPM) and the linear relationship of torque  $Vr_o$  vs. flow rate combine to provide 21x the reference power at  $Vt_o = 1.5, Vr_o = 0.1, N_{RE}=6$  (bottom left) and 50x the reference power at  $Vt_o = 1.5, Vr_o = 0.1, N_{RE}=8$  (bottom right).

### 3.1.6 Nozzle Flow

Nozzles are simulated using COMSOL to visualize flow path and pressure drop. This is a reversible process assuming smooth nozzles with no loss (Figure 3-6).

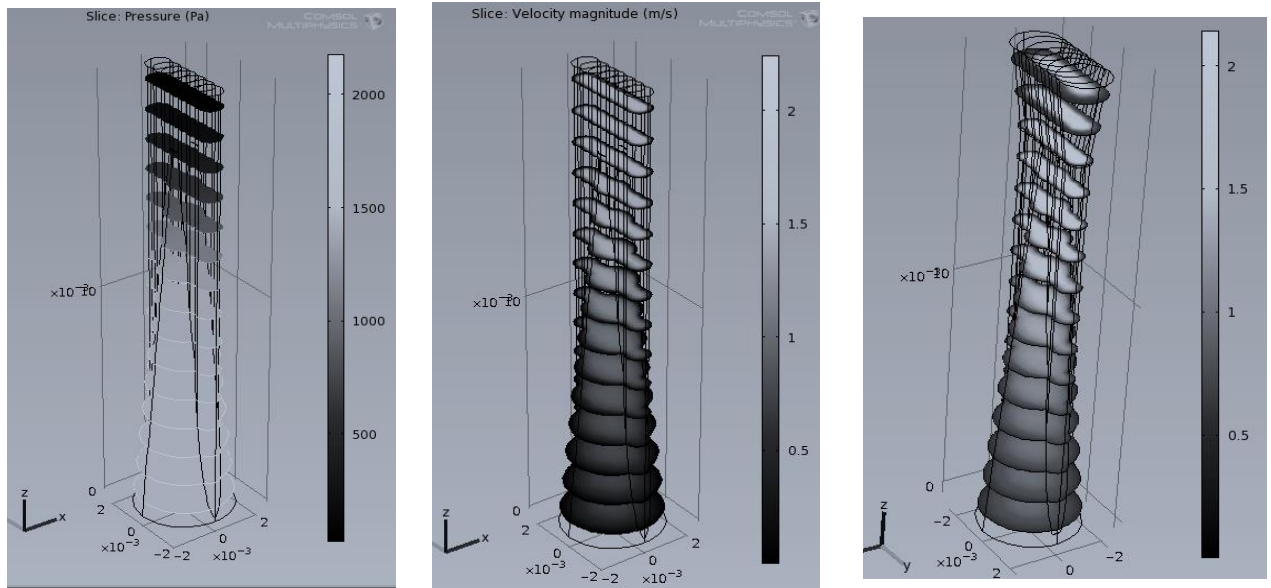


Figure 3-6: Nozzle drop and exit velocity profiles studied using COMSOL. (Left) Nozzle 4 pressure drop in Pascal. (Middle) Nozzle 4 flow velocity in m/s. (Right) Nozzle 7 velocity in m/s. The model design is shown in Figure 2-2. Boundary conditions are set to the following: atmospheric pressure at the exit, water flow rate of  $10 \text{ cm}^3/\text{s}$ , and parabolic velocity profile at the nozzle input. Nozzle flow is laminar and nozzle walls are smooth.

## 3.2 Comparison of Experimental Efficiency and Predicted Efficiency

This section compares the experimental results from fabricated turbines with performance predictions based on analytical flow solution. The predicted results use the experiment pressure head, experiment flow rate, RPM, and turbine dimensions. The prediction does not account for any torque loss, and thus indicates the upper limit of shaft power. We estimate torque loss suffered by the test system from the predicted torque and later employ it to map the test results onto the predicted and ideal results.

A linear relationship is observed between the predicted and experimental efficiencies over the flow rate range, with scale factor depending on the rotor-nozzle pairs. Figure 3-7(left) shows this relationship for the three rotors (R1, R3, R4) with the nozzle-3. Shaft power loss is caused by turbulence inside the rotor and by the swirling of

the trapped fluid in the gaps between rotor and the enclosure. Rotors with lesser number of disks and higher interdisk space will suffer more percentage torque loss due to this and this tendency is observed with rotor-4 (with 8 disks and 500  $\mu\text{m}$  interdisk space), having the greatest loss factor of 0.65 compared rotor-1 (with 20 disks and 125  $\mu\text{m}$  interdisk space) with a loss factor of 0.54.

Figure 3-7(right) shows the linear relationship between the predicted and experimental efficiencies for the three nozzles (N3, N4, and N7) with the rotor-1. Lower nozzle exit velocity results in slower flows, with lesser chance of turbulence in the rotor. Nozzle-7 with higher exit area of 7.14  $\text{mm}^2$  suffers lower torque loss compared to the smaller exit area nozzles N3 (2.28  $\text{mm}^2$ ) and N4 (3.28  $\text{mm}^2$ ).

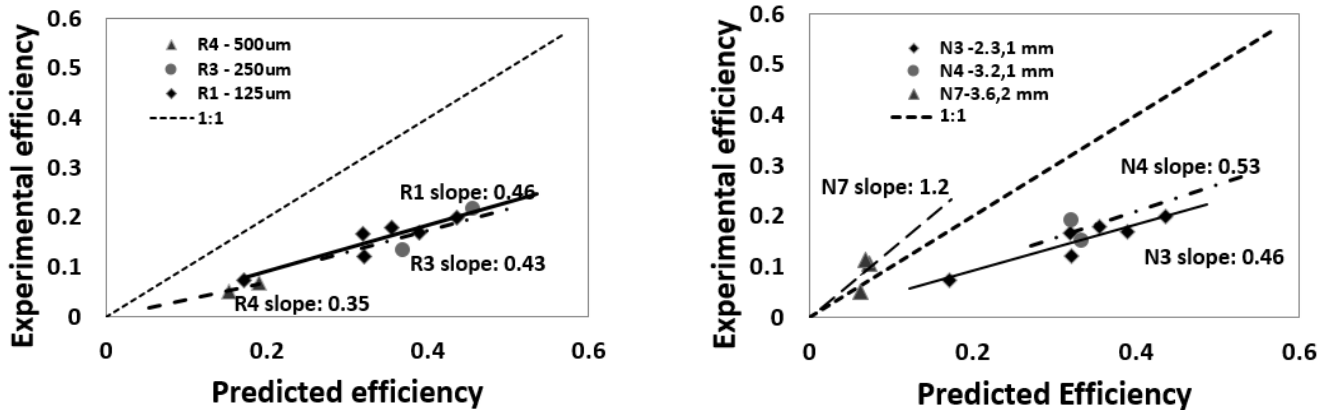


Figure 3-7: Experimental efficiency vs. predicted efficiency. (Left) Experimental efficiency has a linear correlation with predicted efficiency for the rotors tested – rotors R1, R3, and R4 (rotor-disk space specified at 125, 250, 500  $\mu\text{m}$ ) with nozzle 3. (Right) Experimental efficiency also has a linear correlation with predicted efficiency for the nozzles tested – nozzles N3, N4, and N7 (nozzle-length, nozzle-width at 2.3, 3.2, 7.2  $\text{mm}^2$  area) with rotor 1.

### 3.3 ANSYS Verification of Flow Model Testing

To verify testing of the rotor flow model, simulations were run using ANSYS/Fluent 13, with the steady laminar solver. The flow domain modeled is bounded by a symmetry plane through the center of an interdisk space, a symmetry plane aligned with the center of a rotor disk, a pressure boundary exhaust at  $r_i$ , a rotating no-slip boundary at the disk face, a no slip boundary condition at the turbine case walls, and a velocity inlet boundary upstream of the nozzle entry to the case (Figure 3-8). A mesh sensitivity study was performed on the nozzle region and the disk region separately, and confirmed that the velocities presented are insensitive to further reductions in element size. These simulation findings are summarized here, and additional details can be found in [24].

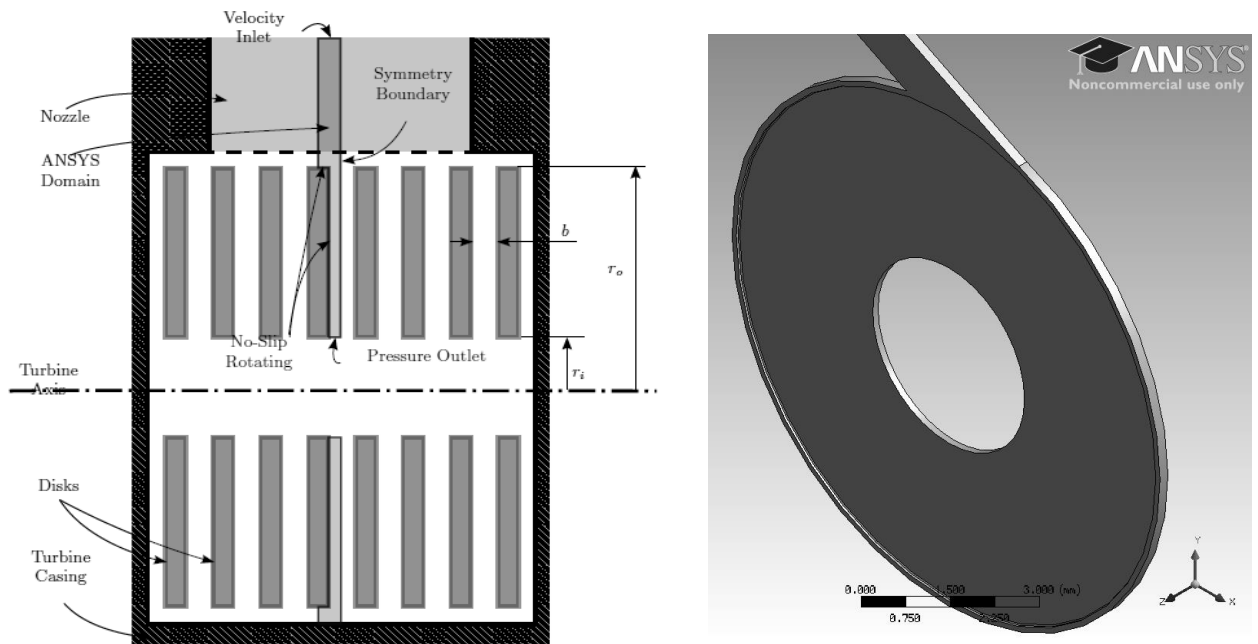


Figure 3-8: (Left) The ANSYS domain (highlighted) is bounded by a symmetry plane through the center of a gap and by a symmetry plane through the center of a disk. The disk edge forms a rotating boundary. (Right) ANSYS geometry.

### 3.3.1 Simulation Variations and Observations

Assuming that the kinetic energy of fluid at the exit of the nozzle is conserved, and deriving the radial component of flow from the mass flow rate considerations, the tangential entry velocity can be derived as  $V_{t_0} = \sqrt{(V_{noz}^2 - V_{r_0}^2)}$ . This would be appropriate if the flow changes direction after it exits the nozzle due to interactions with the turbine casing. Correlation between ANSYS efficiencies and predicted efficiencies is reasonably good (Figure 3-9, left). However, other factors that are difficult to predict – for example, the constriction effect of finite disk thickness – also have an effect on the inlet tangential velocity.

For the sake of comparison with the ANSYS model, the inlet tangential velocity can also be set to the velocity calculated by ANSYS. This separates flow-entry issues, allowing a comparison of the velocity profile in the rotor as calculated by ANSYS with the velocity profile as predicted by the analytical model; the correlation between ANSYS efficiency and predicted efficiency improves considerably as a result (Figure 3-9, right). This is true even though the analytical model assumes axial symmetry but the flow in ANSYS is injected through a nozzle with a finite arc length. As such, the analytical model

accurately predicts the physics of the flow inside the rotor, but a more detailed analysis of what occurs in the nozzle exit and rotor entry is necessary.

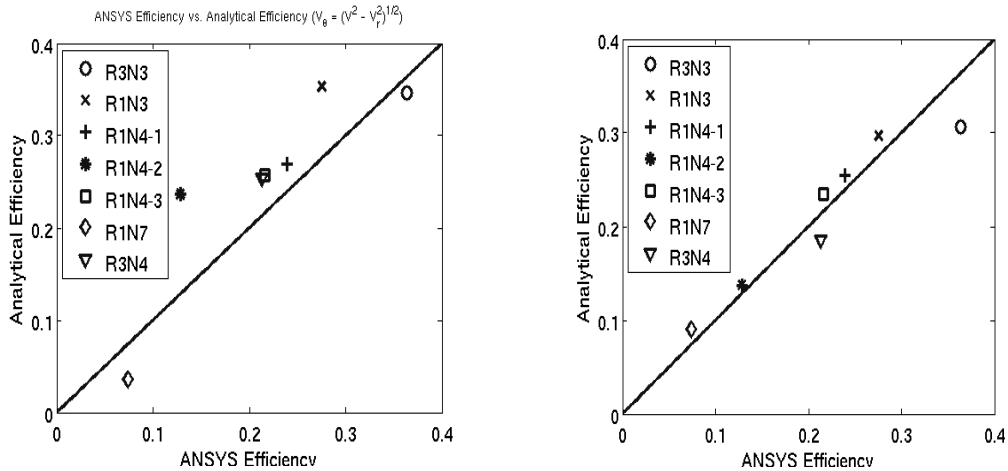


Figure 3-9: (Left)  $V_{t_o}$  based on velocity vector:  $V_{t_o} = \sqrt{V_{noz}^2 - V_r^2}$ . (Right)  $V_{t_o}$  matched to ANSYS.

### 3.3.2 Simulated Systems and Results

Table 3-1 lists a set of tests to verify the experimental and predicted results for the fabricated rotors.

### 3.3.3 Performance Trend Comparison

Decreasing the interdisk space increases efficiency in ANSYS, in the test data, and in the predicted data (Figure 3-10, left). In this analysis, total mass flow rate and radial velocity are held constant, while the number of disks and disk spacing  $b$  are varied. Increasing the velocity to the rotor at the inlet by decreasing the nozzle area (preserving mass flow rate) increases efficiency, but only up to a certain point. This is observed in ANSYS, test data, and the predicted data for N3, N4, and N7 (Figure 3-10, right). Operation of the Tesla turbine relies on converting a pressure head to kinetic energy, which is then transferred to the rotor, so a higher fluid velocity increases efficiency.

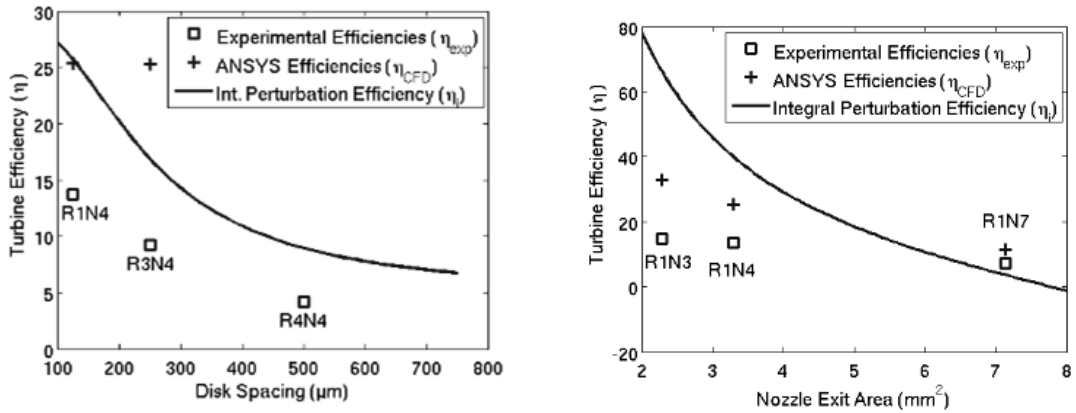


Figure 3-10: (Left) Efficiency vs. disk spacing. The smaller the disk spacing, the higher the efficiency. The smooth curve is the trend predicted by the integral perturbation solution, and the rotors and nozzles for the experimental and ANSYS results are indicated. (Right) Efficiency vs. nozzle area. The smaller the nozzle area, the higher the nozzle exit velocity and the higher the efficiency for the tests simulated. The trend as well as the experimental and ANSYS data are plotted.

Table 3-1: Dimensions and operating points of ANSYS simulations. Rotor# and Nozzle# ID correspond to those in Table 2-1 and Table 2-2. Nozzle angles are measured from the radial direction to nozzle flow direction at the center of the nozzle.

| Rotor-<br>Nozzle-<br>ID | #<br>Disks | Space<br>b μm | Nozzle<br>Angle | Nozzle<br>Area<br>mm <sup>2</sup> | Flow<br>rate<br>cm <sup>3</sup> /s | Nozzle<br>velocity<br>m/s | Rotor<br>RPM | ANSYS<br>efficiency<br>% |
|-------------------------|------------|---------------|-----------------|-----------------------------------|------------------------------------|---------------------------|--------------|--------------------------|
| R1-N3                   | 20         | 125           | 63.5            | 2.8                               | 10                                 | 4                         | 5760         | 33                       |
| R1-N4-1                 | 20         | 125           | 63.5            | 3.8                               | 12                                 | 3.43                      | 6020         | 28.8                     |
| R1-N4-2                 | 20         | 125           | 63.5            | 3.8                               | 3                                  | 0.857                     | 528          | 18.3                     |
| R1-N4-3                 | 20         | 125           | 63.5            | 3.8                               | 12                                 | 3.43                      | 5500         | 25.4                     |
| R1-N7                   | 20         | 125           | 52.7            | 7.6                               | 12                                 | 1.5                       | 5070         | 11.5                     |
| R3-N3                   | 13         | 250           | 63.5            | 2.8                               | 10                                 | 3.82                      | 5770         | 36.2                     |
| R3-N4                   | 13         | 250           | 63.5            | 3.8                               | 12                                 | 3.2                       | 5110         | 24.4                     |

### 3.3.4 Conclusions:

A rotor flow model, accommodating different fluid flow profiles is investigated and it is observed that the flow rate through the rotor can be increased with rotor surface roughening without sacrificing efficiency. When the roughness factor, a multiplier to Poiseuille number, is increased from 1 to 3, the flow profile in the interdisk spacing changes from parabolic to uniform. The rotor can be operated at a proportionally higher speed enabling increase in the rotor power density by  $\sim 3^3$ , a cubic order.

ANSYS results indicate that for our test turbines, the integral perturbation analysis of the rotor flow, based on full peripheral admission agrees with the ANSYS results run using single nozzle at 10%-20% admission. The comparisons are performed over the flow rate indicator range of 0.01 to 0.12 which covers the recommended operating range. In short, single nozzles can be used in place of full admission nozzles.

From the simulations, it is observed that the performance of the ideal turbine is higher than 55% for the whole operation range. The predicted performance based on the experimental setup and the calculated experimental efficiency are about 2/3 and 1/3 of the ideal turbine efficiencies. This is in concurrence with the discrepancies we observe between the theoretical projections and practical implementations in published works.

In the next chapter the types of performance losses in the turbine are explored and the corresponding models and findings are discussed.

# Chapter 4

## 4 Turbine Mechanical Losses and Mapping Test System Performance to the Ideal Turbine

A major goal of this dissertation is to establish a thorough understanding of turbine loss mechanisms at the scales of interest so that strategies can be developed to minimize them. In this chapter, these losses are modeled and applied to a 2 mm, 4 cm, and 30 cm turbine to cover the micro to big range, and also to a test system with rotor-1 and nozzle-4. Overall, turbine mechanical losses fall into two categories: loss of head and loss of shaft power. Loss models enable mapping of experimental efficiency onto predicted efficiency at test conditions, and onto theoretical efficiency at ideal conditions. Mechanical to electrical conversion losses for hydro power is < 10% and this is not included in here [31].

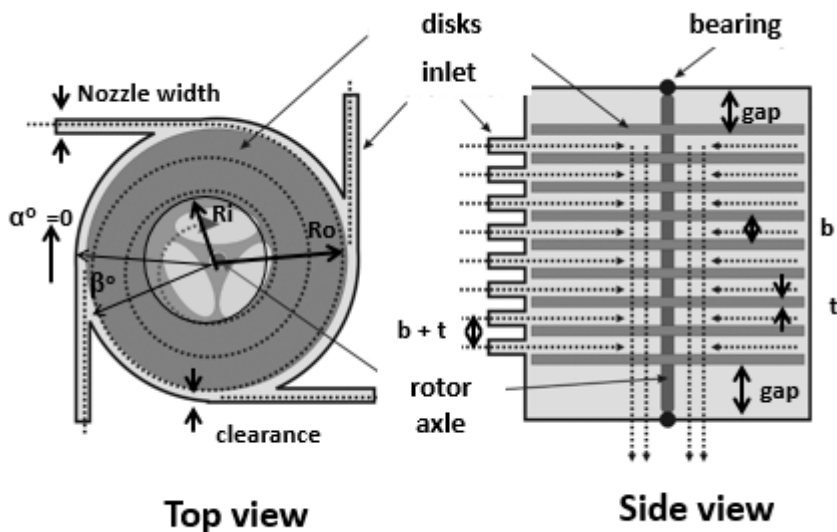


Figure 4-1 : Turbine hardware naming convention used in this chapter to study the losses.

## 4.1 Loss Models and Estimation

Primary turbine Mechanical losses result from a number of factors:

- 1) Fluid frictional loss in the nozzle, in the clearance between rotor and housing and in the interdisk space.
- 2) Unused head loss from volume leakage caused by inadequate sealing.
- 3) Unused kinetic energy loss and path loss at the exhaust
- 4) Impact loss caused by geometry mismatch between the nozzle exit and rotor entry
- 5) Turbulence loss inside the rotor
- 6) Mechanical loss in the bearing.

### Turbine Losses

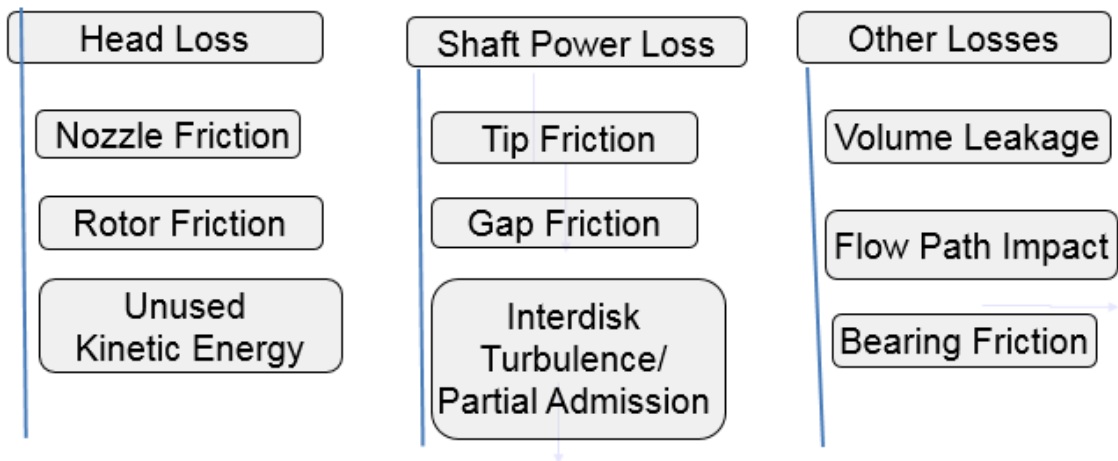


Figure 4-2: Turbine loss model is categorized into head loss, shaft power loss that are part of the turbine hardware and operation and other losses that are more implementation dependent. These loss estimates are applied to our turbine model, and turbine performance is evaluated for various flow profiles.

The losses are broadly grouped under two categories as shown in Figure 4-2. Loss in input power due to friction in the nozzle, friction in the rotor and the unspent kinetic energy at the exit are modeled under head loss. Loss of output power due to fluid trapped in gaps and at tips of the rotor as well as loss due to turbulence near the disk entry and exhaust are modeled under shaft power (torque) loss. Enclosure-rotor interface losses such as leakage loss, entry impact loss, exit path loss, and bearing loss are grouped under other loss and are estimated from published literature.

## 4.2 Head Loss Contributors

### 4.2.1 Nozzle Loss

Nozzle loss is calculated using the Darcy-Weisbach equation, based on  $L_{noz}$ , nozzle length,  $D_{noz}$ , hydraulic diameter and  $V_{noz}$ , nozzle velocity ( Eq. 4-1). The friction factor is a complex function of nozzle Reynolds number and roughness ratio. Moody presented the friction factor in a set of graphs as a function of the Reynolds number and pipe roughness ratio ( [26]), and Kandlikar [20] modified the Moody diagram to account for micro structures with a roughness factor greater than 0.05. For the range of turbines presented here, the maximum roughness factor is set at 0.05 and a piecewise approximation to the Moody diagram is applied to derive the friction factor (Figure 4-3).

$$P_{nozLoss} = (fric)(L_{noz}/D_{noz})( V_{noz}^2/2 g) \quad 4-1$$

$$D_{noz} = 2 W_{noz} H_{noz}/(W_{noz} + H_{noz}) \quad 4-2$$

$$RE_{noz} = D_{noz} V_{noz}/\nu \quad 4-3$$

$$rough_{noz} = \epsilon/D_{noz} \quad 4-4$$

$$fric = \text{Moody graphs} ( RE_{noz} rough_{noz}) \quad 4-5$$

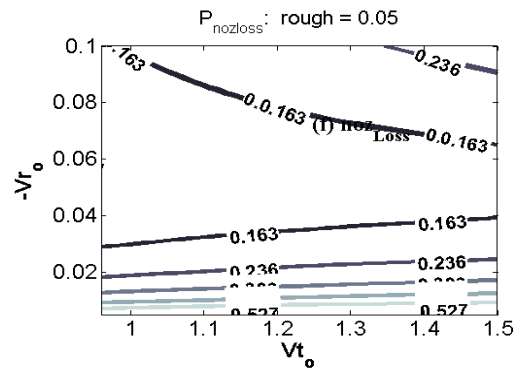
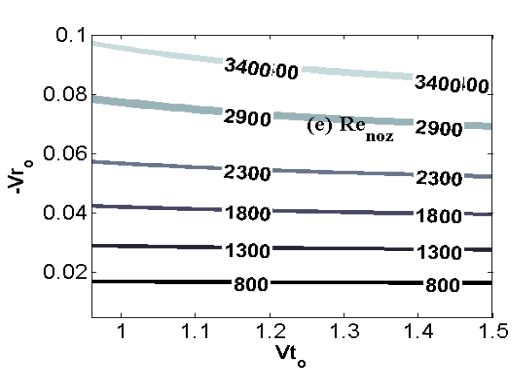
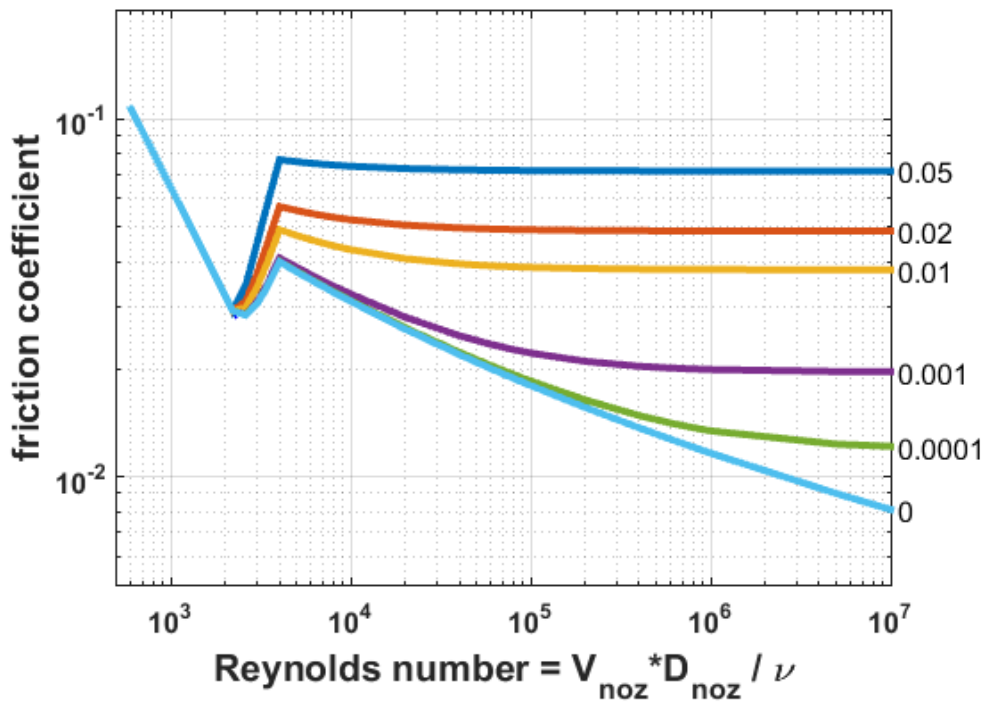


Figure 4-3: (Top) Moody diagram used in this research [25]. Transitional region 2300 to 4000 (from laminar to turbulence) is undefined and is to be avoided, though in the figure a linear interpolation is used to show the transition. (Both bottom) Nozzle loss for R1-N4 at  $V_{r0}=0.06$ ,  $V_{t0}=1.1$ . (Bottom left) Nozzle Reynolds number 2300 at reference. (Bottom right) Non-dimensional head loss 0.17 and nozzle loss = 14.3% at reference.

Frictional loss is estimated for nozzles N3, N4, and N7 over tested flow rates of 2 cm<sup>3</sup>/s to 12 cm<sup>3</sup>/s. The Reynolds number varies from 700 to 8000 in the nozzles, resulting in

laminar to turbulent flow. For turbulent flow, the roughness factor of the nozzles is applied to derive the nozzle drop. Because the nozzles are fabricated using 3D rapid plastic prototyping with 50  $\mu\text{m}$  resolution, a roughness factor of 0.05 is applied for the head calculations in the turbulent flow regions, resulting in head loss ranging from 5 to 3000 Pascal. This corresponds to a range of 0.1% to 10% of the measured turbine head. It is notable that as the turbine scales down, nozzle losses increase due to lower Reynolds number at low flow rate and due to higher roughness factor at high flow rate. The nozzle Reynolds number and non-dimensional nozzle loss for R1-N4 are shown in Figure 4-3. The minimum nozzle loss is about 10% of the head at Reynolds number of 2300 for the test rotor.

Smaller  $D_{\text{noz}}$  results in higher roughness ratio and higher nozzle velocity increasing the nozzle loss. Larger  $L_{\text{noz}} / D_{\text{noz}}$ , higher the nozzle loss, as this is a multiplicative factor for the loss.

#### 4.2.2 Kinetic Energy Loss at Exhaust

Higher tangential and radial fluid velocities relative to rotor speed result in inefficient transfer of the fluid energy because fluid exits the rotor with unspent kinetic energy.

$$KE_{\text{out}} = 0.5 ( (W_i + \xi_i)^2 + V_{\text{ro}}^2 / \xi_i^2 ) \quad 4-6$$

This loss is already accounted for in the ideal turbine efficiency.

#### 4.2.3 Rotor Loss Fraction

A portion of the pressure drop inside the rotor is irreversible. This is included in the pressure drop computation and is derived from the rotor equations (Eqs. 3-8, 3-13, 3-16, 4-6). Rotor frictional loss corresponds to the difference between the total head (dynamic and static) spent in the rotor and the torque output of the rotor (Eq. 4-7).

$$\text{Rotor}_{\text{loss}} = P_{\text{ideal}} - KE_{\text{out}} - R_{\text{momentum}} \quad 4-7$$

### 4.3 Shaft Power Loss Contributors

#### 4.3.1 Disk Friction Loss

Water trapped in the gaps between the enclosure and the end disk of the rotor will rotate at about half speed and inflict frictional loss. An additional frictional loss occurs in the clearance  $c$  between the cylindrical enclosure walls and the rotor tips (thickness  $t$ )

for each disk (Figure 4-4, Top left). Both of these losses are analyzed using a single disk in a closed enclosure. Daily [27] showed that power loss due to disk friction is proportional to torque  $\omega^3 r_o^5$ . Disk friction loss can therefore be defined as a fraction of shaft power. Frictional torque loss due to the gap depends on whether the disk Reynolds number is laminar or turbulent and on whether the flow in the gap is merged or separate. Daily defines four regions : 1) merged laminar flow ; 2) separate laminar flow; 3) merged turbulent flow; and 4) separate turbulent flow, where merged and separate corresponds to the flow characteristic between the rotating end disk of the rotor and the stationary enclosure wall. In here, piecewise linear approximation is used on Daily's diagrams for separate flows (Eqs. 4-10, 4-12).

$$RE_{gap} = \omega r_o^2 / \nu \quad 4-8$$

$$C_1 = C_{lam\_merged} = 2\pi r_o / s RE_{gap} \quad 4-9$$

$$C_2 = C_{lam\_separate} = (2.61 + 2.5 s/r_o) / RE_{gap}^{0.5} \quad 4-10$$

$$C_3 = C_{turb\_merged} = 0.0622 r_o^{0.25} / s^{0.25} RE_{gap}^{0.25} \quad 4-11$$

$$C_4 = C_{turb\_separate} = (0.074 + 0.08 s/r_o) / RE_{gap}^{0.2} \quad 4-12$$

$$C_{gap} = \max(C_1, C_2, C_3, C_4) / N_{disks} \quad 4-13$$

The multiplicative constant is derived for all the four regions at different gap ratios. (Eqs.4-9 to 4-13). Daily's graph is redrawn to display the range used in this research (Figure 4-4 – Top Right). A merged flow assumption is valid for the test turbines due to the small gap size. From the equations it can be seen that a bigger gap to radius ratio results in smaller losses. This gap friction loss is shared by all disks, and the loss due to tip friction also occurs for every disk. The tip friction loss increases with disk thickness to clearance ratio and is inversely proportional to the Reynolds number of the fluid trapped in the clearance (Eq. 4-14). The non-dimensional torque loss per disk is given by the addition of gap and tip coefficients (Eq. 4-15).

$$C_{tip} = 4\pi \nu t/c \omega r_o^2 \quad 4-14$$

$$T_{\text{gapLoss}} = 0.5 r_o / b (C_{\text{gap}}); T_{\text{tipLoss}} = 0.5 r_o / b (C_{\text{tip}})$$

4-15

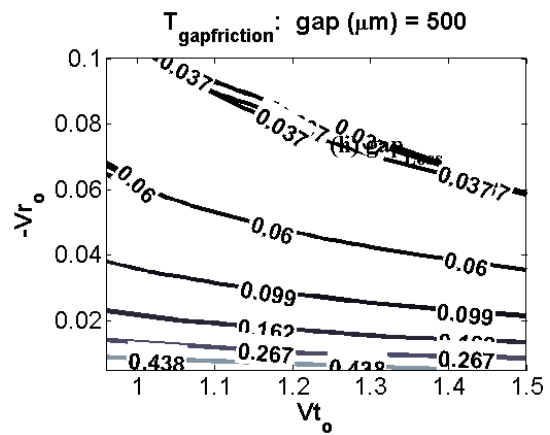
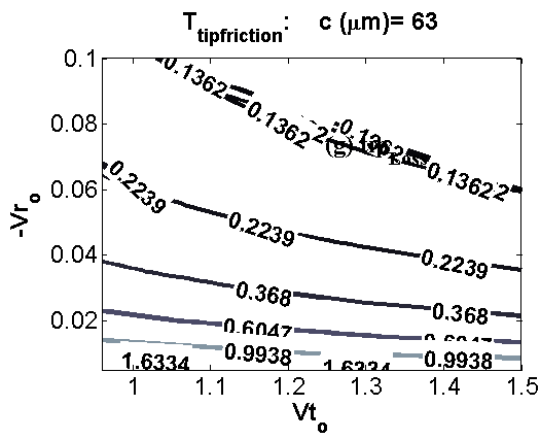
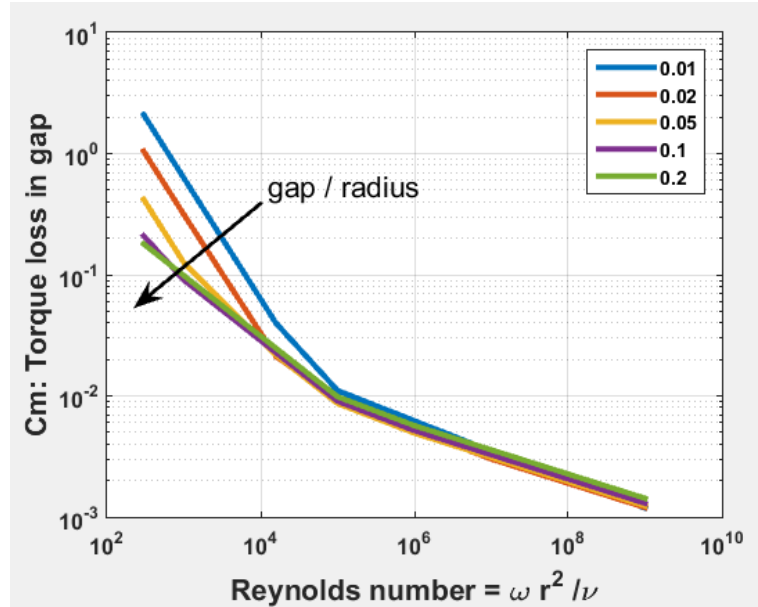
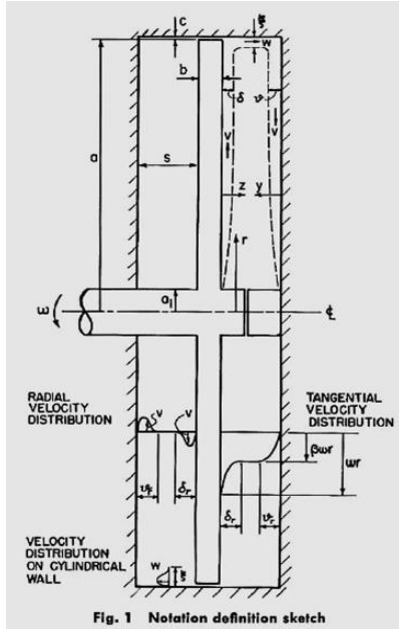


Figure 4-4: Disk friction [26]. (Top left) Rotor and housing for disk friction measurement. (Top right) Gap friction coefficient (torque multiplier) used in this dissertation. (Bottom, both) Non-dimensional torque loss factors for R1-N4 at  $Vr_o=0.09$ ,  $Vt_o=1.5$ . (Bottom left) Tip friction loss 4% and (Bottom right) Gap friction loss 1.1% at reference.

The tip friction and gap friction torque loss factors for R1-N4 are given in Figure 4-4. These losses are significant at low flow parameters. At the test operating regions it varied up to 15% of the torque generated.

Performance loss due to fluid trapped in the gap can be reduced by increasing the gap and also the number of disks. Because tip friction depends on  $t/c$ , decreasing disk thickness or increasing clearance improves performance. The effect of tip loss increases as the turbine scales down.

#### 4.3.1 Rotor Turbulence Loss

Loss can also occur due to turbulence near the rotor exhaust. Nendl [32] developed the visco-geometric constant  $\alpha_N$ , which defines flow between corotating disks at any radial position  $r$  as laminar for  $\alpha_N < 10$ , transitional for  $10 < \alpha_N < 20$ , and turbulent for  $\alpha_N > 20$

$$\alpha_{N(r)} = 0.25 RE_{\text{rot}} / (\xi_i \xi_r) \quad \text{where } \xi_r = r/r_o \quad 4-16$$

In the operating range of the turbines in this paper, this constant is maintained at less than 8, keeping the flow laminar and eliminating turbulence loss.

#### 4.3.2 Partial Admission

The rotor model assumes that the flow in the interdisk space has radial symmetry (3.1). Full peripheral admission could assure this symmetry. But full peripheral admission requires very thin slit nozzles, due to the small value of radial to tangential velocity – a basic requirement for Tesla turbine operation. Many thin nozzles around the rotor increase nozzle loss bringing down the efficiency. In our designs we are using one or more discrete slit nozzles around the rotor. ANSYS simulations of the rotor does not indicate any loss due to this (3.3.4). Matsch and Rice discuss the deviation in symmetry due to partial admission [33] at flow rate indicator  $Vr_o > 0.1$ . In this work we recommend design constraints to limit flow rate indicator to  $< 0.1$  to minimize this variation.

### 4.4 Other Losses

There are other head loss and shaft power loss which could cause as much as 10% efficiency loss. In here the losses in the flow path due to leakage and path bends is grouped under head loss and losses due to bearing friction, possible flow turbulence in the interdisk spacing are grouped under torque loss (shaft power loss.)

#### 4.4.1 Leakage

Leakage from water escaping between the periphery of the rotor and the enclosure due to inadequate sealing also contributes to loss in efficiency

#### 4.4.2 Leading and Trailing Flow Losses

When fluid exiting the slit nozzles encounters a disk edge or a rotor disk gap, this results in impact loss. At the exhaust, the fluid is shunted 90° and suffers losses depending on the position of the disk in the rotor assembly ([28], Figure 4-5), which can be modeled as a second-order function of flow rate [33]. This is included in our loss model, and is estimated to have a much lower impact on overall loss compared with the first-order flow rate effect for our test systems.

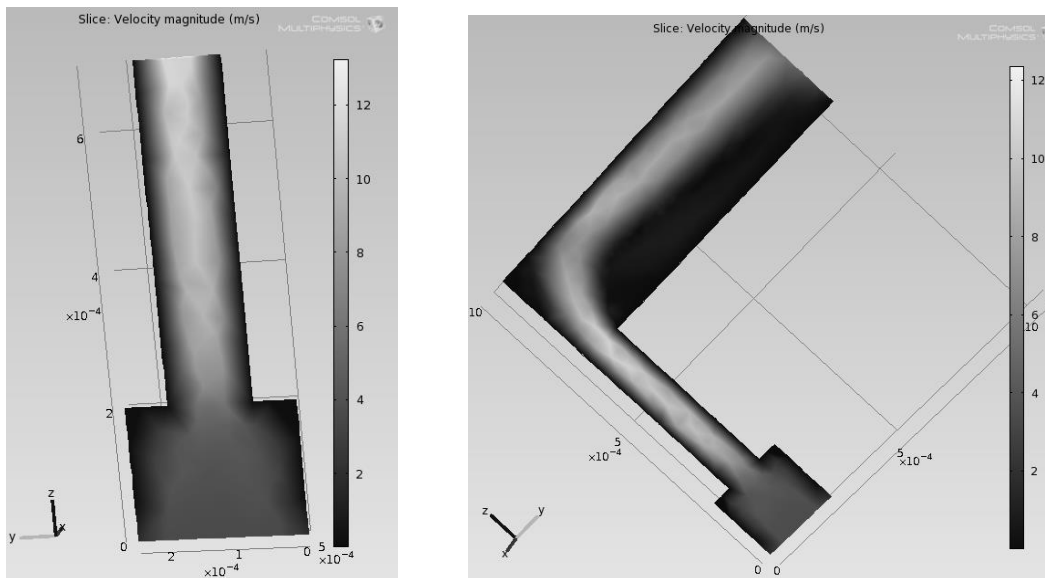


Figure 4-5: Flow path visualization at the entry and exit of the rotor. (Left) Flow path bending around the disk edges into 125  $\mu\text{m}$  interdisk space from the 250  $\mu\text{m}$  nozzle exit (entry) at the bottom. (Right) Flow path making a 90° turn at the exit.

#### 4.4.3 Bearing Loss

Bearing loss is a function of speed. In our testing, bearing loss is accounted for in the deceleration of the rotor, and is modeled as a polynomial function of flow rate. Previous research has concluded that the combined losses from leakage, leading and trailing paths, and bearings amounts to less than 10% [34], [18].

$$(\text{othe head and shaft power losses}) < 0.1$$

## 4.5 Mechanical Efficiency Estimate with all Losses

The efficiency of the system including major losses can be calculated using the derivations in Eqs. 3-18, 3-19, 4-6, 4-7 and 4-15.

$$\text{head}_{\text{loss}} = P_{\text{nozloss}} + \text{Rotor}_{\text{loss}} + \text{KE}_{\text{out}} + \text{head}_{\text{other}} \quad 4-17$$

$$\eta_{\text{head}} = R_{\text{momentum}} / (R_{\text{momentum}} + \text{head}_{\text{loss}}) \quad 4-18$$

$$\eta_{\text{shaft}} = (1 - T_{\text{gaploss}} - T_{\text{tiploss}} - \text{torque}_{\text{other}}) \quad 4-19$$

$$\eta_{\text{system}} = \eta_{\text{head}} \eta_{\text{shaft}} \quad 4-20$$

## 4.6 Estimated Turbine Performance with Losses

Performance of three turbines with diameters 2 mm, 4 cm, and 30 cm (micro, small, and big) and of test turbine R1-N4 is analyzed using these turbine flow models and loss models. The roughness factor  $\epsilon$  for the nozzles is set higher as the turbine scales down due to manufacturing needs. The tip clearance  $c$  is increased to keep the tip loss below 1%, with the assumption that leakage can be minimized with proper sealing. To minimize size dependency in the gap friction loss, the gap clearance  $s$  is kept proportional to spacing and the number of disks is kept proportional to radius. The roughness for the disks and the Reynolds number ( $PO$ ,  $n$ ,  $N_{RE}$ ) are set higher as the turbine scales down, without affecting efficiency (Figure 3-5). The operating details for the four turbines are given in Table 4-1.

Sankey diagrams for each system along with ideal efficiency, actual efficiency, power density, and nozzle Reynolds number over a range of non-dimensional flow indicators are given in Figure 4-6 for 2 mm, Figure 4-7 for 4 cm, and Figure 4-8 for 30 cm turbines. The loss due to unspent kinetic energy is shown separate, to include more details. The diagrams show regions of stable operation with close to 60% efficiency for all the three turbines. Here, the interdisk spacing is designed based on constant power density across the turbine range (5.5). The clearance and gap space are increased here about an order to minimize the tip and gap losses.

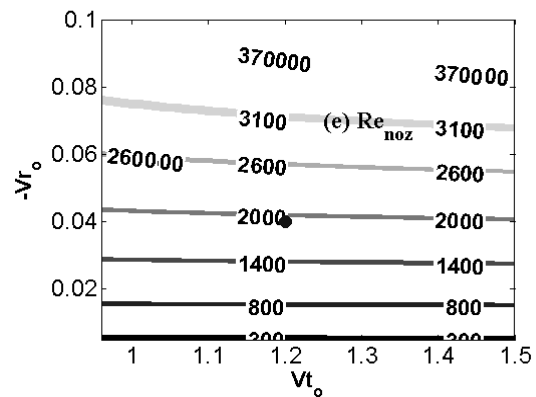
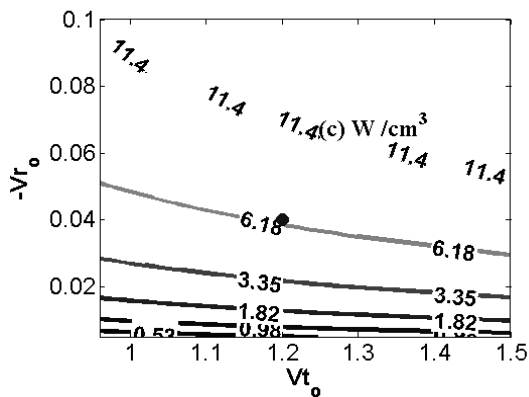
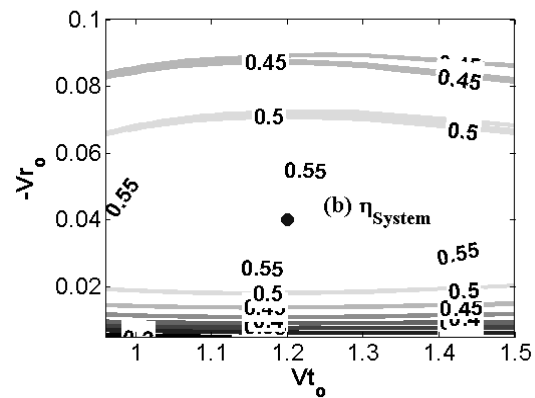
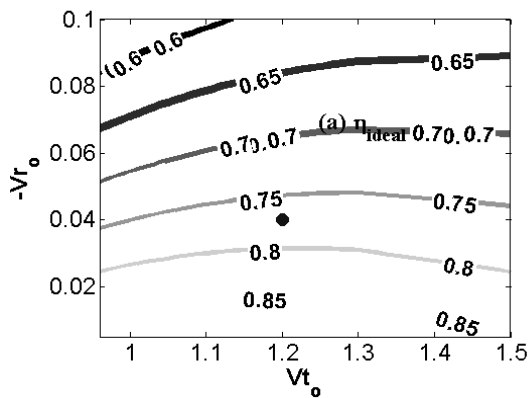
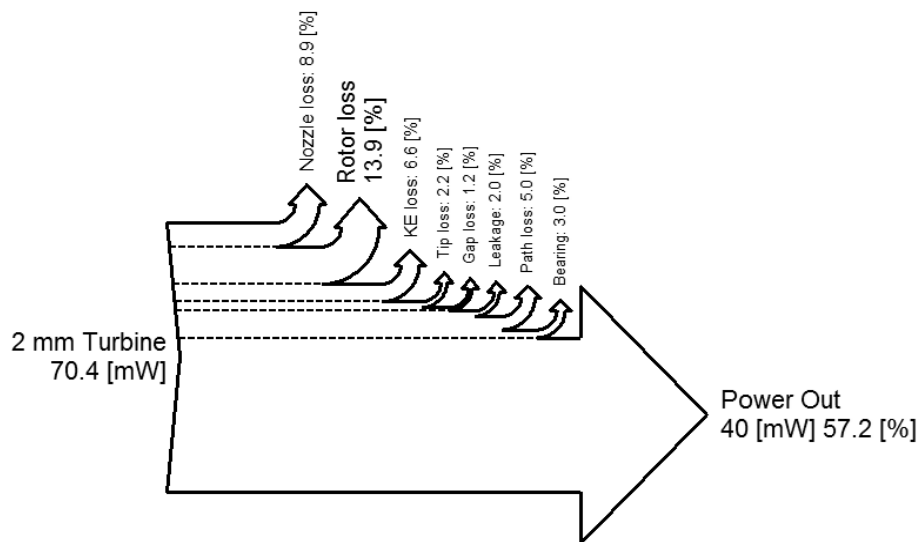


Figure 4-6: 2 mm turbine;  $b=35\mu m$ ,  $n=5$ ,  $NRE=8$ ,  $RPM=62500$  (Table 4-1) (Top) Sankey diagram, derived at reference point  $Vr_0=0.04$ ,  $Vt_0=1.2$ ,  $Re_{rot}=1.28$ . (Middle left) Ideal turbine efficiency. (Middle right) Lossy turbine efficiency. (Bottom left) Power density. (Bottom right) Nozzle Reynolds number.

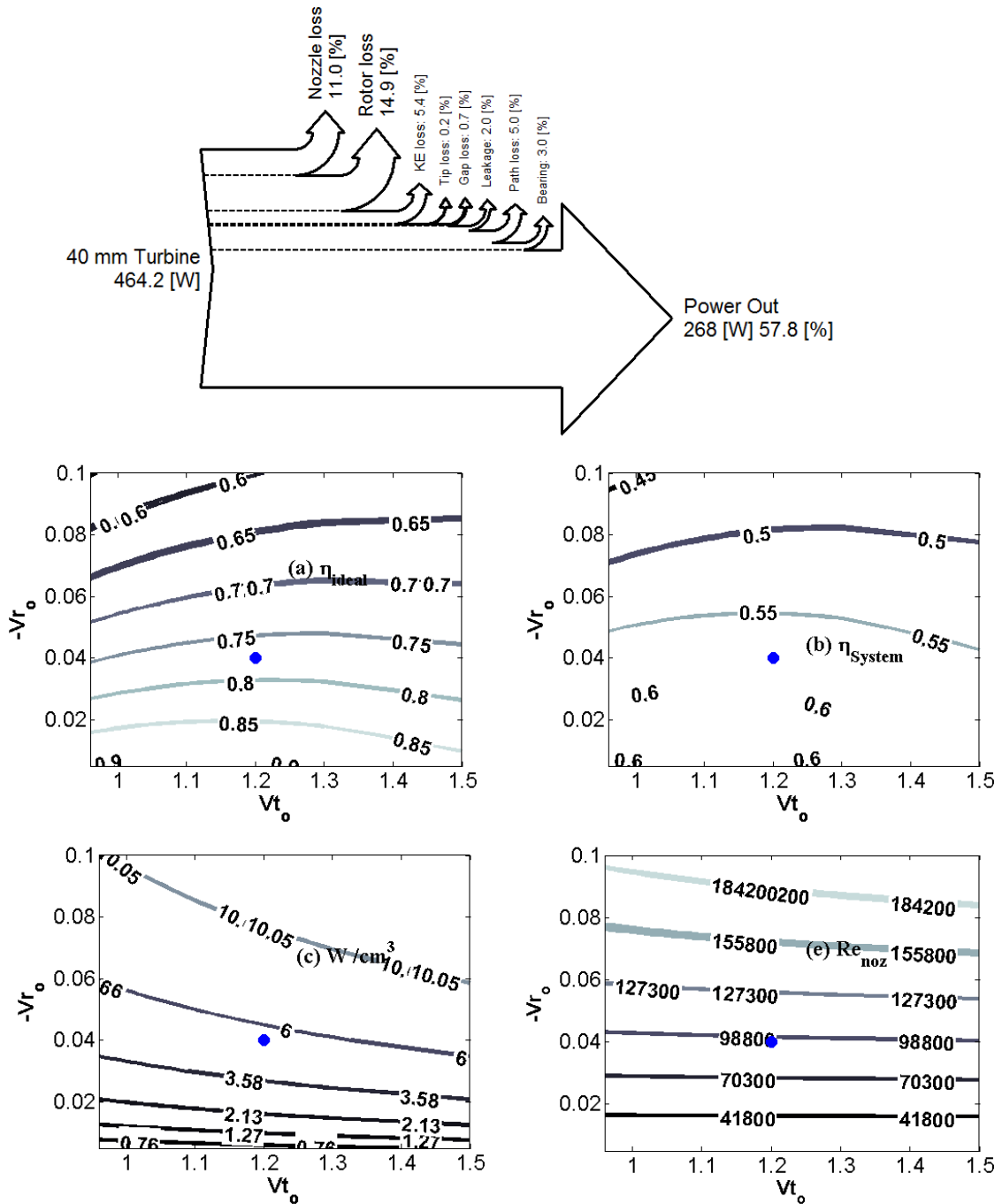


Figure 4-7: 4 cm turbine;  $b=86\mu m$ ,  $n=3.5$ ,  $NRE=6$ ,  $RPM=7700$  (Table 4-1) (Top) Sankey diagram, derived at reference point  $Vr_o=0.04$ ,  $Vt_o=1.2$ ,  $RE_{rot}=0.96$ . (Middle left) Ideal turbine efficiency. (Middle right) Lossy turbine efficiency. (Bottom left) Power density. (Bottom right) Nozzle Reynolds number.

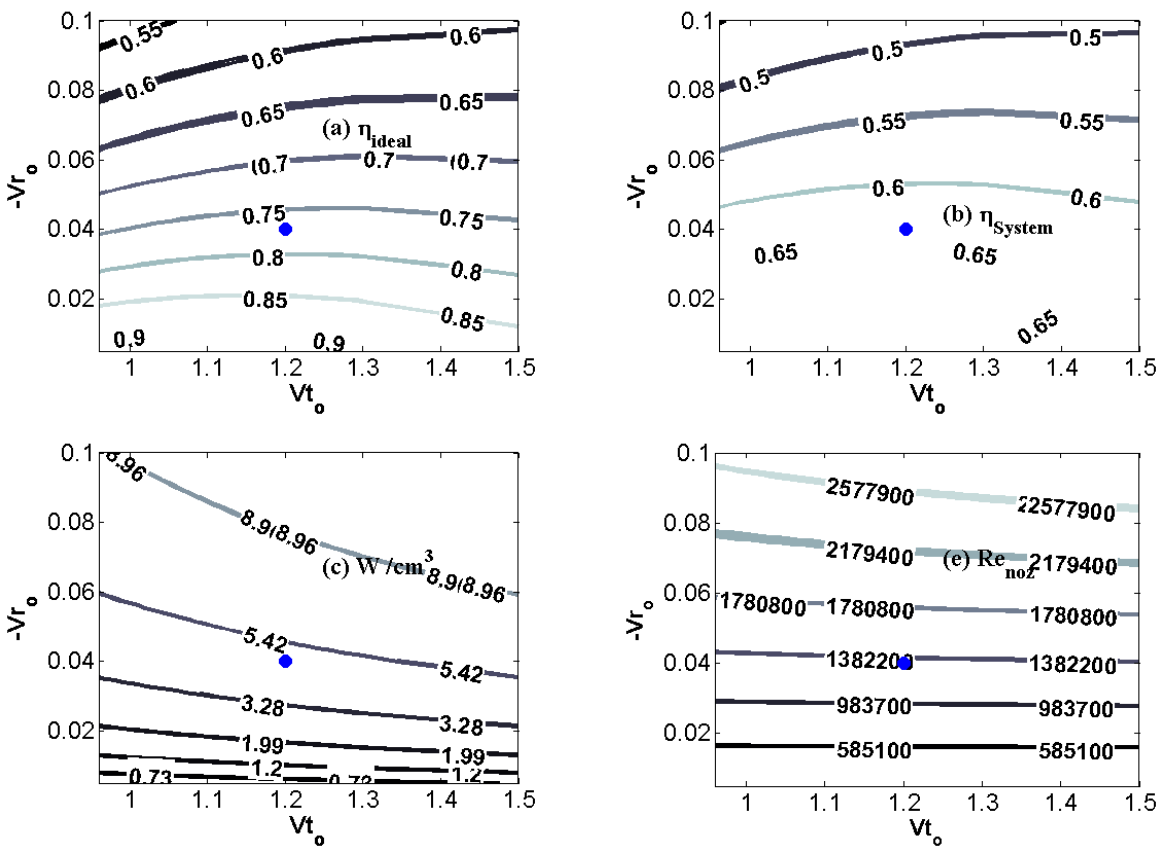
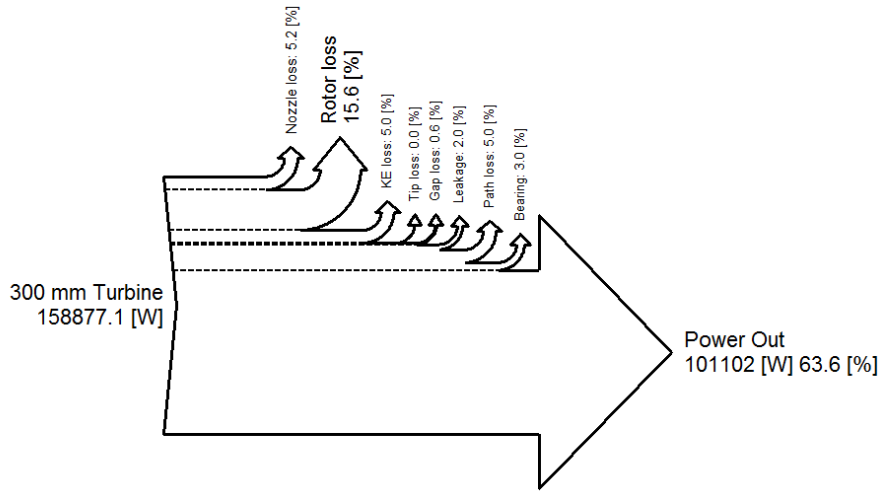


Figure 4-8: 30 cm turbine;  $b=157\mu m$ ,  $n=2$ ,  $NRE=4$ ,  $RPM=1930$  (Table 4-1); (Top) Sankey diagram, derived at reference point  $Vr_o=0.04$ ,  $Vt_o=1.2$ ,  $RE_{rot}=0.64$ . (Middle left) Ideal turbine efficiency. (Middle right) Lossy turbine efficiency. (Bottom left) Power density. (Bottom right) Nozzle Reynolds number.

### 4.7 Test Turbine Performance Evaluation and Mapping

The Sankey diagram shown in Figure 4-9 depicts the expected performance of test rotor-1 with nozzle-4 operating at 8 cm<sup>3</sup>/s flow rate and 0.98 m head. Nozzles 1, 2, 4, 6, and 8 are all of same type, only difference being the exit angle. In this performance evaluation nozzle-4 angle is varied from tangential to 45° to the rotor. This is to study the exit angle impact and to choose the optimum angle for the nozzle.

The turbine efficiency with respect to nozzle angle and RPM is given in Figure 4-10. The optimum output for the given input conditions is 26 mW at 33% efficiency at about 10° nozzle angle. Nozzle-4 angle is the closest to tangent, but its center is at about 26° to the tangent. Our experimental calculations for this nozzle results in about 14 mW power at 18.3% efficiency. Both nozzle-4 design angle and the optimum nozzle angle are mapped on the efficiency plot. Much of the loss in the performance is probably due to the wide angles covered by our test nozzles.

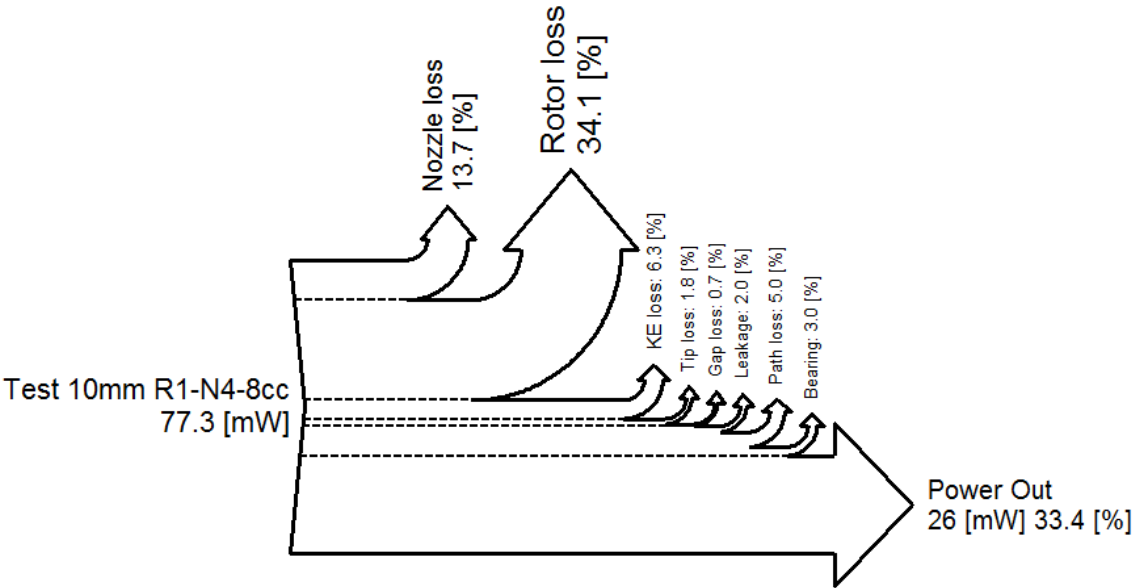


Figure 4-9: Sankey diagram on test turbine mechanical power output using nozzle-4 structure. Here the optimum angle for nozzle-4 is used in calculating, resulting in better efficiency. Setup: R1-N4; 8 cm<sup>3</sup>/s, b=125µm, n=2, N<sub>RE</sub>=5, Vr<sub>o</sub>=0.09, Vt<sub>o</sub>=1.5 (Table 4-1).

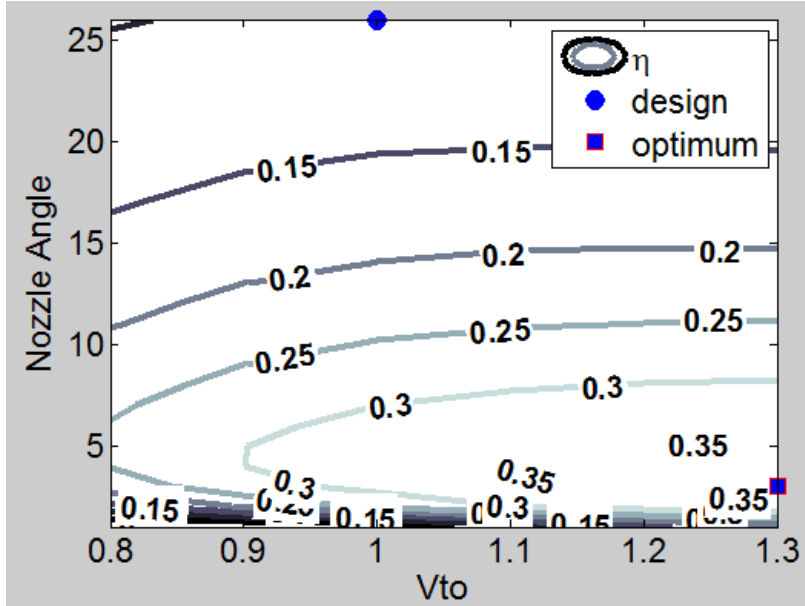


Figure 4-10: Rotor-1, Nozzle-4 performance at various nozzle exit angle and RPM. Efficiency increases as the nozzle angle is close to being tangential to the rotor.

Table 4-1: Turbine Hardware and Operating Specifications

| Turbine diameter | Space b - $\mu\text{m}$ | Thick t - $\mu\text{m}$ | Disks | $\xi_i$ | Gap s - mm | Clearance c - $\mu\text{m}$ | Rough $\epsilon$ | Profile n (PO) | $N_{RE}$ |
|------------------|-------------------------|-------------------------|-------|---------|------------|-----------------------------|------------------|----------------|----------|
| 2 mm (micro)     | 35                      | 18                      | 19    | 0.4     | 1          | 53                          | 0.05             | 5 (48)         | 8        |
| 4 cm (small)     | 86                      | 43                      | 155   | 0.35    | 2.6        | 200                         | 0.01             | 3.5 (36)       | 6        |
| 30 cm (big)      | 157                     | 79                      | 635   | 0.3     | 4.8        | 1500                        | 0.001            | 2 (24)         | 4        |
| 1 cm (R1-N4)     | 125                     | 125                     | 20    | 0.47    | 0.5        | 65                          | 0.05             | 2 (24)         | 5        |

## 4.8 Mapping Experimental Results to Ideal Performance

In here the head loss factor and the shaft power lost factors are derived for the test system runs and a mapping methodology is used to verify the loss factors.

### 4.8.1 Test Rotor Performance Analysis

An ideal performance surface for rotor 1 is generated with  $Vr_o = 0.1$ ,  $\xi_i = 0.4645$ ,  $n = 2$ , while the flow tangential velocity parameters and the Reynolds number vary across the experimental range. The predicted and experimental performance of the three nozzles R1-N3, R1-N4, and R1-N7 at an estimated flow rate indicator of  $\sim 0.1$  ( $0.08 < Vr_o < 0.11$ ) is picked and mapped onto the ideal rotor 1 surface (Figure 4-11).

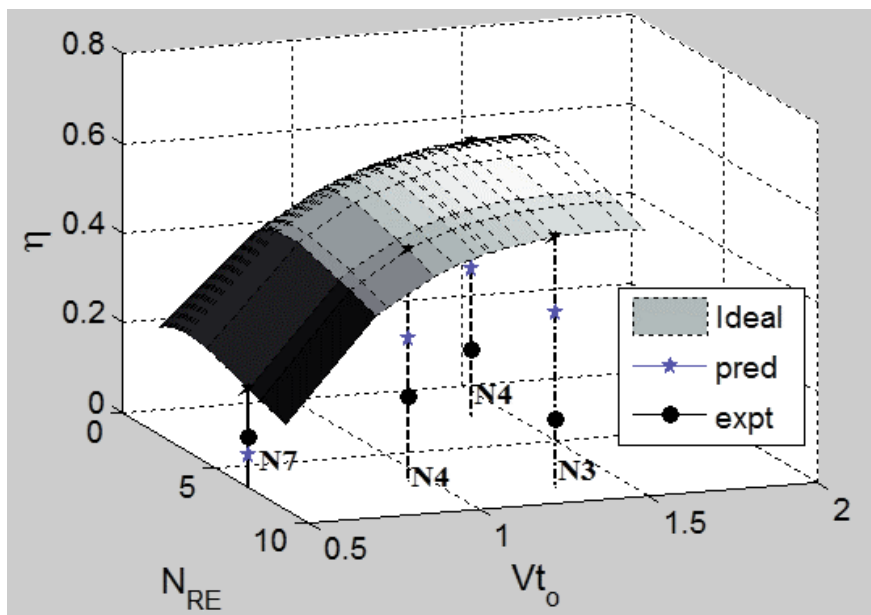


Figure 4-11: Rotor 1 performance surface, projection of experimental and predicted efficiencies for N3, N4, and N7 onto the ideal efficiency surface of R1 with flow profile  $n = 2$ ,  $Vr_o = 0.1$ .

For the test system with rotor 1 and nozzles 3, 4, and 7, tangential velocity, pressure drop, and momentum transfer are compared with the 30 cm reference turbine (Figure 4-12). At the exit, rotor 1 exhibits higher tangential velocity compared with the reference rotor. Momentum analysis shows that for rotor 1, nozzles 3, 4, and 7 are approximately 85%, 60%, and 25% as efficient as the 30cm reference system (respectively). The pressure drop in the rotor is also higher in the test system, reducing overall efficiency.

## 4.8.2 Test System Model

The test system model is derived in two steps:

- 1) Head loss  $p_{loss}$  is modeled as a polynomial in flow rate, and the coefficients ( $a_0$ ,  $a_1$ ,  $a_2$ ) are derived by regression from ideal heads and corresponding test heads at different flow rates.
- 2) Shaft power loss  $T_{loss}$  is modeled as the average percentage loss of prediction efficiencies. Major disk friction loss is a linear function of torque, and this is also seen in our experiments (Figure 3-7). For this system,  $a_0=0$ ,  $a_1= 1.81$ ,  $a_2= 0.017$ ,  $T_{loss} = 0.586$ ,  $q$  is in  $cm^3/min$ , and  $p_{loss}$  is in Pascal. These estimates are used to map the ideal turbine efficiency to predicted efficiency  $\eta_{id2pr}$  first, and then to experimental efficiency  $\eta_{id2ex}$  (Eqs.4-24, and 4-25 ).

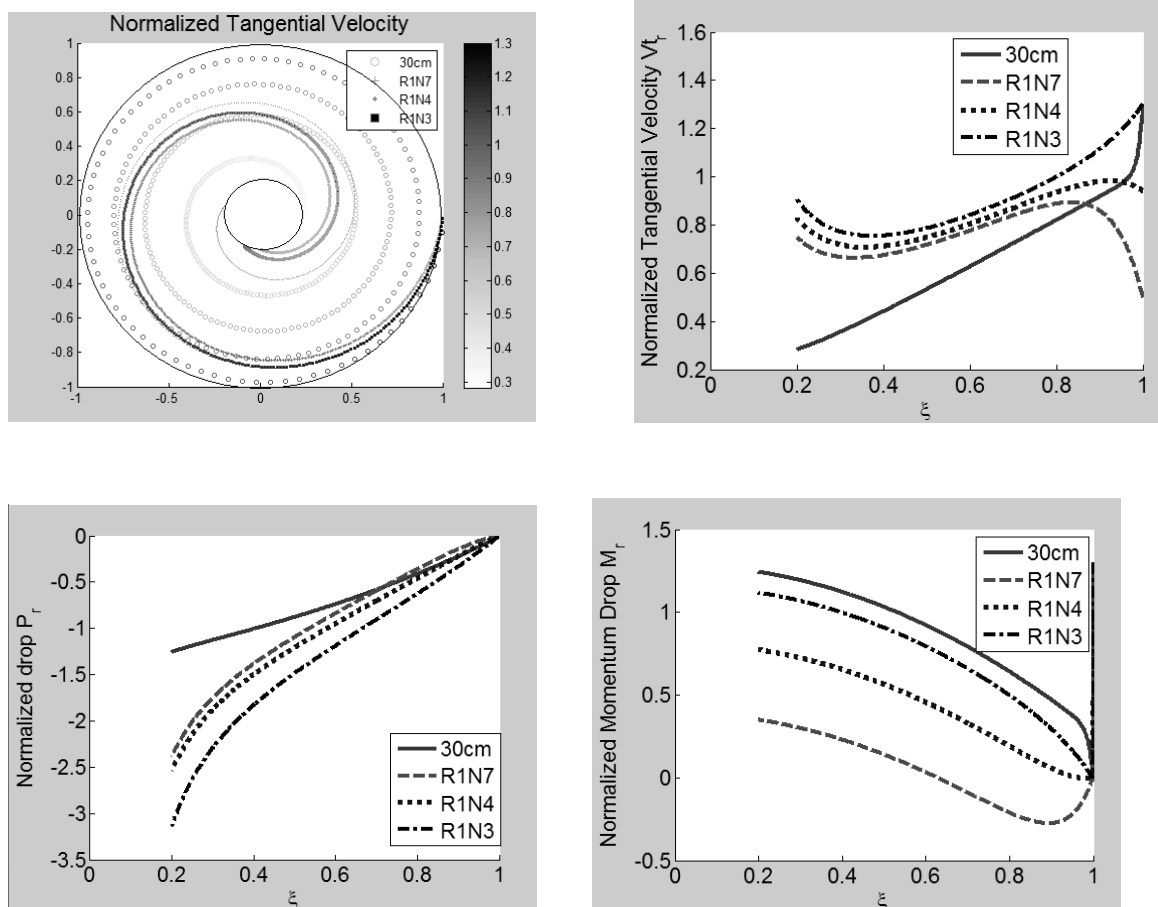


Figure 4-12: Test rotor 1 performance for nozzles 3, 4, and 7 vs. 30 cm reference rotor. (Top left) Normalized tangential velocity in the flow path, inside the rotor. (Top right) Normalized tangential velocity with respect to rotor radius ratio. (Bottom left) Pressure drop and (Bottom right) momentum transfer with respect to radius ratio. All test nozzle curves show higher unspent kinetic energy, higher pressure drop, and lower torque transfer compared with the reference turbine. Nozzle 7 performance is especially poor.

$$(a_2, a_1, a_0) = \text{polynomial\_order\_2}(q, (p_{\text{ideal}} - p_{\text{expt}})) \quad 4-21$$

$$p_{\text{loss}} = a_0 + a_1 q + a_2 q^2 \quad 4-22$$

$$T_{\text{loss}} = \langle \{(\eta_{\text{pred}} - \eta_{\text{expt}})/\eta_{\text{pred}}\} \rangle \quad 4-23$$

$$\eta_{\text{id2pr}} = \left( P_{\text{ideal}} / (P_{\text{ideal}} + P_{\text{loss}}) \right) (\eta_{\text{ideal}}) \quad 4-24$$

$$\eta_{\text{id2ex}} = (1 - T_{\text{loss}}) (\eta_{\text{id2pr}}) \quad 4-25$$

### 4.8.3 Analytical-to-Experimental Mapping

Rotor 1, nozzle 3 tests are conducted at flow rates ranging from 2 cm<sup>3</sup>/s to 15 cm<sup>3</sup>/s. The experimental, predicted, and ideal efficiencies are derived using test and theoretical efficiencies (Eqs. 2-1, 3-18, and 3-19), and mapping is generated using the polynomial approximations for the losses (Eqs. 4-24, 4-25). Figure 4-13 shows the momentum efficiency, the ideal efficiency, the predicted and the experimental efficiencies along with the corresponding two mappings.

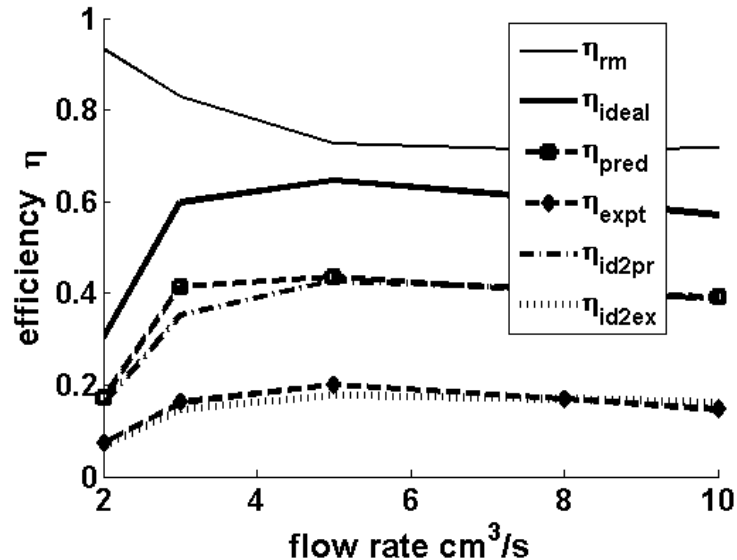


Figure 4-13: R1-N3 test system efficiencies. Ideal turbine efficiency maps first to the prediction ( $\eta_{\text{id2pr}}$ ), then to the experimental efficiency ( $\eta_{\text{id2ex}}$ ).

#### 4.8.4 *Conclusion*

In this chapter, we discussed the losses in a turbine. The hardware and operating parameters that contribute to various losses are identified over the wide range of turbines from 2 mm in diameter to 500 mm in diameter. The study also included our 1 cm-test turbines; it quantified the losses and provided an ideal performance surface for rotor-1.

From this study, we see that the loss behavior is dependent on the rotor size, increasing as the rotor scales down. The next chapter investigates in detail the effect of scaling on the turbine performance and recommends constraints on the design for maximizing torque transfer while minimizing the losses. Examples of constant power density designs and designs for particulate mediums are discussed.

# Chapter 5

## 5 Design Constraints, Scaling Criteria and Sensitivity Analysis

---

In this chapter, a set of design constraints is developed based on the research described in the previous chapters. Scaling the properties of a Tesla turbine is also discussed, and the effects of scaling for constant head, disk spacing, and power density are analyzed. Two kinds of designs with examples are given. First provides a design specification using a constant power density approach with no restrictions on inputs and the second provides an optimum design, given the input specification for head, flow rate and particulate size. Performance of theoretical and practical turbines from the published papers are evaluated and the observed discrepancies are reconciled.

### 5.1 Design Approach

With control over the flow profile and the operating Reynolds number, non-dimensional rotor behavior can be maintained across scaling (Figure 3-5). By selecting flow and hardware parameters based on scaling, the various loss factors can be greatly minimized.

### 5.2 The Optimal Rotor

The five dimensionless parameters  $n$ ,  $V_{to}$ ,  $V_{ro}$ ,  $RE_{rot}$ , and  $\xi_i$  that affect rotor performance are studied in order to pick an operating range for lossless turbines. These parameters also control the number of revolutions that fluid makes before exiting the rotor.

#### 5.2.1 Flow Profile $n$

Uniform flow with  $n=5$  broadens the efficiency curves covering higher rotor speeds relative to parabolic flow with  $n=2$ . With micro rotors, for which the fluid path inside the rotor is short, higher speeds are needed to achieve higher power and watt-range power density. As demonstrated earlier (Disk Roughness and Flow Profile), the profile of the flow depends on surface roughness – a linear relationship exists between the roughness factor and the resulting profile. In this research, profile  $n$  is varied from  $n=5$  for micro 2 mm rotors to  $n=2$  for big 400 mm rotors.

### 5.2.2 Rotor Reynolds Numbers, $RE_{rot}$ and $N_{RE}$

The rotor flow Reynolds number  $RE_{rot}$  is proportional to the rotational Reynolds number  $N_{RE}$  and to the flow rate indicator  $V_{ro}$ . Power output and power density increase as  $RE_{rot}$  increases within the laminar region of operation. Efficiency can be maintained at the same higher level by controlling the fluid profile from parabolic to uniform as  $RE_{rot}$  ( $N_{RE}$ ) increases.  $RE_{rot}$  varies between 0.16 and 4.0 for the water turbines presented here, with an optimum value from 1.28 for 2 mm rotors to 0.64 for 400 mm rotors.

### 5.2.3 Non-dimensional Fluid Tangential Velocity, $V_{to}$

For a normalized average tangential velocity  $V_{to}$  of less than 1, the rotor imparts a portion of its torque to the fluid, resulting in a sharp drop in shaft power and efficiency. When  $V_{to}$  approaches 1, the fluid makes many turns inside the rotor before it reaches the exhaust, transferring a large portion of its momentum to the rotor but at low power. As  $V_{to}$  increases above 1, the power transfer also increases but efficiency drops because of the increase in kinetic energy loss at the exhaust. Tesla himself suggested a normalized velocity of 2.0 [5], and Lawn [2] used values between 0.8 and 1.3. The experiments here suggest that the optimum range for  $V_{to}$  is between 1.1 and 1.3, where a power density gain of 20% can be achieved for an efficiency loss under 5%.

### 5.2.4 Non-dimensional Flow Rate indicator, $V_{ro}$

As normalized radial velocity  $V_{ro}$  decreases, efficiency increases and power density decreases. When radial velocity is high, efficiency drops but power density increases. The optimum range is between 0.01 and 0.09.

### 5.2.5 The Exhaust to Rotor Radius ratio, $\xi_i$

When the exhaust radius is larger than 0.6, fluid exits the rotor without transferring all of its momentum. When the exhaust radius is smaller than 0.2, the rotor's Reynolds number might exceed the Nendl limit of 10, and the fluid at the exhaust can turn turbulent – wasting fluid momentum. The optimum range for this parameter is between 0.3 and 0.4 (Figure 3-4).

## 5.3 Minimizing Losses

In an ideal turbine, efficiency would be determined by the rotor pressure drop  $P_i$  and the kinetic energy at the rotor input  $KE_{in}$ . In a real system, there are many sources of loss, and (importantly) these are scale-dependent. Figure 4-6, Figure 4-7, and Figure 4-8 show the performances of a 2 mm, a 4 cm, and a 30 cm rotor both with no loss and with all losses.

### 5.3.1 Head Loss Minimization

Nozzle loss is the most significant contributor to head loss. All other head loss contributors can be minimized by good design practices, but nozzle loss depends on turbine dimensions and operating flow rates. As turbines scale down, the nozzle Reynolds number  $RE_{noz}$  drops, increasing loss. The following observations are relevant to scaling in this regard.

We can minimize nozzle loss by operating near the peak laminar Reynolds number wherever feasible. This corresponds to  $RE_{noz} \sim 2200$ . For higher Reynolds number, nozzle loss can be minimized by lowering  $rough_{noz}$ , the relative roughness. The effect of Reynolds number in the transition range from laminar to turbulent is not defined. This corresponds to  $RE_{noz}$  values from 2300 to 4000. This region can be avoided by changing the operating regions and the nozzle dimensions.

A conceptual drawing for nozzle implementation is shown in figure below.

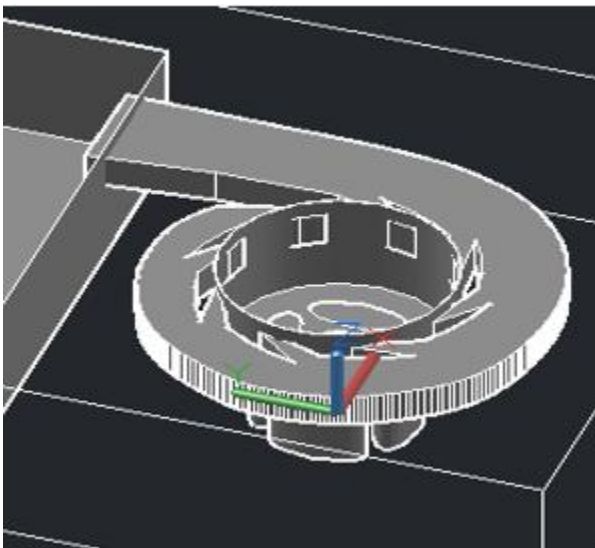


Figure 5-1: Spiral Nozzle: Eight slit nozzles scanning the entire rotor stack located around the rotor. Length of the nozzles is small. The width of the slit nozzles are shown exaggerated. Normally the nozzle slit width for this implementation is less than  $5^\circ$

The nozzle loss scales with  $L_{noz}/D_{noz}$ , the length to hydraulic diameter of the nozzle. So the length of the nozzle should be minimized using techniques such as plenum chambers [15].

Having many small nozzles around the rotor increases the nozzle loss, due to the decrease in  $D_{noz}$ , the hydraulic diameter. Number of nozzles should be minimized.

The orientation of the nozzles should be close to tangential to the rotor.

### 5.3.2 *Shaft Power Loss Minimization*

The trapped fluids between the enclosure and the rotor can cause very high loss to the turbine performance. In Figure 4-4, it can be seen that the test rotor performance is largely limited by this loss.

Gap loss can be reduced by increasing the gap between the end disks and the enclosure. When gap value is greater than  $20*(b+t)$ , this loss reduces to less than 5%. It is also improved by reducing fluid entrapment in the gap with better sealing and drainage (Eq. 4-9).

Because tip friction depends on  $t/c$ , decreasing disk thickness or increasing clearance improves performance (Eq. 4-14). When increasing rotor tip clearance, proper sealing should be provided to prevent fluid from escaping through the clearance into the gaps at the ends of the rotor [27].

Higher rotor speed increases the Reynolds number  $RE_{gap}$ , thus reducing tip loss. However, higher rotor speed increases bearing loss.

Maintaining the Nendl number at less than 10 minimizes turbulence loss in the rotor path. The Nendl number is proportional to  $RE_{rot}$  and indirectly proportional to  $\xi^2$  (Eq. 4-16) and imposes additional constraints on exhaust designs.

### 5.3.3 *Minimizing Other Losses*

Volume leakage loss, entry impact loss, exhaust path loss and bearing loss correspond to almost 10% of turbine efficiency and most of it can be recovered using targeted designs.

The end disks and the turbine enclosure at the end disks can be made larger to contain the fluid volume in the rotor space, reducing volume loss. Labyrinth sealing arrangements can also be used to reduce leakage.

Impact loss at the leading edge can be minimized by reducing disk thickness.

Shaft-less rotors accommodate higher power transfer while maintaining the desired exhaust area. Roughening the rotor surface increases the momentum transfer while maintaining the efficiency.

Using air or magnetic bearings for small and micro turbines and ball bearings for bigger turbines minimizes bearing loss, thus improving efficiency.

A table is presented with the parameters, suggested operating values, constraints, and their effects on turbine performance (Table 5-1), with the goal of maximizing efficiency and power density for a given head and flow specification.

## 5.4 Scaling Approach

A practical approach can scale turbines using customer preference for desired RPM, power density, or efficiency. Various scaling functions applied to rotor dimensions determine their effect on overall turbine efficiency and power density. A hydro turbine with a 300 mm rotor with 210  $\mu\text{m}$  interdisk space is used as the reference rotor to study these effects.

### 5.4.1 *Scaling Rotor Hardware Parameters*

Scaling of the rotor diameter and the nozzle and turbine dimensions can be related to rotor dimensions. However, a proportional scaling down of the whole turbine is not optimal, as the power density varies inversely with the fourth power of scaling in this case. Beans [5] investigated performance sensitivity to interdisk spacing and showed about an order of magnitude's difference in power output for the same-sized rotor with different disk spacing.

To study this, the radius is scaled by  $r_{\text{scale}}$  and the interdisk space is scaled by a power  $k$  of  $r_{\text{scale}}$  -  $b_{\text{scale}} = (r_{\text{scale}})^k$ , where  $k = 0.0, 0.15, 0.33, 0.5, \text{ and } 0.8$ . Using  $k = 0.5$ , turbines can be designed to operate at a given pressure head. At  $k = 0.33$  the scaling preserves power density, at  $k = 0.8$  the scaling preserves power, and at  $k = 0$  rotor speed (RPM) can be maintained. At  $k = 0.15$ , the reference turbine scales to the 1 cm test turbine. The effect of  $k$  on interdisk spacing, power density, RPM, power, head and flow per disk is shown for the 1 mm to 400 mm in Figure 5-2. In this graph, 300mm rotor diameter corresponds to the reference rotor and all the parameters are given in the scale of the corresponding parameters of that rotor.

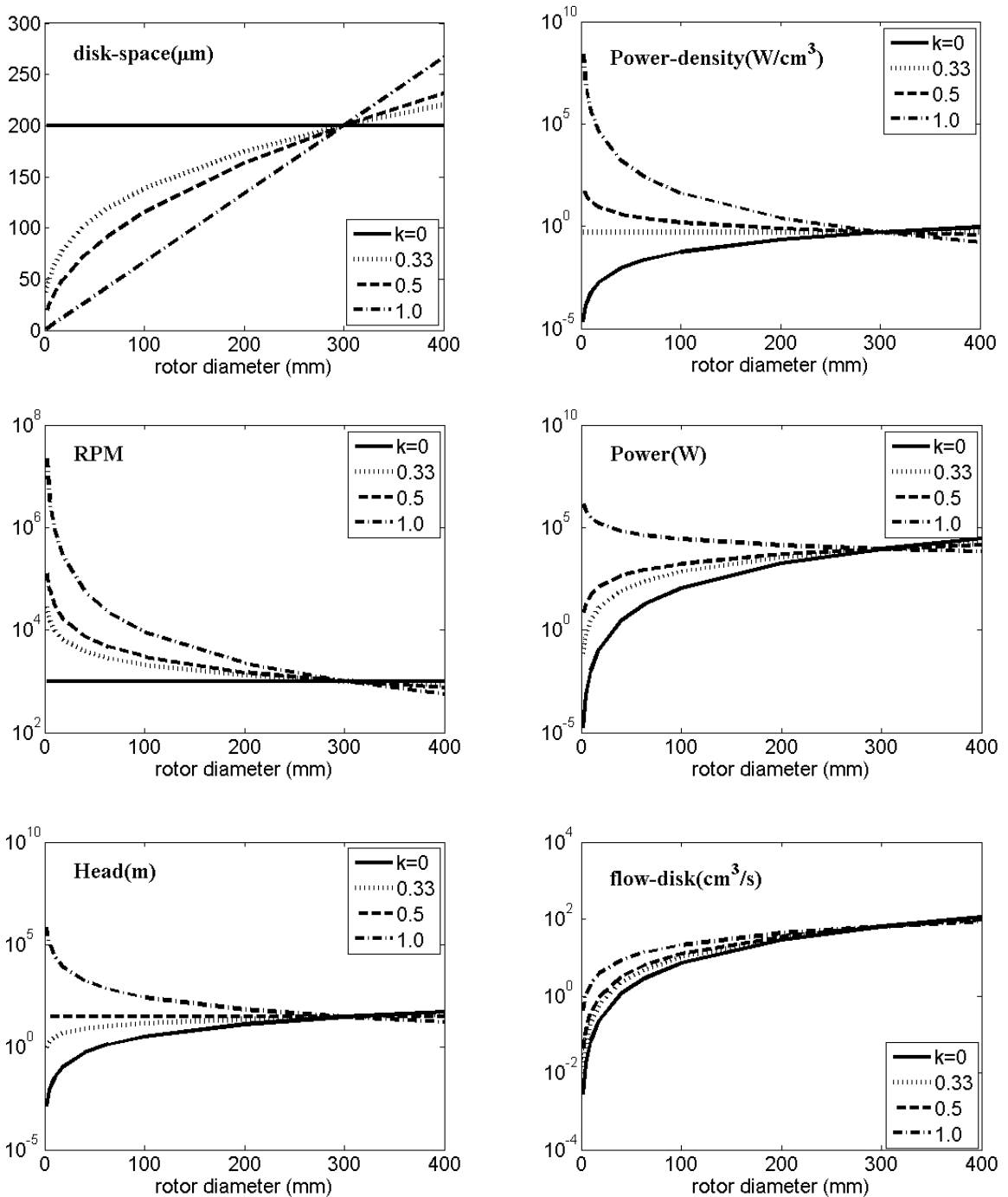


Figure 5-2: Effect of scaling exponent  $k$  on (Top left) interdisk space, (Top right) power density, (Middle left) RPM, (Middle right) power output, (Bottom left) head, and (Bottom right) flow rate per disk, while maintaining optimal non-dimensional operating parameters (based on a 300 mm reference turbine).

## 5.5 Design for Constant power density over the Range of 2 mW to 20 kW Turbines

Optimization for scaling involves the following method, with a power density of about  $2 \text{ W/cm}^3$  as the target for design. To standardize across practical rotors, we keep the rotor height equal to its radius, the disk thickness  $t$  to half of interdisk space  $b$ , the tip clearance to the larger of 1% of the radius  $r_o$  or  $0.2*(t+b)$ , the gap to  $2*(t+b)$ , and the nozzle roughness parameter  $\epsilon$  inversely proportional to the radius. The medium is taken to be particulate-free which makes it feasible to design down to 2 mW power.

A three-level approach is used to design and to specify operating regions for the turbines while scaling across the 1 mm to 400 mm diameter range. First, an operating parameter set for the range is generated at  $k = 0.33$  to provide at least 35% efficiency. Next, power scaling  $k$  for interdisk space is tuned to provide tighter power/cm<sup>3</sup> across the range. Finally, interdisk spacing is tuned linearly to adjust the mean power density to  $2 \text{ W/cm}^3$ .

The test rotors have a diameter of 1 mm, 4 mm, 10 mm, 20 mm, 40 mm, and 200 mm, and the maximum efficiency operating points are derived for each within a range of power density. The resulting parameters  $V_{to}$ ,  $V_{ro}$ ,  $n$ ,  $N_{RE}$ , and  $\xi_i$  are used to derive the operating parameters for all rotors from 1 mm to 400 mm in diameter using piecewise interpolation. The maximum RPM at 1 mm rotor is 130,000. Power density varies 30:1 from  $38 \text{ W/cm}^3$  to  $1.3 \text{ W/cm}^3$ , with efficiency variation from 0.54 to 0.71 (Figure 5-3).

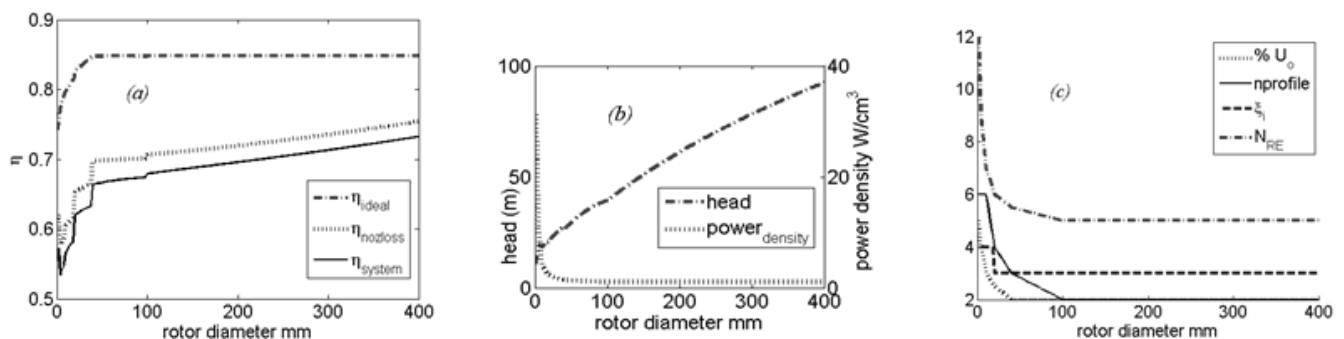


Figure 5-3: Level-1 design for 1 mm to 400 mm diameter rotors;  $k = 0.33$ ,  $V_{to} = 1.3$ , minimum interdisk spacing is  $30 \mu\text{m}$ . (Left) System efficiency (turbine with nozzle and disk friction loss) variation 0.54 to 0.73. (Center) Power density variation  $38 \text{ W/cm}^3$  to  $1.3 \text{ W/cm}^3$ . (Right) Flow control parameters.

Interdisk spacing for the small rotors is increased to lower the relative power density of the smaller rotors, as well as the speed of the rotor. A study for  $k$  from 0.29 to 0.33 along with minor modifications to the optimized parameters determined that  $k = 0.3$  minimized the power density variation to 2:1 (from  $4.4 \text{ W/cm}^3$  to  $2.2 \text{ W/cm}^3$ ) while keeping efficiency in the range of 0.41 to 0.75 (Figure 5-4).

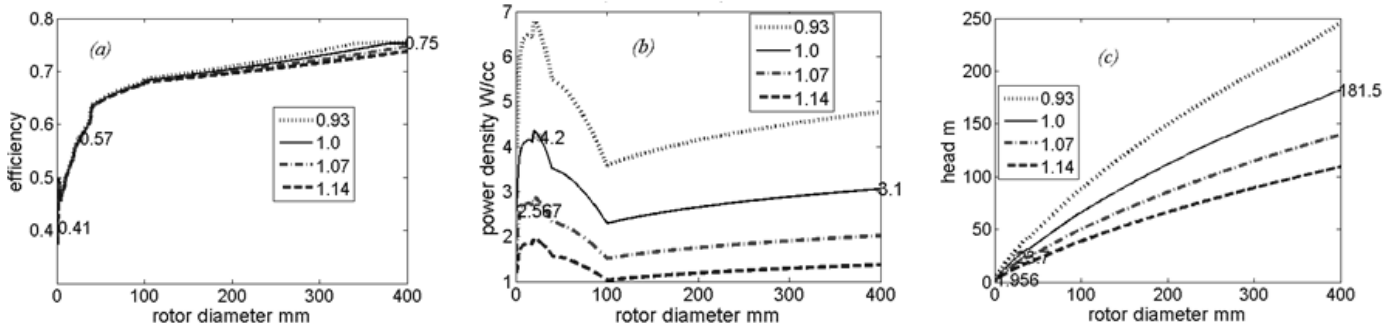


Figure 5-4: Design graphs for 1 mm to 400 mm diameter rotors;  $k = 0.3$ ,  $NRE = 5$ ,  $Vr_o$  and  $Vt_o$  adjusted to meet the desired efficiency and power density,  $b = 32.5 \mu\text{m}$  for 1 mm rotor at scaling = 1. Level-3 optimization with interdisk space linear scaling at 0.93, 1.0 (Level-2, solid line), 1.07, and 1.14. Level-2, parameter range at scaling = 1. (Left) System efficiency 0.41 to 0.75 (mostly constant over the scaling range). (Center) Power density  $2.2 \text{ W cm}^3$  to  $4.4 \text{ W cm}^3$ . (Right) Head 2 m to 180 m.

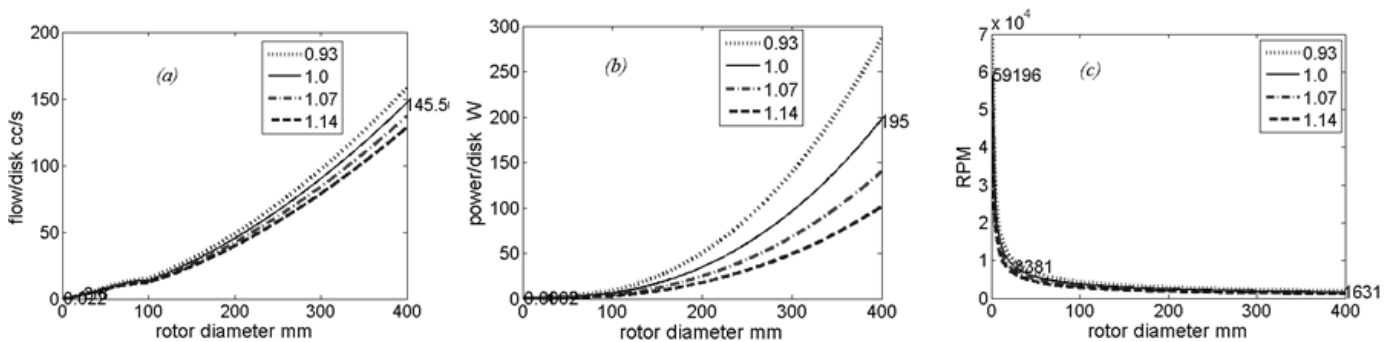


Figure 5-5: Level-3 design graphs for rotors from 1 mm to 400 mm in diameter; all parameters as in Figure 5-4. (Left) Flow rate / disk is from  $20 \text{ mm}^3/\text{s}$  to  $160 \text{ cm}^3/\text{s}$ . (Center) Power in watts/disk varies by approximately 300% as interdisk space scaling varies by 21%. (Right) RPM varies by 42% in the same range.

A one percent change to interdisk spacing results in about minus six percent change to spacing is studied at four 7% steps, varying from -7% to +14% (Figure 5-4 and Figure 5-5). With minor changes to interdisk spacing, the power/disk can be tuned almost 1:3

without significant change to efficiency or RPM. Table 5-2 shows sample designs for four turbines, from micro to big, using 1.5 W/cm<sup>3</sup> specifications.

### 5.5.1 Design Constraint Table

Table 5-1: Turbine design parameters and constraints

| name  | Value Range  |
|---|--|
| b interdisk space                               | 10* particulate size < b ; b ↑ power density ↓<br>filter the medium to minimize b ; b nominal < 200 μm               |
| ε aspect ratio = b / r <sub>o</sub>             | Smaller than 0.05 to satisfy the assumptions in the rotor flow characterization. ε nominal < 0.01                    |
| ξ <sub>i</sub> , radius ratio                   | 0.3 < ξ <sub>i</sub> < 0.4 ; 0.4 for micro to 0.3 to large turbines  |
| t disk thickness                                | t < b/2, as minimum as possible, but enough disk mass to support the power/disk. t ↓ tip loss ↓                      |
| c clearance                                     | (b + t) < clearance to keep tip loss < 2%  |
| s gap   | 20*(b+t) < gap to keep the gap loss < 2% ; higher the rotor radius or lower the flow indicator , higher the gap loss |
| V <sub>noz</sub> nozzle velocity                | V <sub>noz</sub> = flow rate /nozzle area  |
| RPM rotor speed                                 | RPM ↑ as radius r <sub>o</sub> ↓ ; RPM ↑ as V <sub>noz</sub> ↑   |
| PO Poiseuille #<br>n profile # =PO/8 -1         | 24 < PO < 48; 2 < n < 5; disk roughening ↑ PO ↑; small rotors need higher PO to achieve good power density.          |
| RE <sub>rot</sub> Rotor RE #                    | 0.64 < RE <sub>rot</sub> < 1.28 ; smaller the rotor, larger the RE <sub>rot</sub>                                    |
| V <sub>r<sub>o</sub></sub> , flow indicator     | 0.01 < V <sub>r<sub>o</sub></sub> < 0.08, nominal value: 0.04 ; V <sub>r<sub>o</sub></sub> ↓ efficiency ↑            |
| V <sub>t<sub>o</sub></sub> , velocity indicator | 1.05 < V <sub>t<sub>o</sub></sub> < 1.5 ; nominal value: 1.2 ; V <sub>t<sub>o</sub></sub> ↑ power density ↑          |
| Q <sub>disk</sub> flow per disk                 | ~ cm <sup>3</sup> /s; Q <sub>disk</sub> proportional to RE <sub>rot</sub> , r <sub>o</sub> , and 1/ε                 |
| N <sub>disks</sub> # of disks                   | Flow rate / Q <sub>disk</sub> - can be split into many smaller rotors.   |
| Nozzle Type                                     | Single slit for smaller rotors , 1-4 slits for larger -  |
| H <sub>noz</sub> slit length                    | Slit covers all the active disks = N <sub>disks</sub> *(b+t)   |
| Nozzle position                                 | Flow direction tangential to the rotor   |
| W <sub>noz</sub> , nozzle width                 | Flow rate / (V <sub>noz</sub> *H <sub>noz</sub> ); can be distributed around the rotor.                              |
| L <sub>noz</sub> , nozzle length                | Minimize to reduce nozzle loss – use Plenum chamber  |

|  |  |
|--|--|
| efficiency indicator = $Q_{\text{disk}} / \omega r_o^3$      | Smaller than 0.001 to achieve rotor efficiency > 70% for smooth disks; this can be increased with disk roughening. |
| $\alpha$ , $N_{\text{endl}} = RE_{\text{rot}} / (4 \xi_i^2)$ | $\alpha < 10$ for Laminar flow in the rotor - nominal = 2.0  |
| $RE_{\text{noz}} = V_{\text{noz}} * D_{\text{noz}} / \nu$    | Close to 2200, for micro and small rotors with low flow.<br>Avoid 2300 – 4000 $RE_{\text{noz}}$ range              |
| Rotor assembly   | Shaft-less rotors to maintain exhaust area while maximizing the active momentum transfer area.                     |
| Bearing  | Air or magnetic bearing to minimize bearing loss as rotor RPM increase when rotor size go down.                    |
| Turbine assembly and operation                               | Minimize volume loss, gap loss and tip loss with specially designed sealing.                                       |

### 5.5.2 Constant Power Density Design Examples

Table 5-2: Possible constant power density Designs for four hydro turbines from micro to big. Here particulate size in the medium is not taken in to account.

| Turbines            | Parameter                           | Big        | Medium     | Small     | Micro     |
|---------------------|-------------------------------------|------------|------------|-----------|-----------|
| Input Specification | Head [m]                            | 75         | 25         | 4         | 2         |
|                     | Flow rate [cm <sup>3</sup> /s]      | 30000      | 1000       | 5         | 1         |
|                     | Power density [W/cm <sup>3</sup> ]  | 1.5        | 1.5        | 1.5       | 1.5       |
| Output              | Power [W]                           | 15430      | 157        | 0.075     | 0.008     |
|                     | Power density [W/cm <sup>3</sup> ]  | 1.23       | 1.48       | 1.68      | 1.4       |
|                     | RPM                                 | 1708       | 3965       | 19727     | 29900     |
| Rotor               | Efficiency                          | 0.7        | 0.65       | 0.46      | 0.48      |
|                     | Radius [mm]                         | 118        | 29         | 2         | 1         |
|                     | Disk space, b [ $\mu\text{m}$ ]     | 167        | 110        | 49        | 40        |
|                     | Disk thickness, t [ $\mu\text{m}$ ] | 83.5       | 55         | 24.5      | 20        |
|                     | Ndisks                              | 572        | 122        | 24        | 15        |
|                     | Radius ratio $\xi_i$                | 0.3        | 0.3        | 0.4       | 0.4       |
| Enclosure           | Disk roughness PO                   | 24         | 24         | 48        | 48        |
|                     | Gap, s [ $\mu\text{m}$ ]            | 500        | 330        | 148       | 120       |
|                     | Clearance, c [ $\mu\text{m}$ ]      | 1180       | 290        | 30        | 24        |
| Nozzle              | Height, Hnoz [mm]                   | 144        | 20         | 1.8       | 0.9       |
|                     | Width, Wnoz [mm]                    | 7.6        | 3.35       | 0.59      | 0.31      |
|                     | Rough ratio [ $\mu\text{m}$ ]       | 0.004 (56) | 0.008 (48) | 0.04 (37) | 0.05 (25) |

|                                    |                             |        |       |      |      |
|------------------------------------|-----------------------------|--------|-------|------|------|
| Resulting dimensionless Parameters | Flow indicator $V_{ro}$     | 0.02   | 0.034 | 0.08 | 0.08 |
|                                    | Velocity indicator $V_{to}$ | 1.3    | 1.23  | 1.15 | 1.15 |
|                                    | Rotor RE # $RE_{rot}$       | 0.4    | 0.68  | 1.6  | 1.6  |
|                                    | Rotational RE# $NRE$        | 5      | 5     | 5    | 5    |
|                                    | Fluid profile $n$           | 2      | 2.7   | 6    | 6    |
| Loss                               | $RE_{noz}$                  | 390000 | 89000 | 4280 | 1630 |
|                                    | Head-loss fraction          | 0.14   | 0.16  | 0.2  | 0.12 |
|                                    | Torque-loss fraction        | 0.03   | 0.03  | 0.07 | 0.11 |

The design examples shown here focus on how to improve the turbine performance, assuming the inputs can be specified to achieve this performance.

## 5.6 Turbine Design for a Given Head, Flow, and Particulate Size

The constant power density design discussed in 5.5, is for a closed-loop system or for an open-loop system with a filtered motive medium – basically, for systems where particulate size in the medium is not a concern. In this chapter, a more general approach is adopted that includes systems with a contaminated medium (rivers, for example, can contain particles up to 500  $\mu\text{m}$  in size). Design graphs for a range of head, flow rate, and particulate size are presented and the effect of these inputs on performance is discussed. The published turbines are mapped on a 3D grid performance space and analyzed. A graphical user interface has also been created to assist with design optimization, described in detail in Appendix page: 124

### 5.6.1 Methodology and Tool

Based on the design constraints and scaling techniques presented so far, and given a set of inputs such as head, flow, and particulate size, the search for an optimum turbine follows these steps:

- 1) The rotor diameter range for the design is set as 2 mm to 500 mm.
- 2) Radius and interdisk space are varied by 11 values each, resulting in 121 turbine designs (found to be adequate for optimum turbine design specification),

- 3) Minimum interdisk space  $b_{\min}$  is set to  $\max(40 \mu\text{m}, 10 \times \text{particulate size})$  to maintain clog-free flow, and interdisk space increment is set to  $\max(20 \mu\text{m}, 0.1 \times b_{\min})$  to determine the optimum spacing and radius combination.
- 4) Minimum radius  $r_{\min}$  is set to satisfy the interdisk space to radius (aspect ratio) requirement of 10, and radius increment is set as  $2 \times r_{\min}$ .
- 5) At each radius and interdisk space,  $RE_{\text{rot}}$ ,  $n$ , and  $\xi_i$  are chosen based on the design constraints specified in the previous section. Dynamic head  $V_{\text{noz}}$  and flow  $Vt_o$  indicators are varied to select a set of four candidate designs with efficiency, power density, aspect ratio and head as optimality criteria at that radius.
- 6) The method is repeated over the radius range (4) at varying interdisk spacing (3) until at least half of the designs are valid and obey all user requirements (for a maximum of four sets of 121 possible designs).
- 7) A selection criteria based on power, power density, and size is applied to recommend four designs, one from each set of all valid designs.

This method is used in redesigning the reference rotor of 150 mm radius, based on its input specifications (40 m head, 30000 cm<sup>3</sup>/s flow rate, and 211  $\mu\text{m}$  interdisk space – corresponding to 21  $\mu\text{m}$  particulate size). Figure 5-6 shows the power and power density curves against the radius range of possible turbines. The optimum design corresponds to a 66 mm radius turbine, with 0.96 W/cm<sup>3</sup> power density, 8200 W power, and an aspect ratio of 2.

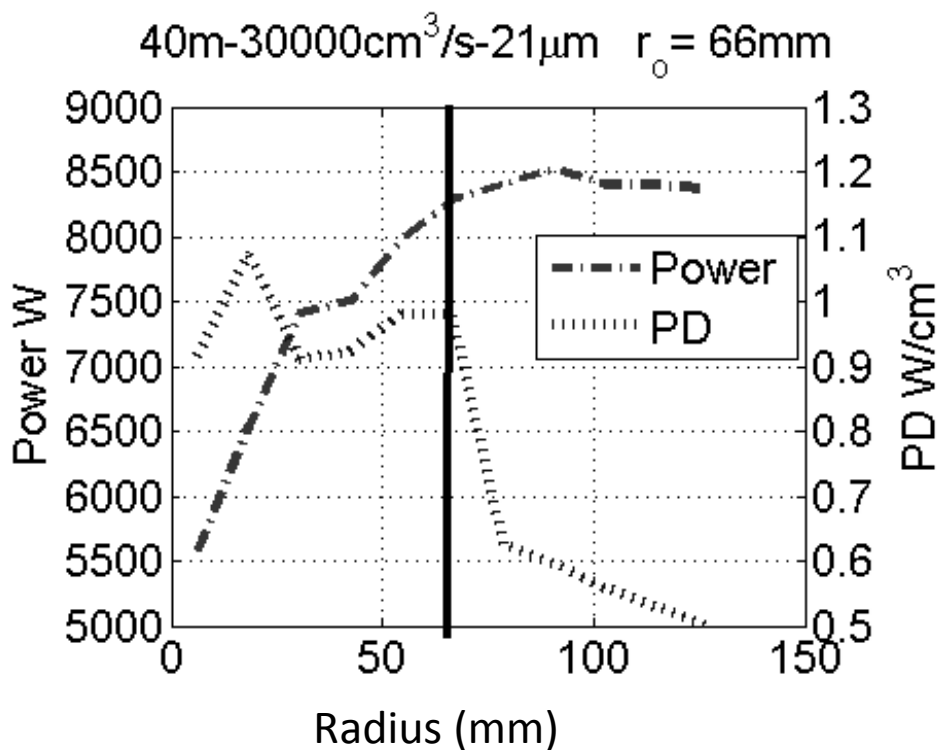


Figure 5-6: Power and power density variations for rotors in radius range from 2 mm to 150 mm at the input specifications of the (150 mm radius) reference rotor. The optimal turbine radius according to our study is 66 mm.

### 5.7 Sensitivity Analysis and Verification

Here, the performance sensitivity of the designed turbine to flow and head variation is analyzed. Figure 5-7 shows efficiency, power density, power, and RPM in relation to head and flow variations for the designed turbine in Figure 5-6. The analysis demonstrates that efficiency is very stable (less than 2% variation) even when head and flow vary by as much as 20%. RPM varies with the head, while power and power density vary with the input power.

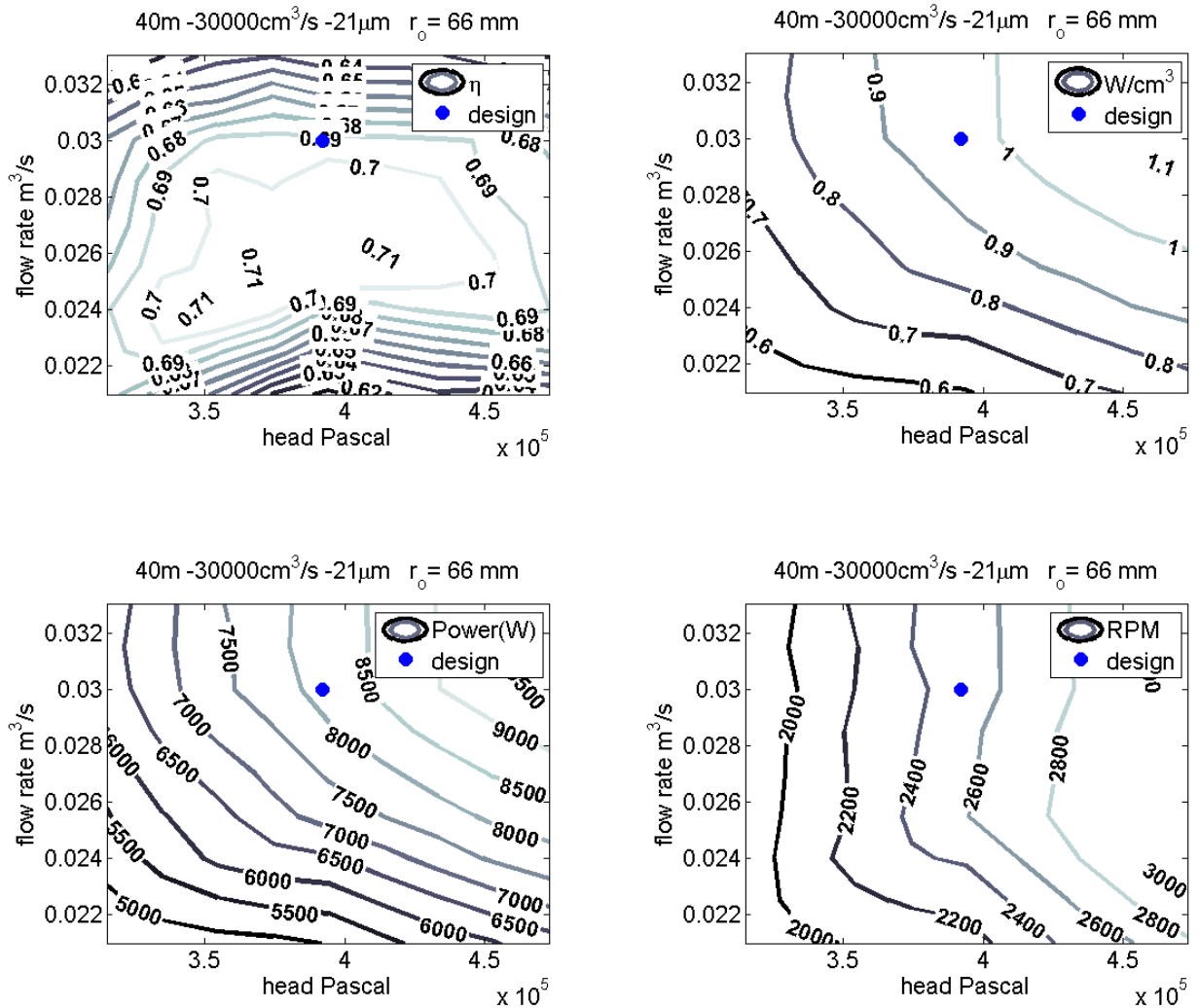


Figure 5-7: Head and flow sensitivity analysis of the designed turbine. (Top right) Efficiency is relatively stable (+/- 2%) over a wide range of input head (+/- 20%) and of input flow (+10%/-20%). Values of (top right) power density, (bottom left) power, and (bottom right) RPM.

## 5.8 Design Graphs and Mapping of Published Turbines

### 5.8.1 Design Graphs

To cover both the current application range and the published turbines, turbines are designed with five variations in head between 2 m and 50 m, four variations in flow rate

between 10 cm<sup>3</sup>/s and 30000 cm<sup>3</sup>/s, and six variations in particulate size ranging from 4 μm to 500 μm.

At each input combination, a turbine design is selected based on efficiency criterion, using the methodology in 5.6.1. Performance and parameters of the designed turbines is presented in Figure 5-8 using 3D slice graphs and following observations are relevant.

Power density increases as dust particles get smaller or as head is increased, at all flow rates

Due to the combined optimality of efficiency and power density, smaller turbines are selected over larger ones in this method with maximum radius at 180 mm.

Smaller the radius, higher the Rotor speed,

In acceptable performance range, efficiency and power density exhibit an inverse relationship.

Larger the flow rate, higher the aspect ratio.

Larger the flow rate, higher the number of disks.

Larger the flow rate, lower the nozzle losses and higher the efficiency

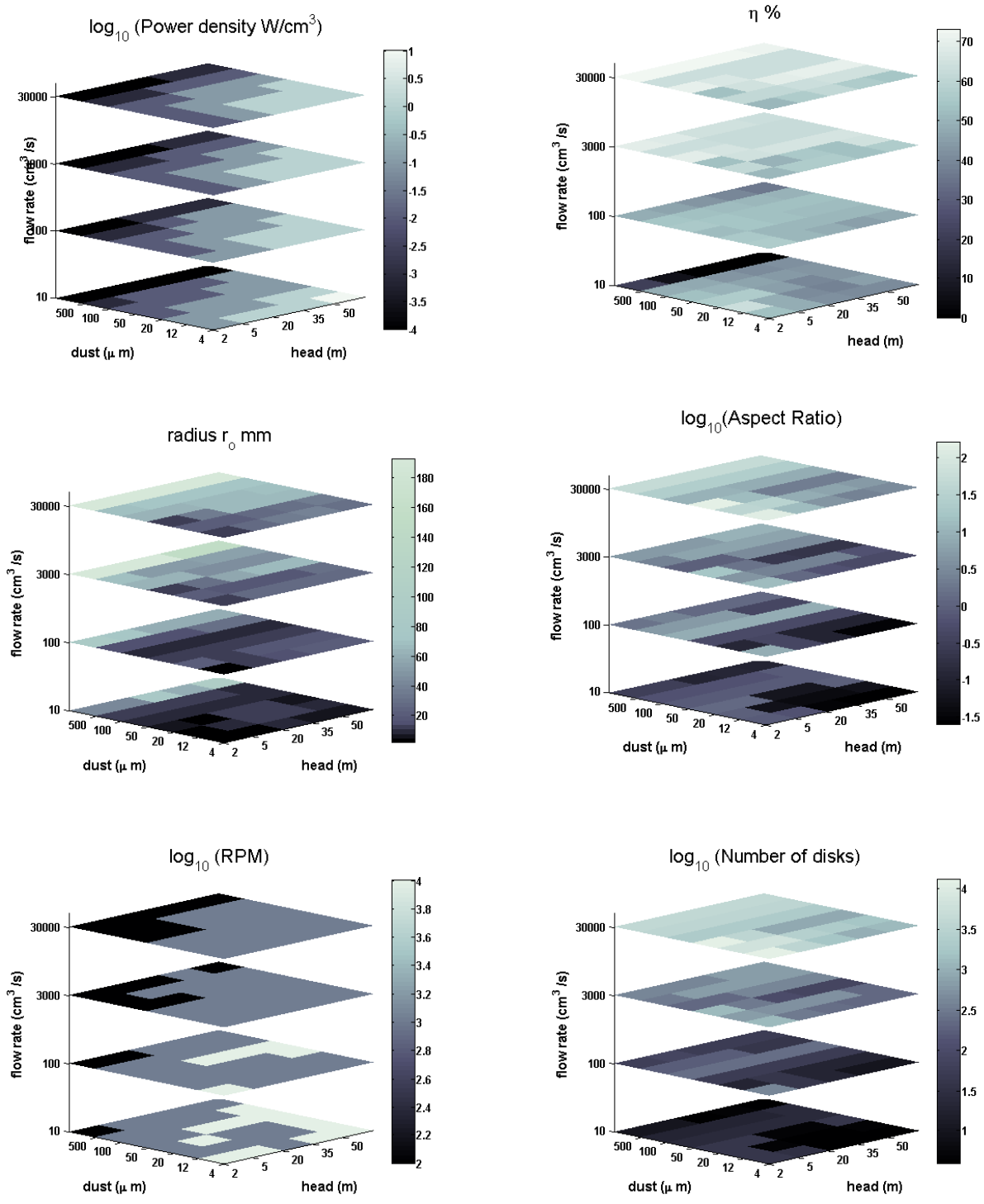


Figure 5-8: 3D slice graphs

### 5.8.2 Mapping of Published Turbines

Four published turbines are redesigned using their input specifications and are shown below on the 3D grid plot of power density and efficiency.

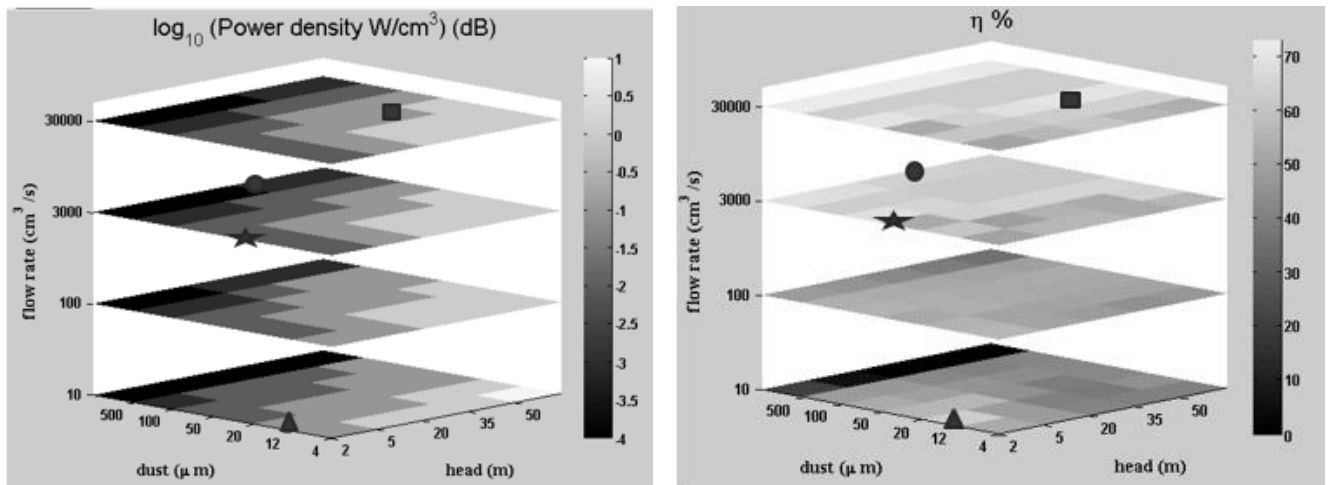


Figure 5-9: Four turbine designs mapped on the 3D grid: 1) triangle - test turbine R1-N4 2) star - the Razak river turbine redesign 3) circle - Ho-Yan's open falls turbine 4) square- Lawn's 30 cm reference hydro turbine. (Left) log10 (power density) plot for 120 turbine designs. Density varies by five orders, and lower dust particle size and higher head both result in higher power density. (Right) Efficiency varies 10% to 70%. In the higher flow range, the inverse relationship between power (efficiency) and power density can be observed.

For the two practical turbines -- test turbine R1-N4 (triangle), and Razak river turbine redesign (star) - the new design efficiency is better than reported, suggesting that the practical turbines designs can be improved with the current design.

For the two theoretical turbines - Ho-Yan's open falls turbine [1] with 5 mW/cm<sup>3</sup> power density and Lawn's 30 cm reference turbine [2] with 85% efficiency - the new design efficiency and power density are lower than reported, suggesting that the practical losses are not taken into account in the theoretical projections of performance.

### 5.8.3 Reconciliation of observed Turbine Discrepancies

Tesla rotors exhibit an inverse square relation between power density and particulate size. For the same head and flow, power density could vary from 2 mW/cm<sup>3</sup> for a 500 μm particulate size to W/cm<sup>3</sup> (~1:400) for a 25 μm particulate size. Due to such high sensitivity, the operation of this turbine at high power density might be limited to closed-loop systems or to open-loop systems with a 200 μm filter.

Tesla rotors also exhibit an inverse relationship between power density and efficiency: higher input head and flow increase power density at the cost of efficiency. In our tests, a 50x power density increase from 0.4 mW to 20 mW was observed at a 50% efficiency loss (from 36% to 18%).

These two tradeoffs are the primary sources of power density variations in published rotors. Ho-Yan's rotor has a 5 mm interdisk space, which can accommodate 500 μm to 1 mm dust particles [1]. At the same input specification, an optimum design resulted in lower performance than reported in the paper: 2 mW/cm<sup>3</sup> power density at 50% efficiency due to losses unaccounted in the paper. However, reducing the interdisk to 1 mm at the same head and flow specification, resulted in 20x increase to power density of 40 mW/cm<sup>3</sup> with slightly higher efficiency of 54%.

In the design graphs, the maximum efficiency is 70% after losses. The published designs do not account for all losses, resulting in claimed efficiencies greater than 85%. As seen in Figure 5-6, for the same input conditions power output (efficiency) can vary by as much as 1 to 2 depending on turbine dimensions and operating parameters. This explains the high variation in the realized efficiency of turbines. For the reference turbine, choosing 150 mm radius design results in about 0.5 mW/cm<sup>3</sup> power density at 67% efficiency, whereas choosing 66 mm radius design doubles up the power density to 0.96 mW/cm<sup>3</sup> at 65% efficiency, a 2% efficiency loss.

Overall, such variations demonstrate the usefulness of design tools for achieving desired power density and efficiency.

### 5.8.4 Designs Examples for Intended Applications

Table 5-3 lists designs for four different applications

1) Razak's low head of 1.2 m and medium flow of 3000 cm<sup>3</sup>/s river turbine [10], is redesigned with two different interdisk space of 200 μm and 500 μm to accommodate different river particulate sizes. A 325% increase in power density for a loss of 15% loss in efficiency can be seen at the lower spacing (200 μm) indicating the need for filters.

2) Williamson's low head of 3.2 m, high flow river turbine [7], is redesigned for medium flow of 12000 cm<sup>3</sup>/s and high flow of 60000 cm<sup>3</sup>/s. The efficiency of 64% and the power density of 90 mW/cm<sup>3</sup> remained the same in both cases, only the length to width of the turbine increased to accommodate the flow increase. This shows we can modularize the turbines and install multiple smaller turbines instead one large.

3) A low flow, low head micro turbine. It is possible to design for 10 cm<sup>3</sup>/s flow and 2 m head with 63% efficiency and 180 mW/cm<sup>3</sup> power density.

4) A low flow, high head Evaporation scavenger. Just increasing the head to 20 m at the same low flow of 10 cm<sup>3</sup>/s results in higher power density of 1.38 W/cm<sup>3</sup> at a lower efficiency of 48%.

Table 5-3: Optimum efficiency design for hydro applications discussed in Chapter 1.3

| Turbines                   | Parameter     | unit                | Razak                |      | Williamson                           |       | Low Flow          |        |
|----------------------------|---------------|---------------------|----------------------|------|--------------------------------------|-------|-------------------|--------|
| Varied parameter and Value |               |                     | Interdisk space (μm) |      | medium/high flow (m <sup>3</sup> /s) |       | low/high head (m) |        |
|                            |               |                     | 200                  | 500  | 0.012                                | 0.06  | 2                 | 20     |
| Input Specification        | Head          | meter               | 1.2                  | 1.2  | 3.6                                  | 3.6   | 2.0               | 20.0   |
|                            | Flow rate     | cm <sup>3</sup> /s  | 3000                 | 3000 | 12000                                | 60000 | 10                | 10     |
|                            | Dust          | μm                  | 20                   | 50   | 20                                   | 20    | 4                 | 4      |
| Output                     | Power         | W                   | 21                   | 25   | 270                                  | 1350  | 0.125             | 0.95   |
|                            | Power density | mW/ cm <sup>3</sup> | 28                   | 6.6  | 90                                   | 90    | 180               | 1380   |
|                            | RPM           |                     | 1194                 | 459  | 1533                                 | 1390  | 9760              | 25700  |
|                            | efficiency    |                     | 0.59                 | 0.7  | 0.64                                 | 0.64  | 0.63              | 0.48   |
| Size                       | height/width  |                     | 5                    | 1.2  | 7.4                                  | 27    | 1.1               | 1.1    |
|                            | Volume        | liter               | 0.37                 | 1.9  | 1.5                                  | 7.5   | 0.0004            | 0.0004 |

|                      |                            |               |       |        |        |        |       |       |
|----------------------|----------------------------|---------------|-------|--------|--------|--------|-------|-------|
| Rotor                | Radius                     | mm            | 23    | 63     | 32     | 35     | 3.7   | 3.7   |
|                      | Disk space, b              | $\mu\text{m}$ | 200   | 500    | 200    | 200    | 120   | 120   |
|                      | Disk thick, t              | $\mu\text{m}$ | 100   | 100    | 100    | 100    | 60    | 60    |
|                      | Ndisks                     |               | 759   | 248    | 1564   | 6419   | 45    | 45    |
|                      | Radius ratio ,<br>$\xi_i$  |               | 0.4   | 0.35   | 0.4    | 0.4    | 0.4   | 0.4   |
|                      | Disk rough,<br>PO          |               | 38.4  | 31.2   | 38.4   | 38.4   | 48    | 48    |
| Enclosure            | Gap, s                     | $\mu\text{m}$ | 6000  | 12000  | 6000   | 6000   | 3600  | 3600  |
|                      | Clearance, c               | $\mu\text{m}$ | 300   | 635    | 320    | 350    | 180   | 180   |
| Nozzle               | Height, $H_{\text{noz}}$   | mm            | 228   | 149    | 470    | 1925   | 8.1   | 7     |
|                      | Width, $W_{\text{noz}}$    | mm            | 4.4   | 6.3    | 4.8    | 5.8    | 0.3   | 0.12  |
|                      | Nozzle roughness           |               | 0.01  | 0.004  | 0.01   | 0.01   | 0.05  | 0.05  |
| Resulting Parameters | Fluid profile, n           |               | 3.8   | 2.9    | 3.8    | 3.8    | 5     | 5     |
|                      | Flow indicator, $Vr_o$     |               | 0.048 | 0.02   | 0.038  | 0.041  | 0.02  | 0.008 |
|                      | Velocity indicator, $Vt_o$ |               | 1.05  | 1.05   | 1.05   | 1.05   | 1.1   | 1.2   |
|                      | RErot                      |               | 0.96  | 0.96   | 0.96   | 0.96   | 1.28  | 1.28  |
|                      | REnoz                      |               | 25800 | 38600  | 50500  | 62000  | 2380  | 2800  |
|                      | REgap                      |               | 65310 | 192780 | 162780 | 180000 | 13780 | 36300 |
|                      | $N_{RE}$                   |               | 5     | 12     | 6.4    | 5.8    | 14.7  | 38    |
|                      | Head indicator, $P_t$      |               | 1.42  | 1.26   | 1.33   | 1.34   | 1.39  | 1.98  |
| Torque indicator, T1 |                            | 0.26          | 0.11  | 0.20   | 0.22   | 0.125  | 0.05  |       |

# Chapter 6

## 6 Conclusions and Future Work

---

### 6.1 Conclusions

#### 6.1.1 *The Value of the Tesla Turbine*

It is possible to fabricate sub-cm Tesla turbines with commercially available technology to achieve over 40% mechanical efficiency.

The rotor can be made modular and stacked to meet the input flow rate without performance degradation, and therefore this design is suitable for tailoring to residential and remote power applications.

#### 6.1.2 *Optimizing Performance*

Smaller-than-cm rotors might require micro structuring of the discs to increase momentum transfer in order to achieve power densities in the watt/cm<sup>3</sup> range.

Open-loop systems will potentially require filters that remove particulates in order to achieve power densities in the watt/cm<sup>3</sup> range.

To achieve higher than watt/cm<sup>3</sup> power density, a fuel-based turbine might be needed.

#### 6.1.3 *The Importance of the Design Tools*

Turbine performance is very sensitive to hardware and to operating parameters, and this is likely the reason for large discrepancies among the performances of published turbines. By applying appropriate design constraints, turbines can be designed with consistent performance.

For the same input specification, multiple designs are possible. A unified design tool can provide these choices for turbine design, making it easier to manufacture and deploy optimized turbines. This can extend the turbines' operating range.

#### 6.1.4 *Practical Limits for Tesla Hydro Turbines*

##### *Lower Limits*

Scaling down below a 1 mm rotor might not be practical for a hydro turbine, for several reasons.

Although Tesla rotors do not have obstructing vanes, particulate size in the fluid dictates the lower limits to interdisk space and rotor radius. The minimum ratio of radius to interdisk space is 20 for optimum rotor function.

As the turbine scales down, the volume of fluid passing through the rotors also declines, and losses increase. This reduces the power available for conversion.

### *Upper Limit*

Scaling above a 400 mm rotor might diminish the Tesla turbine's advantages in manufacturability and maintainability. With current manufacturing technology, the performance of a Tesla turbine can potentially be made to match that of an inertial turbine. However, the advantage over inertial turbines for high power applications is not clear

## 6.2 Future Work

When considered in conjunction with fabrication capabilities, this research provides a guide to what is achievable in terms of scaling down these systems. It also provides a tool for exploring Tesla turbine operation. However, more work on disk micro structuring is needed in order to enhance the friction coefficient and improve the power density of the turbine as it scales down. More work on full admission need to be investigated as losses due to partial admission increase as the rotor scales down.

Some of the losses are not modeled or derived, but estimated from published papers. Mechanical to electrical conversion is not addressed in this research. A practical implementation is needed to evaluate the turbine design tool for power generation and to tailor it to a particular application.

Though the research here focuses specifically on water turbines, the design tool can be used for any fluid. Because Tesla turbines and Tesla pumps operate on the same principle, the conclusions in this dissertation can also be extended to Tesla pump specifications. A future step could additionally extend the analysis here to compressible flow and to two-phase flows, which would potentially enable solar CHP and CPVT implementations.

## Bibliography

---

- [1] B. P. Ho-Yan, "Tesla Turbine for Pico Hydro Applications," *Guelph Engineering Journal*, vol. 4, pp. 1-8, 2011.
- [2] R. W. Lawn M. J, "Calculated Design Data for the Multiple-Disk Turbine using Incompressible Fluid," *Journal of Fluids Engineering, Transactions of the ASME*, vol. 96, no. 3, pp. 252-258, 1974.
- [3] G. A. Hoya G. P, "The design of a test rig and study of the performance and efficiency of a Tesla disc turbine," *Proceedings of the Institution of Mechanical Engineers, Part A: Journal of Power and Energy*, vol. 223, pp. 451-465, 2009.
- [4] R. C. North, "An Investigation of the Tesla Turbine," Mechanical Engineering, University of Maryland, 1969.
- [5] E. Beans, "Performance Characteristics of a Friction Turbines," Mechanical Engineering, Pennsylvania State University, 1961.
- [6] Armstrong J. H., "An investigation of the performance of a modified Tesla Turbine," M.E. department, Georgia Institute of Technology, Atlanta, 1952.
- [7] S. J. S. B. H. J. D. Williamson, "Low head pico hydro turbine selection using a multi-criteria analysis," Sweden, 2011.
- [8] Tesla N..United States of America Patent 1,061,206, 1913.
- [9] A. Camacho, "The Design of a Micro-Turbogenerator," Duke University, Durham, NC, 2011.
- [10] Y. M. M. S. Z. Z. J.A.Razak, "Application of Crossflow Turbine in Off-Grid Pico Hydro Renewable Energy System," *Recent Advances in Applied Mathematics*, pp. 519-526, 2010.
- [11] Kalogirou S.A., "Seawater desalination using renewable energy sources," *Progress in Energy and Combustion Science*, pp. 242-281, 2005.
- [12] V. P. Carey, "Assessment of Tesla Turbine Performance for Small Scale Rankine Combined Heat and Power Systems," *Journal of Engineering for Gas Turbines and Power*, vol. 132, pp. 122301-1 122301-8, 2010.
- [13] W. Rice, "An Analytical and Experimental Investigation of Multiple Disk Turbines," *Journal of Engineering for Power*, vol. 87, pp. 29-36, 1965.

- [14] L. E. M. B. C. R. Deam T. R., "On Scaling Down Turbines to Millimeter Size," *Journal of Engineering for Gas Turbines and Power*, vol. 130, pp. 052301--9, 2008.
- [15] S. B. Guha A., "Experiment and analysis for an improved design of the inlet and nozzle in Tesla disc turbines," *Journal Power and Energy*, vol. 224, no. 2, pp. 261-277, 2009.
- [16] S. A. J. a. A. H. Epstein, "AN INFORMAL SURVEY OF POWER MEMS," in *The International Symposium on Micro-Mechanical Engineering*, 2003.
- [17] F. Herrault, B. C. Yen, C.-H. Ji, Z. Spakovszky, J. H. Lang and M. G. Allen, "Fabrication and Performance of Silicon-Embedded Permanent-Magnet Microgenerators," *Journal of MicroMechanical Systems*, vol. 19, no. 1, pp. 4-13, 2010.
- [18] D. R. F. V. Jan Peirs, "A microturbine for electric power generation," *Sensors and Actuators A*, vol. 113, pp. 86-93, 2004.
- [19] V. G. I. Z. M. M. M. Krishnan, "A micro Tesla Turbine for power generation from low pressure heads and evaporation driven flows," in *Solid-State Sensors, Actuators and Microsystems Conference (TRANSDUCERS), 2011 16th International*, Beijing, 2011.
- [20] D. S. A. L. C. J. B. T. S. G. Kandlikar, "Characterization of surface roughness effects on pressure drop in single-phase flow in minichannels," *Phys. Fluids 17*, 100606, 2005.
- [21] P. D. a. C. N. G. Croce, "Three-dimensional roughness effect on microchannel heat transfer and pressure drop," *Int. J. Heat Mass transfer*, p. 5249, 2007.
- [22] G. Gamrat, "An Experimental Study and Modelling of Roughness Effects on Laminar Flow in Microchannels," *Journal of Fluid Mechanics*, pp. 399-423, 2008.
- [23] L. M.J, "An investigation of Multiple-Disk Turbine performance parameters," Arizona State University, 1972.
- [24] Romanin V. D., "Theory and Performance of Tesla Turbines," Mechanical Engineering Department, U.C. Berkeley, Berkeley, 2012.
- [25] V. Romanin and V. G. Krishnan, "Experimental and Analytical study of sub-watt scale Tesla turbine performance," in *Proceedings of the ASME 2012 IMECE*, Houston, 2012.
- [26] L. Moody, "Friction Factors for Pipe Flow," *Transactions of the A.S.M.E.*, vol. 66, no. 8, pp. 671-684, 1944.
- [27] N. R. E. Daily J. W, "Chamber Dimension Effects on Induced Flow and Frictional Resistance of Enclosed Rotating Disks," *Journal of Basic Engineering, Transactions of ASME*, vol. 82, pp. 217-230, 1960.
- [28] Ladino A. F. R., "Numerical simulations of the flow field in a Friction-type Turbine ( Tesla Turbine)," Institute of Thermal Powerplants, Vienna University of Technology, Vienna, 2004.

- [29] R. V. C. V. M. M. Krishnan V.G., "Design and Scaling of Microscale tesla turbines," *Journal of Micromechanics and Microengineering*, 2013.
- [30] W. Rice, "Tesla Turbomachinery," in *Handbook of Turbomachinery*, CRC Press, 1994.
- [31] Eurelectric "Preservation of Power" and VGB, "Efficiency in Electricity Generation," Union of the electricity industry -eurelectric, Brussels, 2003.
- [32] D. Nendl, "Eine Theoretische Betrachtung der Tesla-Reibungspumpe," *VDI-Forsch.Heft 527*, pp. 29-36, 1973.
- [33] R. W. Matsch L., "Flow at Low Reynolds number with Partial Admission between Rotating disks," *Journal of Applied Mechanics*, pp. 768-770, 1967.
- [34] Y. G. L. Z. T. X. H. D. Yun Zeng, "Torque Model of hydro turbine with inner energy loss characteristics," *Sci China Tech*, vol. 53, pp. 2826-2832, 2010.

# Appendix

## Appendix - A: Design Tool

---

### A.1 Methodology

Design Tool program is written in MATLAB (Figure A--1)

Design Tool: In 'Design Tool' GUI, user specifies the following: particulate size in  $\mu\text{m}$  (dust), head in meter (head) and flow rate in  $\text{cm}^3/\text{sec}$  (flow), flow medium (medium). The design is meant for incompressible fluid (water). A list of valid designs are outputted for the user to investigate along with four recommended designs.

Multiple interdisk spacing (b) greater than ten times the particulate size (non-clogging) and multiple radii (r) greater than  $20*b$  (satisfy rotor equation simplifications) are chosen. At each (r, b) combination, 'Design Turbine' selects four candidate designs for the given head, flow, radius and interdisk space, applying the design constraints (Table 5-1: Turbine design parameters and constraints).

Design Turbine: Candidates for given radius, interdisk space, head and flow rate:

Turbine performance is investigated using 'Evaluate Turbine' varying  $V_{t0}$  (tangential flow) and  $V_{noz}$  (dynamic head) parameters. All other hardware and operating parameters are derived from input specifications and design constraints for the particular radius.

'Evaluate Turbine': Investigates the turbine performance: It calculates momentum, all losses and shaft power delivered based on algorithms described in 'Analytical and Computational Turbine Models' and 'Loss Models and Estimation' and creates a performance summary for the given operating points.

All designs that is within +1%/-5% of the input head are chosen and four that correspond to - maximum efficiency (power), maximum power density (size), reasonable turbine aspect ratio ( $0.5 < \text{Height/Width} < 10$ ), and closest to input head - are selected. For some (r, b) combinations valid designs may not be available.

The program default setting selects 11 interdisk spacing and 11 radius setting based on the interdisk spacing, resulting in a maximum of 121 turbine design sets per criterion.

One turbine design is selected in a set based on three levels of sorting: 1. High power (higher than 90% of maximum power); 2. High power density (higher than 80% maximum power density in the selected); and 3. Closest to the input head in the sub selection. The design performance is evaluated on its sensitivity to input head and flow variations using 'Analyze Sensitivity' program. Figure 5-6 shows performance of valid turbines at inputs of 40 m head, 30000 cm<sup>3</sup>/s flow rate and 21 μm particulate size for the maximum efficiency (power) criterion, with the recommended turbine radius at 66 mm. Figure 5-7 shows the sensitivity graphs for the design at 66 mm.

Analyze Sensitivity: Performance variations for +/-20% head, flow rate:

Here all turbine specifications are given. Only the input head and flow rate are varied. Under varying input conditions, the turbine control algorithm can adjust the nozzle flow and RPM to maximize performance. So at each head and flow, rotor speed (RPM) and flow rate ( $V_{r_o}$ ) are varied and the resulting turbine performance parameters are calculated using 'Evaluate Turbine' algorithm. The optimum operation points are chosen for maximum efficiency and the corresponding performance data is chosen for that head and flow. This is repeated over the input variation range and the performance sensitivity graphs are generated.

Outputs: All the valid rotor radii are listed. User can get the hardware and operating design data on any turbine by selecting the rotor in the designed turbines (radii list) and criterion in the four criteria list.

A subset of four designs are recommended. Power, Power density, Aspect ratio, RPM of the recommended turbines are plotted over the entire range of rotor radius.

Sensitivities of Power, Power density and RPM to input head and flow variations are plotted for the recommended high efficiency turbine.

## A.2 Design Tool Flow Chart

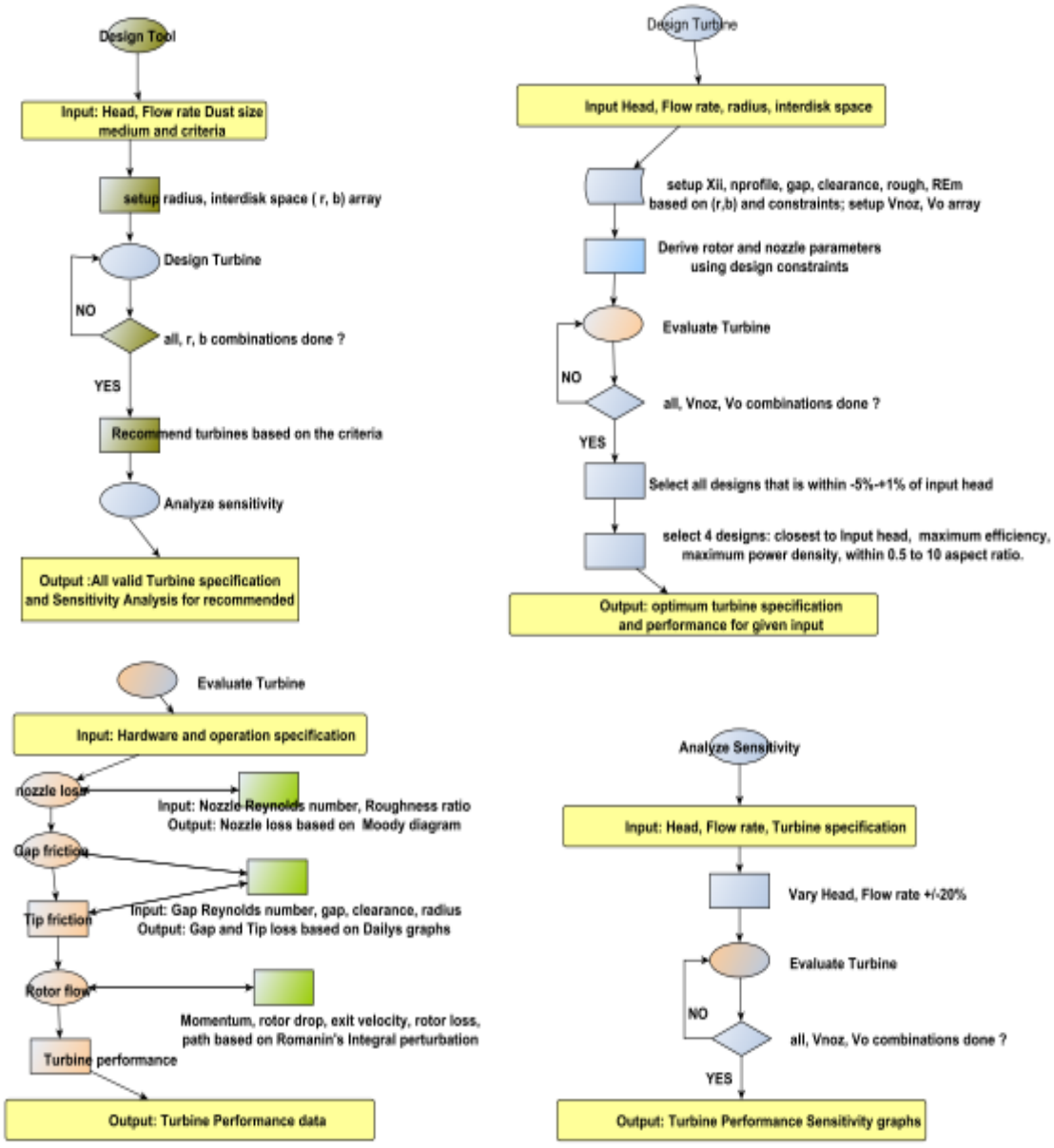


Figure A--1: Design Tool program flow chart

## A.3 MATLAB Code

### A.3.1 *Design\_Turbine*

```
function [designs]=Design_turbine(head_m, flow_cc,dust_um, medium, rbt, plots)
% Inputs: head, flow, dust, medium, radius, space, thickness information
% outputs : set of possible designs based on power.
% sets up design parameters based on constraints and inputs and evaluates
% the design by varying operating points and selects four designs .

if(nargin < 1)
    head_m = 40; flow_cc=30000; dust_um = 21; medium = 'water';
    rbt = [ 66e-3 210e-6 105e-6]; plots = [ 1 1 1 1 1];
end

%set up user input ;
user.application = medium; user.method = 'voVn';
user.headm = head_m; user.flowcc = flow_cc;
user.dustum = dust_um; user.task = 'design';
user.radius = rbt(1); user.space = rbt(2); user.thick = rbt(3);

% setup turbine hardware and operating parameters
[setVar] = Design_setup(user);
rotor = setVar.rotor; flowvar = setVar.flowvar;
headIn = setVar.userinp.headIn; flowIn = setVar.userinp.flowIn;

% evaluate urbine performance
[eval] = evaluate_turbine(setVar);
head = eval.userout.head;
eta = eval.userout.eta;
powerout = eval.userout.powerout;
powerin = eval.userout.powerin;
flow = flowvar.flow;

% pick the optimum turbine based on head and powerout (efficiency).
% derive closest head to input head (dIh) and highest power (dIp) indices
dIh= find(abs(head-headIn) == min(min(abs(head-headIn))));
dIp= find(powerout == max(max(powerout)));
% collect all designs that are within -5%/+1% of the input head
klow= 0.05 ; khigh= 0.01; head_temp = head;
head_temp(find(headIn-head_temp < -khigh*headIn))=0;
head_temp(find(abs(headIn-head_temp) > klow*headIn))=0;
K = head_temp > 0 ; z = K.*powerout; %all heads within -5% - 1% head range
if sum(sum(z))~=0;
    dI=find(z==max(max(z))); valid=1 ;% highest power within 0.95-1.01 head
else
```

```

dI = dIh; valid = 0 ; %check the closest head index
end
refcol = ceil(dI/size(head,1));
refrow = dI -(refcol-1)*size(head,1) ;

% plot sankey diagram of the turbine
turbineLabel = [ num2str(2*rotor.radius*1000),' mm '];
if (plots(5) ==1)
    inputs = powerin(dI) ; unit= 'w';
    if (inputs < 1) ; inputs = inputs*1000; unit = 'mw'; end ;
    losses = [eval.sankey.nozloss(dI) eval.sankey.rotorloss(dI) eval.sankey.keIoss(dI)...
        eval.sankey.tiploss(dI) eval.sankey.gaploss(dI)...
        eval.sankey.leakloss(dI) eval.sankey.pathloss(dI)
eval.sankey.bearing(dI)*eval.userout.torqueff(dI)]*inputs;
    labels = {turbineLabel, 'Nozzle loss', 'Rotor loss', 'KE loss', 'Tip loss', 'Gap
loss', 'Leakage', 'Path loss', 'Bearing', 'Power Out'};
    sep =[1,2,3,5,8];
    drawSankey(inputs, losses, unit, labels, sep)
end

% setup input, performance and recommended turbine for the tested radius and space
designs.setVar = setVar;
designs.eval = eval;
designs.select.dI =dI; designs.select.valid = valid;
designs.select.dIh = dIh; designs.select.dIp = dIp; designs.select.k =length(k);
if(valid == 1)
disp(['done design at radius = ',num2str(rotor.radius*1000),', space =
',num2str(rotor.space*1e6)]);
else
disp(['head is not enough for design at radius = ',num2str(rotor.radius*1000),', space
= ',num2str(rotor.space*1e6)]);
end

```

*Published with MATLAB® R2013a*

### A.3.2 Evaluate\_Turbine

```
function [ evaluation] = evaluate_turbine(turbine_setup )
% evaluate the performance of the turbine at the setup
% input: tesla turbine design and operating parameters
% output: performance data -power,power density ,efficiency, sankey losses...

%turbine_setup =
%struct('allvar',setup,'invar',userinp,'rotHW',rotor,'nozHW',nozzle, ...
%'flowvar',operation,'nozvar',nozlossI,'gapvar',gaplossI,'rotvar',rotorflowI);

setup = turbine_setup.allvar;
nozinp = turbine_setup.nozvar;
gapinp = turbine_setup.gapvar;
rotinp = turbine_setup.rotvar;
userinp=turbine_setup.invar;
rotor = turbine_setup.rotHW;
nozzle = turbine_setup.nozHW;
flowvar = turbine_setup.flowvar;

%%calculate the nozzle loss - use Moody %diagram
[nozL] = NozzleLoss(nozinp);

%Gap and Tip torque loss coefficients according to Daily
% calculate the losses and normalize to torque coefficient T1.
[gapL] = GapTipLoss(gapinp);

%calculate the rotor flow based on Romanin's integral perturbation method
% The rotor flow and drop characteristics
[rFlow] = RotorFlow(rotinp);

%Loss factors taken from published work - Piers and Zeng : less than 10%
%other_headLoss = leakloss + flowPathLoss other_torqLoss = bearingLoss ;

    Pnozout = rFlow.ProtorIn*(1+setup.leakloss + setup.pathloss); % other head loss:
    Pt = Pnozout+ nozL.Pnozloss;
; % turbine head + nozzle loss
    head_efficiency = rFlow.momentdif./Pt ;

% setup torque loss factors
cmTip = min(gapL.cmtip_T1./rFlow.T1rotor,0.9);
cmGap = min(gapL.cmgap_T1./rFlow.T1rotor,0.9);

% torque loss due to gap and tip frictions
T1loss = (1-cmTip -cmGap) *(1-cmTip).*(1-cmGap); % local variable
torque_efficiency = (T1loss - setup.bearingloss) %T1loss .*(1-
setup.bearingloss);
% T1lossScale: Torque, coefficient after other torque losses
T1 = rFlow.T1rotor.*torque_efficiency;
```

```

eta = head_efficiency.*torque_efficiency; %= T1./( 2*pi*Uo.*Pt)
eta_encf = rFlow.etaturbine.*T1loss; % enclosure losses:gap tip loss
eta_nozf = rFlow.etaturbine.*Pnozout./Pt; % noz loss

% dimensional calculations and efficiency check
head = Pt.*setup.headnorm;
torque = T1.*setup.torquenorm;
powerin = head.*flowvar.flow;
powerout = torque.*flowvar.omega.*rotor.Ndisks;
powercc = 1e-6.*powerout./rotor.rotorVol./2; % double rotor vol.

% system efficiency with derived head or actual head if it is specified
if (userinp.headIn > 0)
    eta_dim = powerout ./ ( userinp.headIn.*userinp.flowIn);
else
    eta_dim = powerout./powerin;
end

% setup for user performance ouput
userout.head =head;
userout.torque = torque;
userout.powerin = powerin;
userout.powerout = powerout;
userout.powercc = powercc;
userout.eta_dim = eta_dim;
userout.torqueeff = torque_efficiency;
userout.headeff = head_efficiency;
userout.eta = eta;
userout.Pt = Pt;
userout.T1 = T1;
userout.etaenc = eta_encf;
userout.etanoz = eta_nozf;

% sankey representation of performance % head losses &
sankey.rotorloss = rFlow.rotorloss ./ Pt ;
sankey.ke loss = rFlow.KEout ./ Pt;
sankey.nozloss = nozL.Pnozloss ./ Pt;
sankey.leakloss = rFlow.ProtorIn.*setup.leakloss ./Pt;
sankey.pathloss = rFlow.ProtorIn.*setup.pathloss ./Pt;
sankey.gaploss = cmGap.*head_efficiency; %torque losses
sankey.tiploss = cmTip.*head_efficiency;
sankey.bearing = setup.bearingloss.*head_efficiency;

evaluation.nozL = nozL;
evaluation.gapL = gapL;
evaluation.rFlow = rFlow;
evaluation.userout= userout;
evaluation.sankey = sankey;

end

```

### A.3.3 Nozzle Loss

```
function [nozout]= NozzleLoss(noz_interface)
% input
REnoz = noz_interface.REnoz; % flow Reynolds number Dnoz.Vnoz / nu
rough = noz_interface.rough; % relative roughness epsilon / Dnoz
KEnoz = noz_interface.KEnoz; % flow kinetic energy at nozzle exit
LbyD = noz_interface.LnozBYDnoz; % Lnoz / Dnoz

% generate friction coefficient
nozout.fric = moody_diagram(REnoz, rough);

% calculate nozzle loss
nozout.Pnozloss = KEnoz.*nozout.fric.*LbyD;

function flow_fric = moody_diagram(REnoz, rough)
laminar = 2300; %Hagen Poisuille equation for laminar
turbulent=4000; % colebrook equation for turbulent
tran_range = turbulent - laminar; %linear interpolation between laminar to turbulent

flag_lam=zeros(size(REnoz));
flag_lam(find(REnoz<laminar))= 1;
flag_turb=zeros(size(REnoz));
flag_turb( find(REnoz>=turbulent))= 1;
flag_tran = ones(size(REnoz));
flag_tran = not(or(flag_lam,flag_turb));

laminar_f = 64./REnoz;
turbulent_f = colebrook(REnoz, rough);
tran_f = laminar_f + (REnoz-laminar)./tran_range.*(turbulent_f-laminar_f);
flow_fric = laminar_f.*flag_lam + tran_f.*flag_tran + turbulent_f.*flag_turb;

function fric=colebrook(RE,rough)
% Colebrook Equation : for turbulent
% fric = Darcy-Weisbach friction factor ; % RE = Reynolds number
% rough = relative roughness ; fric=zeros(size(RE)); f0=0.04;
[row col] = size(RE);
for i=1:row
    for j = 1:col
        for k=1:5
            f0=(2*log10(rough/3.7+2.51/RE(i,j)/sqrt(f0)))^-2;
        end
        fric(i,j)=f0;
    end
end
end
```

### A.3.4 Gap and Tip Torque Losses

```

function [gapout]= GapTipLoss(Daily_interface)

% Daily disk friction
% emperical equations for Cm , the torque coefficients.
% Torque-disk friction = Cm* 0.5*rho*omega^2*r_o^5 for each side
% torque at tip = (Cm*0.5*r_o/b) * rho*omega^2*r_o^4*b
% water flow is assumed to be not restricted at the bottom exhaust
% disk friction coefficient Cm - s - rotor to enclosure axial clearance
% a = radius of the rotor ; REgap = flow reynolds in gap = omega*ro^2/nu

% R = omega*ro^2/nu
% regime 1: 2*pi/(s/a)/R % laminar merged boundary
% regime 2: (2.61+2.5*sBYr)/R^0.5 % laminar separate boundaries
% regime 3: 0.0622/(s/a)^.25 /R^0.25 % theory ( as 1 - turbulent)
% regime 4: (0.074+0.08*sBYr)/R^0.2 % as 2 - turbulent

REgap = Daily_interface.REgap; % Reynolds number of the trapped flow
sBYr = Daily_interface.sBYr; % gap / disk radius
Ndisks = Daily_interface.Ndisks; % number of disks
bBYr = Daily_interface.bBYr ; % normalizing factor to T1 ; b/ro

if (sBYr < 0)
cm_gap = 0*REgap;
else
    cgap1 = 2*pi./sBYr ./REgap; % laminar merged
    cgap2 = (2.61+2.5*sBYr)./sqrt(REgap); % laminar separate
    cgap3 = 0.0622 ./sBYr^0.25 ./REgap.^0.25; % turbulent merged;
    cgap4 = (0.074+0.08*sBYr)./REgap.^0.2; % turbulent merged;

    z2(1, :, :) = cgap1'; z2(2, :, :) = cgap2'; z2(3, :, :) = cgap3'; z2(4, :, :) = cgap4';
    for i = 1:size(cgap1,1) ; cgap(i, :) = max(z2(:, :, i)); end
    gapout.cm_gap = cgap./Ndisks; gapout.cmgap_T1 = 0.5./bBYr .*gapout.cm_gap;
end

% tip friction
% Torque-tip friction = Ctip* 0.5*rho*omega^2*r_o^5 for each disk
% = (Ctip*0.5*r_o/b) * rho*omega^2*ro^4*b
% coquette flow is assumed
% Ctip = 4*pi *t *nu/ (ro^2*c*omega); c=tip clearance, t=disk thickness

tBYc = max(0,Daily_interface.tBYc); % disk thickness / clearance
gapout.cm_tip = 4*pi.*tBYc ./REgap; gapout.cmtip_T1 = 0.5 ./bBYr .*gapout.cm_tip;

End

```

### A.3.5 Rotor Flow Characterization

```

function [Pic, wic] = RotorFlow(rotorflow)
% Inputs an array and evaluates rotor drop and tangential flow for each
% element, based on Integral perturbation algorithm (Vincent Romanin)
REm = rotorflow.REm; % Rotor reynolds number
Xii = rotorflow.Xii; % ri / ro
n = rotorflow.nprofile;
Uo = rotorflow.Uo; % radial flow rate indicator
wo = rotorflow.hatwo; % relative tangential flow rate indicator

delx = -(1-Xii)/2000; % compute - 2000 iteration from entry to exit
lengthi = floor(abs((1-Xii)./delx) );
kw1 = (2*n+1)./(n+1); %
kp1 = 4./kw1; %
kw2a = 8*(2*n+1)./REm; %
kw3a = REm./(8*(n+1)); %

for io = 1: size(REm,1)
for jo = 1: size(REm,2)
% setup for each initial conditions
hatwo = wo(io,jo);
Re_star = REm(io,jo);
Vro = Uo(io,jo);
kw2 = kw2a(io,jo);
kw3 = kw3a(io,jo);
kw4 = kw2./2; %
kp2 = 4./kw3; %
POA = 0*hatwo ; % initialize pressure drop and relative velocity
hatwi = hatwo ; %

% Use analytical expression for wr and compute Pr
for i = 1:lengthi
x = 1 + delx*(i);
% Use analytical wr to compute Pr
delp = kp1.*(Vro.^2./x.^3 + hatwi.^2./x) + ...
4.*hatwi + 2.*x + kp2.*Vro.^2./x;
POA = delp.*delx + POA;
% analytical wr
hatwi = kw3./x + ((hatwo - kw3)./x).*exp(kw4.*(x.^2-1));
end
wic(io,jo)= hatwi;
Pic(io,jo) = POA;

end
end

```

```

Vi = wic + Xii; Ui = Uo./Xii;

rotorout.hatWi= wic;
rotorout.Pic = Pic;
rotorout.Ui = Ui;
rotorout.Vi = Vi;
rotorout.NRE = 4*Uo.*REm;
rotorout.momentdif = Vo - vi.*Xii;
rotorout.Tlrotor = 2*pi*Uo.*rotorout.momentdif;
rotorout.Pirot = abs(0.5*Pic);
rotorout.KEin = 0.5*(Vo.^2 + Uo.^2);
rotorout.KEout = 0.5*(Vi.^2 + Ui.^2);
rotorout.Protor = rotorout.Pirot + rotorout.KEin - rotorout.KEout;
rotorout.rotorloss = rotorout.Protor - rotorout.momentdif;
rotorout.statichead = rotorout.Pirot - rotorout.rotorloss;
rotorout.dynamichead = rotorout.KEin - rotorout.KEout;
rotorout.reaction = rotorout.statichead./(rotorout.statichead + rotorout.dynamichead);
rotorout.ProtorIn= rotorout.Protor+ rotorout.KEout;
rotorout.etamomentum = rotorout.momentdif./Vo;
rotorout.etarotor = rotorout.momentdif./rotorout.Protor;
rotorout.etaturbine = rotorout.momentdif./rotorout.ProtorIn;

```

*Published with MATLAB® R2013a*

### A.3.6 Sensitivity of Designed Turbine to Head and Flow Variations

```

function [ sensitivity ] = Sensitivity_turbine(turbine)

flowvar = turbine.setVar.flowvar; userinp = turbine.setvar.userinp;
dI = turbine.select.dI;

omega = flowvar.omega(dI);
% vary input head by +/- 20% and flow by +10%/- 30%
% rotor speed is varied to find the stable operating points for different
% head and flow combinations for the specified turbine.
scalehead= [0.8:0.05:1.2]; xref = 5;
scaleflow= [0.7:0.05:1.1]; yref = 7;
[a b] = ndgrid(scaleflow,scalehead);
e1 = min(0.9,a*0.9).*a;
e2 = min(0.9,b*0.9).*sqrt(b);
omegaMin = omega*(e1.*e2);
f1 = max(1.1,a*1.1).*a;

```

```

f2 = max(1.1,b*1.1).*sqrt(b);
omegaMax = omega*(f1.*f2);
omegainc = omega*0.02;
flowv = userinp.flowIn*a;
headv = userinp.headIn*b;
xvarh=[]; yvarf= []; fhs_pwr = 0*flowv; fhs_eta = 0*flowv; fhs_rpm = 0*flowv;

plotv=
struct('xref',userinp.headIn,'yref',userinp.flowIn,'xvar',scalehead.*userinp.headIn, ...
      'yvar',scaleflow.*userinp.flowIn,'xlab','head Pascal','ylab','flow m3/s');

for i = 1:length(scaleflow);
    for j = 1:length(scalehead);

        Flow = flowv(i,j); Head = headv(i,j);
        omega = [ omegaMin(i,j):omegainc:omegaMax(i,j)];
        [sensitivity_analysis] = Sensitivity_check(Flow, Head, omega, turbine);
        sI = sensitivity_analysis.sI;

        if (sensitivity_analysis.powerout>0);
            fhs_pwr(i,j) = sensitivity_analysis.powerout;
            fhs_eta(i,j) = sensitivity_analysis.eta;
            fhs_rpm(i,j) = sensitivity_analysis.RPM;
            fhs_pcc(i,j) = sensitivity_analysis.powercc;
        end

    end
end

%flowheadSen= [ fhs_rpm fhs_pwr fhs_eta fhs_pcc];
sensitivity.analysis = sensitivity_analysis;
sensitivity.RPM = fhs_rpm; sensitivity.eta = fhs_eta;
sensitivity.powerout = fhs_pwr; sensitivity.powercc = fhs_pcc;
sensitivity.plotv = plotv;

end

```

### A.3.7 Analyze Sensitivity for a Particular Head and Flow

```

function [flowheadsensitivity ] = Sensitivity_check( flow, head, omegav, turbine )
% [flowheadSen] = Design_check(Flow, Head, omega, turbineSpec);
% performance of a turbine at off design head , flow, and speed

%default set up for water

```

```

anaVar = Sensitivity_setup(flow, head, omegav, turbine);
analysis = evaluate_turbine(anaVar);

headIn = anaVar.userinp.headIn; RPM = anaVar.flowvar.RPM;
head = analysis.userout.head; eta = analysis.userout.eta;
powerout = analysis.userout.powerout; powercc = analysis.userout.powercc;

% pick the optimum turbine (sI) based on head and powerout (efficiency).
% derive closest head to input head (sIh) and highest power (sIp) indices
    sIh= find(abs(head-headIn) == min(min(abs(head-headIn))));
    sIp= find(powerout == max(max(powerout)));
% collect all designs that are within -5%/+1% of the input head
klow= 0.05 ; khigh= 0.01; head_temp = head;
head_temp(find(headIn-head_temp < -khigh*headIn))=0;
head_temp(find(abs(headIn-head_temp) > klow*headIn))=0;
K = head_temp > 0 ; z = K.*powerout; %all heads within -5% - 1% head range
if sum(sum(z))~=0;
    sI=find(z==max(max(z))); valid=1; % highest power within 0.95-1.01 head
else
    sI = sIh; valid = 0 ; %check the closest head index
    disp(' head is not enough for this operation'); % closest to input head
end

flowheadsensitivity.anaVar = anaVar;
flowheadsensitivity.analysis = analysis;
flowheadsensitivity.powerout = powerout(sI);
flowheadsensitivity.powercc = powercc(sI);
flowheadsensitivity.RPM =RPM(sI);
flowheadsensitivity.eta = eta(sI);
flowheadsensitivity.valid = valid;
flowheadsensitivity.sI = sI;
end

```

*Published with MATLAB® R2013a*

### A.3.8 Setup constants and variables for Design

```

function [ setup_I ] = Design_setup(userInput)
% sets up Turbine operation psrsmeters based on the user inputs of head,
% flow, dust, medium, and desired radius, interdisk space. 2 sets of
% operating parameters are varied to pick the optimum performance points.
% Other parameters are derived using design constraints.

```

```

% medium - only water is used in this simulation - though different motive
% media can be used by supplying all its parameters ie, density, dynamic
% viscosity and temperature coefficient. As the number of variables is
% high, following selection rules are applied based on the variables.

% Method

%default set up for water
rho = 1000; % kg/m^3
mu = 1.002e-3; %Pa*s, water at 20 C
nu = mu/rho ; % kinematic viscosity m^2/s
Cp = 4.181e6 ; % water specific heat : joule/m^3/K

hydro = struct('medium','water','density',1000,'viscosity',1.002e-3, ...
    'kinematicViscosity',1.002e-6,'specificHeat',4.18e6);

% setup based on user input
headIn = userInput.headm*9801; % Pascal meter*rho*g
flowIn = userInput.flowcc*1e-6; % flow rate in m^3/s
dust = userInput.dustum*1e-6; % particulate size in m
medium = userInput.application;
r_o = userInput.radius; % rotor radius in m
b = userInput.space; % interdisk space in m
t = userInput.thick; % interdisk space in m

if(medium == 'water')
rho = hydro.density; % kg /m^3
mu = hydro.viscosity; % Pa sec ; water at 20 deg
nu = mu./rho; % kinematic viscosity m^2/sec
Cp = hydro.specificHeat ; % joule /m^3/K
end

% setup hw and operating parameters based on the radius
rv = [0.5 1 2 5 10 15 20 25 30 35 40 45 50 55 60 65 70 75 80 85 90 95 100 ...
    150 200 240]*1e-3; % m

% nvar = [ 5*ones(1,6) 3.8*ones(1,6) 2.9*ones(1,9) 2*ones(1,14)];
% [x y]=polyfit(rv,nvar,3); nv = x(4) + x(3)*rv + x(2)*rv.^2 + x(1)*rv.^3
nv = [ 5.12 5.09 5.03 4.92 4.67 4.47 4.28 4.10 3.92 3.75 3.59 3.44 3.3 ...
    3.17 3.05 2.94 2.84 2.74 2.65 2.56 2.49 2.42 2.35 2 2 2 2 2 2 2 2];
remv = 0.64*(nv+1)./3; % varies from 1.28 to 0.64
xiiv = nv./30 + 0.2332; % varies from 0.4 to 0.3
roughv = [ 0.05*ones(1,3) 0.02*ones(1,3) 0.01*ones(1,6) 0.004*ones(1,9)
    0.001*ones(1,14)];

indro = max(find(r_o>=rv));
%fixed parameters for a given disk-radius, space, thicknedd
xii = xiiv(indro); % ri/ro increase as radius decrease
REm = remv(indro) ; % Use P0 and profile relationship

```

```

roughc = roughv(indro)          ; % fabrication limitation
nprofile = nv(indro)           ; % disk micro structuring
Numnoz = 1;

%if (headIn > 0) % user specified head
% Vo, Vnoz varied ; REM is given , Uo derived
voa = [ 1.05:0.05:1.5];          % Vo
vnoza = [ 0.6:0.02:0.98]; % Vnoz/Vnoz_max
plotv= struct('refcol',6,'refrow',2,'xvar',vnoza.^2,'yvar',voa,'xlab','Dynamic
Head','ylab','vt_{o}');
Vnoz_max = sqrt(2*headIn/rho);
[Vo vnoz] = ndgrid(voa,vnoza); % tangential velocity and dynamic head
onesarray = ones(size(Vo));
Vnoz = Vnoz_max .* vnoz;
REm = REm.*onesarray;          % REm constant based on r_o
Uo = 0.*onesarray;
for uiter=1:4                  % derive Vtip, Uo, omega from REm and Vnoz
Vtip = Vnoz./sqrt(Vo.^2 + Uo.^2); %
Uo = nu*r_o/(4*b^2).*REm./Vtip; %
end

Nnoz = Numnoz.*onesarray;
omega = Vtip./r_o;
Vrad = Uo.*Vtip;
Qdisk = 2*pi*r_o*b.*Vrad;      % derive flow and Ndisks from Qdisk

if (flowIn > 0) %flow given; calculate Ndisks
    flow = flowIn;;
    Ndisks = ceil(flowIn./Qdisk);
else %flow not specified - new design- cubic rotor
    Ndisks= onesarray.*ceil(2*r_o/(b+t));
end
flow = Ndisks.*Qdisk;
Vtan = Vo.*Vtip;

% nozzle angle, area, height, width, hydraulic diameter and length
Anoz = flow./Nnoz ./ Vnoz; % area/nozzle
Hnoz = (b+t)*Ndisks; % initial setting
wnoz= max(b,Anoz./Hnoz) ; % minimum wnoz width = b; nozloss constraint
Hnoz = Anoz./wnoz; % adjustment with wnoz constraints
ARCnoz= 360*wnoz./(2*pi*r_o);
SLITdisk = Hnoz./Ndisks;
Dnoz = 2*wnoz ./ (1+wnoz./Hnoz); % hydraulic diameter
Lnoz = min(0.1,max(0.005,8*Dnoz)); % nozzle length has a min. length requirement
ANGnoz = 180/pi *(pi/2 - atan2(Vtan, Vrad));
rotorVol = (b+t).*Ndisks.*pi.*r_o.^2; %
diskarea = pi*(1-Xii^2)*r_o^2.*Ndisks;
aspect = (b+t).*Ndisks./(2*r_o);
gap = 0.1*r_o;

```

```

clearance = max((b+t),0.01*r_o);

% operation independent; only rotor hw dependent
rotor.radius = r_o;
rotor.space = b;
rotor.thick = t;
rotor.Xii = Xii;
rotor.nprofile = nprofile;
rotor.gap = gap;
rotor.clearance = clearance;

% flow parameter dependent
rotor.Ndisks = Ndisks;
rotor.rotorVol = rotorVol;
rotor.diskarea = diskarea;
rotor.aspect = aspect;

%rotor = struct('radius',r_o,'space',b,'thick',t,'Xii',Xii, ...
%'nprofile',nprofile,'gap', gap, 'clearance', clearance, ...
%'Ndisks',Ndisks, 'rotorVol',rotorVol,'aspect',Aspect,'diskarea',diskarea);

nozzle.area = Anoz;
nozzle.width = wnoz;
nozzle.height = Hnoz;
nozzle.length = Lnoz;
nozzle.DiaHyd = Dnoz;
nozzle.arc = ARCnoz;
nozzle.angle = ANGnoz;
nozzle.slit = SLITdisk;
nozzle.num = Nnoz;
nozzle.rough = roughc;

% nozzle = struct('width',wnoz,'height',Hnoz,'hydDia',Dnoz,'length',Lnoz, ...
% 'angle',ANGnoz,'arc',
ARCnoz,'area',Anoz,'SLITdisk',SLITdisk,'number',Nnoz,'rough',roughc);

RPM = 30/pi.*omega;
powerIn = headIn.*flowIn;
pwr = powerIn./rotor.diskarea;

lBYd = Lnoz./Dnoz;
sBYr = gap./r_o;
tBYc = t./clearance;
bBYr = b./r_o;

rotvar.hatwo = Vo-1;
rotvar.Uo = Uo;
rotvar.Vo = Vo;
rotvar.REm = REm;

```

```

rotvar.anaflag = 1;
rotvar.Xii = rotor.Xii;
rotvar.nprofile = rotor.nprofile;

%rotvar= struct('REm',REm,'hatWo',Vo-
1,'Uo',Uo,'Vo',Vo,'Xii',rotor.Xii,'nprofile',rotor.nprofile,'anaflag',anaflag);

flowvar.RPM =RPM;
flowvar.omega = omega;
flowvar.Vnoz=Vnoz;
flowvar.Vtip = Vtip;
flowvar.Vrad = Vrad;
flowvar.Vtan = Vtan;
flowvar.flow = flow;
flowvar.Qdisk = Qdisk;

%flowvar=
struct('Qdisk',Qdisk,'flow',flow,'vnoz',Vnoz,'Vtip',Vtip,'Vtan',Vtan,'Vrad',Vrad,'omega',
omega,'RPM',RPM);

KEnoz = 0.5*(Vo.^2+Uo.^2);
REnoz = Vnoz.*Dnoz./nu;
nozvar= struct('KEnoz',KEnoz,'REnoz',REnoz,'rough',nozzle.rough,'lBYd',lBYd);

REgap = r_o.^2.*omega./nu;
gapvar = struct('REgap',
REgap,'sBYr',sBYr,'tBYc',tBYc,'Ndisks',rotor.Ndisks,'bBYr',bBYr);

setup.headnorm = rho.*Vtip.^2;
setup.torquenorm = rho.*Vtip.^2.*r_o.^2*b;
setup.pwr = pwr;
setup.leakloss = 0.02;
setup.pathloss = 0.05;
setup.bearingloss = 0.03;
setup.plotv = plotv;

userinp.headIn = headIn;
userinp.flowIn = flowIn;
userinp.powerIn = powerIn;
userinp.medium = medium;
userinp.dust = dust;

% userinp = struct('headIn',headIn,'flowIn',flowIn,'powerIn',powerIn, ...
% 'dust',dust,'medium',medium);
setup_I =
struct('setup',setup,'userinp',userinp,'rotor',rotor,'nozzle',nozzle,'flowvar',flowvar,'n
ozvar',nozvar,'gapvar',gapvar,'rotvar',rotvar);
end

```

### A.3.9 Setup Variables to Analyze Design's Sensitivity

```
function [ anaVar ] = Sensitivity_setup(flowInv, headInv, omegav, turbine )
%setup for turbine sensitivity to head and flow ;
%Vnoz and omega are varied for each head and flow value and the best
%performance point is selected.

anaVar = turbine.setVar;
rho = 1000; % kg/m^3
mu = 1.002e-3; %Pa*s, water at 20 C
nu = mu/rho ; % kinematic viscosity m^2/s
Cp = 4.181e6 ; % water specific heat : joule/m^3/K

flowvar=turbine.setVar.flowvar; userinp = turbine.setVar.userinp;
dI = turbine.select.dI; headIn = userinp.headIn; flowIn = userinp.flowIn;
rotor = turbine.setVar.rotor;nozzle = turbine.setVar.nozzle;
nozvar = turbine.setVar.nozvar;

vnoza = [0.9:0.02:1.1]*flowvar.Vnoz(dI)* sqrt(headInv /userinp.headIn);
omegaa = omegav ;
[ omega vnoz] = ndgrid(omegav, vnoza);
onesarray = ones(size(omega));
Vtip = omega.*rotor.radius;
flow=onesarray.*flowInv;
Qdisk = flow./rotor.Ndisks(dI);
Vrad = Qdisk ./ ( 2*pi*rotor.radius*rotor.space); Uo = Vrad./Vtip;
Vtan = sqrt(vnoz.^2 - Vrad.^2); Vo = Vtan./Vtip;

% update all new variables and set fixed desired variables
anaVar.rotor.Ndisks = rotor.Ndisks(dI);
anaVar.rotor.rotorVol = rotor.rotorVol(dI);

anaVar.rotvar.hatWo = Vo-1;
anaVar.rotvar.Uo = Uo;
anaVar.rotvar.Vo = Vo;
anaVar.rotvar.REm = Vrad.*4*rotor.space.^2 ./ ( nu*rotor.radius);

anaVar.flowvar.RPM =30/pi.*omega;
anaVar.flowvar.omega = omega;
anaVar.flowvar.Vnoz=vnoz;
anaVar.flowvar.Vtip = Vtip;
anaVar.flowvar.Vrad = Vrad;
```

```

anaVar.flowvar.Vtan = Vtan;
anaVar.flowvar.flow = flow;
anaVar.flowvar.Qdisk = Qdisk;

anaVar.nozvar.KEnoz = 0.5*(Vo.^2+Uo.^2);
anaVar.nozvar.REnoz = Vnoz.*nozzle.DiaHyd(dI)./nu;
anaVar.nozvar.lBYd = nozvar.lBYd(dI);
anaVar.gapvar.Ndisks = rotor.Ndisks(dI);
anaVar.gapvar.REgap = rotor.radius.^2.*omega./nu;

anaVar.userinp.headIn = headInv;
anaVar.userinp.flowIn = flowInv;
anaVar.userinp.powerIn = headInv.*flowInv;

anaVar.setup.pwrD = anaVar.userinp.powerIn./anaVar.rotor.diskarea;
anaVar.setup.headnorm = rho.*Vtip.^2;
anaVar.setup.torquenorm = rho.*Vtip.^2.*rotor.radius.^2.*rotor.space;
end

```

*Published with MATLAB® R2013a*

### A.3.10 Turbine Performance graphs

```

function [ table ] = Output_turbine( Out_turbine ,index, plots, fname )
%UNTITLED3 Summary of this function goes here
% Detailed explanation goes here

if (nargin < 1)
    load turbinespec.mat
    Out_turbine = turbinespec;
    plots = [0 0 0 0 0];
    four_peaks = Out_turbine.fourIndex;
    index = four_peaks(1,1);
    fname = ['test1.xls']
end

four_peaks = Out_turbine.fourIndex;
user_turbine = Out_turbine.turbines{index}; tI = index;
sortMatrix = Out_turbine.sortMatrix;
nvalid = length(sortMatrix);
eval = user_turbine.eval; dI = user_turbine.select.dI;

% plot graphs
radius = sortMatrix(:,2); powerout = sortMatrix(:,3);
powercc = sortMatrix(:,4); RPM = sortMatrix(:,5); aspect = sortMatrix(:,7);
eta = sortMatrix(:,8); space = sortMatrix(:,9);

```

```

if (plots(1) ==1);
% plot 4 peaks selected across the rotor range on efficiency
figure(100); plot(radius,powerout,'Linewidth',2); hold on;
plot(radius(four_peaks(:,1)),four_peaks(:,2),'sr');hold off;
xlabel('radius mm','interpreter','tex', 'FontSize',16);
ylabel('Power (W) ', 'interpreter','tex', 'FontSize',16);
end;

if (plots(2) == 1);
% plot powerout, power density and aspect ratio of turbines across the range.
figure(101);
axlabs = {'RPM' ' '; 'Pwrcc(W/cc)'; ' \eta_{system} '};
leglabs = { 'RPM'; 'pwrcc'; '\eta'};
plot([radius(tI) radius(tI)], [min(RPM) max(RPM)], 'k', 'Linewidth',2)
hold on
text(radius(round(5)),RPM(5)+0.005, ' -.- RPM', 'fontsize',14);
text(radius(tI+1),0.85*max(aspect), ' \eta', 'fontsize',14);
plotyyy(radius,aspect,radius,powercc,radius,eta,axlabs,'plot','plot',0.01,leglabs)
xlabel('radius mm','interpreter','tex', 'FontSize',16);
Title = ['radius mm = ',num2str(radius(tI)), ' ', space '\mum = ', num2str(space(tI))];
title(Title,'interpreter','tex','FontSize',16);
% text is using powercc axis
text(radius(ceil(nvalid*1/2)),powercc(ceil(nvalid*2/3)), ' ... powercc ', 'fontsize',14);
%text(max(radius)*0.6,0.005, ' -.- aspect', 'fontsize',14);
grid on;

end

if (plots(3) == 1);
%plot sankey of the recommended turbine
%figure(103)
turbineLabel = [ num2str(2*radius(tI)), ' mm '];
inputs = eval.userout.powerin(dI) ; unit= 'W';
if (inputs < 1) ; inputs = inputs*1000; unit = 'mw'; end ;
losses = [eval.sankey.nozloss(dI) eval.sankey.rotorloss(dI) eval.sankey.keLoss(dI)...
eval.sankey.tiploss(dI) eval.sankey.gaploss(dI)...
eval.sankey.leakloss(dI) eval.sankey.pathloss(dI)
eval.sankey.bearing(dI)*eval.userout.torqueff(dI)]*inputs;
labels = {turbineLabel, 'Nozzle loss','Rotor loss','KE loss','Tip loss','Gap
loss','Leakage', 'Path loss', 'Bearing','Power Out'};
sep =[1,2,3,5,8];
drawsankey(inputs, losses, unit, labels, sep)
end

[sensitivity] = Sensitivity_turbine(user_turbine)

if (plots(4) ==1);

```

```

ylab = sensitivity.plotv.ylab; xlab = sensitivity.plotv.xlab;
yvar = sensitivity.plotv.yvar; xvar = sensitivity.plotv.xvar;
yref = sensitivity.plotv.yref; xref = sensitivity.plotv.xref;

%leg2='design'; plott = [0.1:0.05:0.9];
Title = [];
zvar = sensitivity.eta ; zlab = '\eta';
plotsen(xvar, yvar, zvar, xlab, ylab, xref, yref, zlab, 'design', Title)

zvar = sensitivity.powercc ; zlab = 'w/cm^{3}';
plotsen(xvar, yvar, zvar, xlab, ylab, xref, yref, zlab, 'design', Title)

zvar = sensitivity.RPM ; zlab = 'RPM';
plotsen(xvar, yvar, zvar, xlab, ylab, xref, yref, zlab, 'design', Title)

zvar = sensitivity.powerout ; zlab = 'Power(w)';
plotsen(xvar, yvar, zvar, xlab, ylab, xref, yref, zlab, 'design', Title)

end

% setup a table for outputting
[table] = getspec(user_turbine, fname);

end

```

*Published with MATLAB® R2013a*

### A.3.11 Turbine Specification Table Generation

```

function [table] = get_Spec(turbine , fname);

    eval= turbine.eval; setVar = turbine.setVar;

    userout = eval.userout; sankey = eval.sankey; dI = turbine.select.dI;
    rFlow = eval.rFlow; gapL= eval.gapL; nozL = eval.nozL;

    setup = setVar.setup; rotor=setVar.rotor; nozzle=setVar.nozzle;
    rotvar = setVar.rotvar; nozvar = setVar.nozvar; gapvar = setVar.gapvar;
    userinp = setVar.userinp; flowvar= setVar.flowvar;

    rho = 1000; mu = 1.002e-3; nu = mu/rho;

% setup variables
    radius = rotor.radius*1e3; space = rotor.space*1e6; thick = rotor.thick*1e6;
    xii = rotor.xii; nprofile = rotor.nprofile; gap = rotor.gap*1e3;
    clearance = rotor.clearance*1e3; Ndisks = rotor.Ndisks(dI); aspect = rotor.aspect(dI);

```

```

rotorVol = rotor.rotorVol(dI)*1e3; diskarea = rotor.diskarea(dI)*1e4;

Nnoz = nozzle.num(dI); rough = nozzle.rough; Anoz = nozzle.area(dI);
Wnoz = nozzle.width(dI); Hnoz =nozzle.height(dI); Lnoz=nozzle.length(dI);
Dnoz = nozzle.DiaHyd(dI); ARCNnoz = nozzle.arc(dI); ANGNnoz=nozzle.angle(dI);
SLITdisk = nozzle.slit(dI);

RPM = flowvar.RPM(dI); omega = flowvar.omega(dI); Vnoz = flowvar.Vnoz(dI);
Vtip = flowvar.Vtip(dI); Vtan = flowvar.Vtan(dI); Vrad = flowvar.Vrad(dI);
flow = flowvar.flow(dI); Qdisk = flowvar.Qdisk(dI);

hatwo = rotvar.hatwo(dI); Uo = rotvar.Uo(dI); Vo = rotvar.Vo(dI) ;
REm = rotvar.REm(dI); anaflag = rotvar.anaflag;

lBYd = nozvar.lBYd(dI); KEnoz = nozvar.KEnoz(dI); RENoz = nozvar.REnoz(dI);

REgap = gapvar.REgap(dI); sBYr = gapvar.sBYr; tBYc = gapvar.tBYc;
bBYr = gapvar.bBYr;

headIn = userinp.headIn; flowIn = userinp.flowIn; powerIn = userinp.powerIn;
medium = userinp.medium ; dust = userinp.dust;

headnorm = setup.headnorm(dI); torquenorm = setup.torquenorm(dI);
leakIn= setup.leakloss; pathlossIn = setup.pathloss; bearingIn = setup.bearingloss;

% output variables
powerout = userout.powerout(dI); powercc = userout.powercc(dI);
powerin = userout.powerin(dI); eta = userout.eta(dI); Pt = userout.Pt(dI);
T1 = userout.T1(dI); head=userout.head(dI); head_ratio=userout.head_ratio(dI);
flow_ratio=userout.flow_ratio(dI); torque = userout.torque(dI);
head_eff = userout.headeff(dI); torque_eff= userout.torqueeff(dI);

nozloss= sankey.nozloss(dI); gaploss = sankey.gaploss(dI);
rotorloss=sankey.rotorloss(dI); tiploss=sankey.tiploss(dI);
keloss=sankey.keloss(dI); leakloss= sankey.leakloss(dI);
pathloss=sankey.pathloss(dI); bearingloss= sankey.bearing(dI);

momentdif = rFlow.momentdif(dI); dynamichead = rFlow.dynamichead(dI)/momentdif;
statichead = rFlow.statichead(dI)/momentdif; NRE= rFlow.NRE(dI);
reaction = statichead/(statichead+dynamichead); Wi = rFlow.hatWi(dI);
etamomentum = momentdif/Vo; etarotor = momentdif/rFlow.Protor(dI);
etaturbine = momentdif/rFlow.ProtorIn(dI); Pi = rFlow.Pirot(dI);
KEin = rFlow.KEin(dI); KEout = rFlow.KEout(dI);

row1 = { 'headIn' 'flowIn' 'dust' 'medium' 'Nnoz' 'rough' }
row2 = { headIn flowIn dust*1e6 'water' Nnoz rough }

```

```

row3 = { 'powerout' 'powercc' 'eta' 'RPM' 'head_eff' 'torque_eff' }
row4 = [ powerout powercc eta RPM head_eff torque_eff]

row5= { 'radius' 'space' 'thick' 'Xii' 'nprofile' 'Ndisks' }
row6 = [ radius space thick xii nprofile Ndisks]

row7 = { 'wnoz' 'Hnoz' 'gap' 'clearance' 'aspect' 'rotorVol'}
row8 = [ wnoz Hnoz gap clearance aspect rotorVol]

row9 = {'ARCnoz' 'ANGnoz' 'SLITdisk' 'Dnoz' 'Lnoz' 'KEout' }
row10 = [ARCnoz ANGnoz SLITdisk Dnoz Lnoz KEout]

row11 = { 'powerin' 'nozloss' 'rotorloss' 'gaploss' 'tiploss' 'keloss' }
row12 = [ powerin nozloss rotorloss gaploss tiploss keloss ]

row13 = {'etarotor' 'etaturbine' 'Pt' 'T1' 'headnorm' 'torquenorm'}
row14 = [ etarotor etaturbine Pt T1 headnorm torquenorm]

row15 = {'head' 'flow' 'powerIn' 'torque' 'head_ratio' 'flow_ratio' }
row16 = [head flow powerIn torque head_ratio flow_ratio ]

row17 = {'leakIn' 'pathlossIn' 'bearingIn' 'leakloss' 'pathloss' 'bearingloss'}
row18 = [leakIn pathlossIn bearingIn leakloss pathloss bearingloss]

row19 = { 'momentdif' 'dynamichead' 'statichead' 'reaction' 'Pi' 'Wi' }
row20 = [ momentdif dynamichead statichead reaction Pi Wi ]

row21 = { 'Qdisk' 'omega' 'Vtip' 'Vrad' 'Vro' 'REm'}
row22 = [ Qdisk*1e6 omega Vtip Vrad Uo REM ]

row23 = {'Vtan' 'Vto' 'Vnoz' 'KEnoz' 'REnoz' 'REgap' }
row24 = [ Vtan Vo Vnoz KEnoz REnoz REgap]

table.label = { row1; row3; row5; row7; row9; row11; row13 };
%table.value = [ row2 ; row4; row6; row8; row10; row12; row14];

if (fname ~= ' ')
xlswrite(fname,row1, 2,'E5'); xlswrite(fname,row2, 2,'E6');
xlswrite(fname,row3, 2,'E7'); xlswrite(fname,row4, 2,'E8');
xlswrite(fname,row5, 2,'E9'); xlswrite(fname,row6, 2,'E10');
xlswrite(fname,row7, 2,'E11'); xlswrite(fname,row8, 2,'E12');
xlswrite(fname,row9, 2,'E13'); xlswrite(fname,row10, 2,'E14');
xlswrite(fname,row11, 2,'E15'); xlswrite(fname,row12, 2,'E16');
xlswrite(fname,row13, 2,'E17'); xlswrite(fname,row14, 2,'E18');
xlswrite(fname,row15, 2,'E19'); xlswrite(fname,row16, 2,'E20');
xlswrite(fname,row17, 2,'E21'); xlswrite(fname,row18, 2,'E22');

```

```

xlswrite(fname,row19, 2,'E23'); xlswrite(fname,row20, 2,'E24');
xlswrite(fname,row21, 2,'E25'); xlswrite(fname,row22, 2,'E26');
xlswrite(fname,row23, 2,'E27'); xlswrite(fname,row24, 2,'E28');

```

```

end

```

```

end

```

### A.3.12 Plot Algorithm: Sankey

Sankey is used for turbine loss analysis. It is taken from the web and modified to suit this research. The original writer and the release statements are in the beginning of the modules.

```

function drawSankey(inputs, losses, unit, labels, varargin)

% drawSankey(inputs, losses, unit, labels, sep)
%
% drawSankey is a matlab function that draws single-direction Sankey
% diagrams (i.e no feedback loops), however, multiple inputs can be
% specified.
%
% inputs: a vector containing the flow inputs, the first of which will be
%         considered the main input and drawn centrally, other inputs will
%         be shown below this.
%
% losses: a vector containing all of the losses from the system, which will
%         be displayed along the top of the Sankey diagram
%
% unit:   a string indicating the unit in which the flows are expressed
%
% labels: a cell list of the labels for the different flows, starting with
%         the labels for the inputs, then the losses and finally the output
%
% sep:    an (optional) list of position for separating lines, placed after
%         the loss corresponding to the indexes provided
%
% For an example, copy and paste the lines below to the command line:
%
% inputs = [75 32]; losses = [10 5 2.8]; unit = 'MW'; sep = [1,3];
% labels = {'Main Input','Aux Input','Losses I','Losses II','Losses III','Output'};
%
% drawSankey(inputs, losses, unit, labels, sep);

```

```

%
% Current Version: 02.11.2009
% Developed by: James SPELLING, KTH-EGI-EKV
% spelling@kth.se
%
% Distributed under Creative Commons Attribution + NonCommerical (by-nc)
% Licensees may copy, distribute, display, and perform the work and make
% derivative works based on it only for noncommercial purposes

%check parameter values%
if (nargin<1)
    inputs = 100; losses = [20 5 5 15 2 2 4]; unit= 'w'
    labels = {'3cm ', 'Nozzle loss','KE out', 'Rotor drop','Disk FrictionLoss','Leakage',
'Path loss', 'Bearing','Power Out'}
    sep =[1,3,4,7]
end

if sum(losses) >= sum(inputs)

    %report unbalanced inputs and losses%
    error('drawSankey: losses exceed inputs, unable to draw diagram');

elseif any(losses < 0) || any(inputs < 0)

    %report negative inputs and/or losses%
    error('drawSankey: negative inputs or losses encountered');

else

    %check for the existance of separating lines%
    if nargin > 4; sep = varargin{1}; end

    %create plotting window%
    figure('color','white','tag','sankeyDiagram');

    %if possible, maximise figure%
    if exist('maximize','file')
        maximize(gcf);
    end

    %create plotting axis then hide it%
    axes('position',[0.15 0 0.75 0.75]); axis off;

    %calculate fractional losses and inputs%
    frLosses = losses/sum(inputs);
    frInputs = inputs/sum(inputs);

    if length(inputs(inputs > eps)) == 1

        %assemble first input label if only one input%
        inputLabel = sprintf('%s\n%.1f [%s]', labels{1}, inputs(1), unit);
    end
end

```

```

else

    %assemble first input label if only several inputs%
    inputLabel = sprintf('%s\n%.1f [%s] %.1f [%%]', labels{1}, inputs(1), unit,
100*frInputs(1));

    end

    %determine first input label font size%
    fontsize = min(13, 10 + ceil((frInputs(1)-0.05)/0.025));

    %draw first input label to plotting window%
    text(0, frInputs(1)/2, inputLabel, 'FontSize',
fontsize, 'HorizontalAlignment', 'right', 'Rotation', 0);

    %draw back edge of first input arrow%
    line([0.1 0 0.05 0 0.4], [0 0 frInputs(1)/2 frInputs(1) frInputs(1)], 'Color',
'black', 'Linewidth', 2.5);

    %set initial position for the top of the arrows%
    limTop = frInputs(1); posTop = 0.4;

    %set initial position for the bottom of the arrows%
    limBot = 0; posBot = 0.1;

    %draw arrows for additional inputs%
    for j = 2 : length(inputs)

        %don't draw negligible inputs%
        if frInputs(j) > eps

            %determine inner and outer arrow radii%
            rI = max(0.07, abs(frInputs(j)/2));
            rE = rI + abs(frInputs(j));

            %push separation point forwards%
            newPosB = posBot + rE*sin(pi/4) + 0.01;
            line([posBot newPosB], [limBot limBot], 'Color', 'black', 'Linewidth', 2.5);
            posBot = newPosB;

            %determine points on the external arc%
            arcEx = posBot - rE*sin(linspace(0,pi/4));
            arcEy = limBot - rE*(1 - cos(linspace(0,pi/4)));

            %determine points on the internal arc%
            arcIx = posBot - rI*sin(linspace(0,pi/4));
            arcIy = limBot - rE + rI*cos(linspace(0,pi/4));

            %draw internal and external arcs%
            line(arcIx, arcIy, 'Color', 'black', 'Linewidth', 2.5);

```

```

line(arcEx, arcEy, 'color', 'black', 'Linewidth', 2.5);

%determine arrow point tip%
phiTip = pi/4 - 2*min(0.05, 0.8*abs(frInputs(j)))/(rI + rE);
xTip = posBot - (rE+rI)*sin(phiTip)/2;
yTip = limBot - rE + (rE+rI)*cos(phiTip)/2;

%draw back edge of additional input arrows%
line([min(arcEx) xTip min(arcIX)], [min(arcEy) yTip min(arcIY)], 'color',
'black', 'Linewidth', 2.5);

%determine text edge location%
phiText = pi/2 - 2*min(0.05, 0.8*abs(frInputs(j)))/(rI + rE);
xText = posBot - (rE+rI)*sin(phiText)/2;
yText = limBot - rE + (rE+rI)*cos(phiText)/2;

%determine label size based on importance%
if frInputs(j) > 0.1

    %large inputs text size scales slower%
    fullLabel = sprintf('%s\n%.1f [%s] %.1f [%%]', labels{j}, inputs(j),
unit, 100*frInputs(j));
    fontsize = 11 + round((frInputs(j)-0.01)/0.05);

elseif frInputs(j) > 0.05

    %smaller but more rapidly scaling losses%
    fullLabel = sprintf('%s: %.1f [%s] %.1f [%%]', labels{j}, inputs(j),
unit, 100*frInputs(j));
    fontsize = 10 + ceil((frInputs(j)-0.05)/0.025);

else

    %minimum text size for input label%
    fullLabel = sprintf('%s: %.2f [%s] %.1f [%%]', labels{j}, inputs(j), unit,
100*frInputs(j));
    fontsize = 10;

end

%draw input label%
text(xText, yText, fullLabel, 'FontSize', min(13,
fontsize), 'HorizontalAlignment', 'right');

%save new bottom end of arrow%
limBot = limBot - frInputs(j);

end

end

```

```

%draw arrows of losses%
for i = 1 : length(losses)

    %don't draw negligible losses%
    if frLosses(i) > eps

        %determine inner and outer arrow radii%
        rI = max(0.07, abs(frLosses(i)/2));
        rE = rI + abs(frLosses(i));

        %determine points on the internal arc%
        arcIX = posTop + rI*sin(linspace(0,pi/2));
        arcIY = limTop + rI*(1 - cos(linspace(0,pi/2)));

        %determine points on the external arc%
        arcEX = posTop + rE*sin(linspace(0,pi/2));
        arcEY = (limTop + rI) - rE*cos(linspace(0,pi/2));

        %draw internal and external arcs%
        line(arcIX, arcIY, 'color', 'black', 'Linewidth', 2.5);
        line(arcEX, arcEY, 'color', 'black', 'Linewidth', 2.5);

        %determine arrow tip dimensions%
        arEdge = max(0.015, rI/3);
        arTop = max(0.04, 0.8*frLosses(i));

        %determine points on arrow tip%
        arX = posTop + rI + [0 -arEdge frLosses(i)/2 frLosses(i)+ arEdge
frLosses(i)];
        arY = limTop + rI + [0 0 arTop 0 0];

        %draw tip of losses arrow%
        line(arX, arY, 'color', 'black', 'Linewidth', 2.5);

        %determine text edge location%
        txtX = posTop + rI + frLosses(i)/2;
        txtY = limTop + rI + arTop + 0.05;

        %determine label size based on importance%
        if frLosses(i) > 0.1

            %large losses have the space for a two line label%
            fullLabel = sprintf('%s\n%.1f [%%]', labels{i+length(inputs)},
100*frLosses(i));
            fontsize = 11 + round((frLosses(i)-0.01)/0.05);

        elseif frLosses(i) > 0.05

            %single line, but still scaling label%
            fullLabel = sprintf('%s: %.1f [%%]', labels{i+length(inputs)},
100*frLosses(i));

```

```

        fontsize = 10 + ceil((frLosses(i)-0.05)/0.025);

    else

        %minimum siye single line label%
        fullLabel = sprintf('%s: %.1f [%%]', labels{i+length(inputs)},
100*frLosses(i));
        fontsize = 10;

    end

    %draw losses label%
    text(txtX, txtY, fullLabel, 'Rotation', 90, 'FontSize', fontsize);
    %text(txtX, txtY, fullLabel, 'Rotation', 0, 'FontSize', fontsize);
    %save new position of arrow top%
    limTop = limTop - frLosses(i);

    %advance to new separation point%
    newPos = posTop + rE + 0.01;

    %draw top line to new separation point%
    line([posTop newPos], [limTop limTop], 'Color', 'black', 'Linewidth', 2.5);

    %save new advancement point%
    posTop = newPos;

end

%separation lines%
if any(i == sep)

    if length(inputs) > 1 && any(inputs(2 : length(inputs)) > eps)

        %if there are additional inputs, determine approx. sep. line%
        xLeft = 0.1*posTop;

    else

        %otherwise determine exact sep. line%
        xLeft = 0.05 * (1 - 2*abs(limTop - 0.5));

    end

    %draw the line%
    line([xLeft posTop], [limTop limTop], 'Color', 'black', 'Linewidth', 2,
'LineStyle', '--');

end

end

```

```

%push the arrow forwards a little after all side-arrows drawn%
newPos = max(posTop, posBot) + max(0.05*limTop, 0.05);

%draw lines to this new position%
line([posTop, newPos],[limTop limTop], 'color', 'black', 'Linewidth', 2.5);
line([posBot, newPos],[limBot limBot], 'color', 'black', 'Linewidth', 2.5);

%draw final arrowhead for the output%
line([newPos newPos newPos+max(0.04, 0.8*(limTop-limBot)) newPos newPos], [limBot,
limBot - max(0.015, (limTop+limBot)/3), (limTop+limBot)/2, limTop + max(0.015,
(limTop+limBot)/3), limTop], 'color', 'black', 'Linewidth', 2.5);

%save final tip position%
newPos = newPos + 0.8*(limTop - limBot);

%determine overall ins and outs%
outputFinal = sum(inputs) - sum(losses);
inputFinal = sum(inputs);

%create the label for the overall output arrow%
endText = sprintf('%s\n%.0f [%s]\n%.1f
[%%]', labels[length(losses)+length(inputs)+1], outputFinal,
unit,100*outputFinal/inputFinal);
fontSize = min(13, 10 + ceil((1-sum(frLosses)-0.1)/0.05));

%draw text for the overall output arrow%
text(newPos + 0.05, (limTop+limBot)/2, endText, 'FontSize', fontSize);

%set correct aspect ratio%
axis equal;

%set correct axis limits%
set(gca, 'YLim', [frInputs(1)-sum(frInputs)-0.4, frInputs(1)+frLosses(1)+0.4]);
set(gca, 'XLim', [-0.15, newPos + 0.1]);
%view(90,90)
end
end

```

*Published with MATLAB® R2013a*

### A.3.13 Design Tool

```

function [turbineSpec ] = Design_Tool(head_m, flow_cc, dust_um, medium, plots)
%inputs turbine input specifications- head(meter), flow(cc/s), dust (um
%size) , medium (water default);
%outputs specifications for valid turbines (out of 121); selects four spread
%over the radius range on power basis,provides sensitivity analysis for the
%top recommended design ( sorted order power, power density and aspect ratio).

if(nargin < 1); head_m = 3.6; flow_cc = 60000; dust_um = 20;
    medium = 'water'; plots = [ 1 1 1 1 0] ; end;

hm= num2str(head_m)   %=str2double(hm)
fccv = num2str(flow_cc) %str2double(fcc) + version info
fcc = num2str(floor(flow_cc))% strip version info
dum= num2str(dust_um)   %=str2double(dum)
%inputs = [hm 'm -' fcc 'cm^{3}/s -' dum '\mum ' ];
savetable = [ hm '_' fccv '_' dum '.xls'];
savefile = [ hm '_' fccv '_' dum '.mat'];

%find 'bmin',the minimum spacing at which valid turbines can be designed to
%support the particulate size; limit minimum 'b' to 30 um.
bmin = max(3e-5,min(5e-3,ceil(10*dust_um)*1e-6));

%step increase bmin by 20 um, to allow operation at lower heads for bmin<1mm;
%step decrease bmin by 5% to allow for higher power density for bmin>= 1mm;
if (bmin < 1e-3); binc = 2e-5; else binc = -0.05*bmin; end;
b_trys = 11; r_trys= 11;rb_array = [];
for i = 1: b_trys      % 11 space increments
    b = bmin + binc*(i-1); bv = b*ones(1,r_trys);
    t = max(3e-5, min(1e-3, round(b/2*1e6)*1e-6)); tv = t*ones(1,r_trys);

%set rmin to satisfy rotor flow constaints,= 15*b; rmax, maximum = 300*b, in 11 steps;
rmin = b*20; rmax = min(0.2, b*400); rinc = max(1,round((rmax - rmin)*1000/(r_trys-
1)))*1e-3;
r = rmin + rinc*[0:r_trys-1]; rb_array = [ rb_array;r' bv' tv'];
end

rbt_array = sortrows(rb_array,1); % setup 121 r,b combinations satisfying constraints
nvalid=0;

    for j = 1:length(rbt_array) % all radius , space combinations;
%get optimum turbine design spec for the rotor with radius r and space b
    [turbinedesign] = Design_turbine( head_m, flow_cc,dust_um, medium,
rbt_array(j,:),plots);

```

```

setVar = turbinedesign.setVar; eval = turbinedesign.eval;
select = turbinedesign.select;
% store valid designs
    if(turbinedesign.select.valid == 1);
        nvalid = nvalid+1;
        turbine{nvalid} = turbinedesign; % structure -valid turbine design
        c_radius{nvalid} = setVar.rotor.radius*1000;
        c_space{nvalid} = setVar.rotor.space*1e6;
        c_powerout{nvalid} = eval.userout.powerout(select.dI);
        c_powercc{nvalid} = eval.userout.powercc(select.dI);
        c_head{nvalid} = eval.userout.head(select.dI);
        c_aspect{nvalid}=setVar.rotor.aspect(select.dI);
        c_rpm{nvalid}=setVar.flowvar.RPM(select.dI);
        c_eta{nvalid} = eval.userout.eta(select.dI);
        c_index{nvalid} = nvalid;
    end
end

% cell to float
index = [c_index{:}]; radius = [c_radius{:}]; space=[c_space{:}];
powerout=[c_powerout{:}];
powercc= [c_powercc{:}]; head=[c_head{:}]; aspect = [c_aspect{:}]; eta= [c_eta{:}]; rpm=
[c_rpm{:}];
headIn = setVar.userinp.headIn;
%disp('number of valid turbines out of ', num2str(iter),'trys is ',num2str(nvalid));
% sort the turbines in the high power, high power density and low aspect order
format shortg;
sortMatrix = [ [index]' [radius]' [powerout]' [powercc]' [rpm]' [abs(headIn-head)]'
[aspect]' [eta]' [space]'];
sIr=2; sIpwr = 3; sIpcc = 4; sIrpm = 5; sIhead=6; sIar = 7; sIeta=8 ; sIb=9; sort3rd =
'hd';
sortpower = flipud(sortrows( sortMatrix,sIpwr)); % descending power
PwrA= sortpower(:,sIpwr); keepPwr = max(ceil(nvalid/4), max(find(PwrA >= PwrA(1)*0.8)));
sortpcc = flipud(sortrows(sortpower(1: keepPwr,:),sIpcc)); % descending pcc
PccA= sortpcc(:,sIpcc); keepPcc = max(ceil(keepPwr/4), max(find(PccA >= PccA(1)*0.9)));
    if (sort3rd=='ar') % power, pd , aspect ratio - head , power, pd criteria
        sortlast = sortrows(sortpcc(1:keepPcc,:),sIar); % ascending aspect ratio
    else % power, pd, closest head for not valid designs
        sortlast = sortrows(sortpcc(1:keepPcc,:),sIhead); % closest head;
    end
end
tI= sortlast(1,1); % chosen turbine index to check sensitivity
disp( [ 'radius(mm) space(micron) powerout(W) powercc(W/cc eta RPM]');
outsort = [sortlast(:,sIr) sortlast(:,sIb) sortlast(:,sIpwr) sortlast(:,sIpcc)
sortlast(:,sIeta) sortlast(:,sIrpm)]
%select 3 more turbines at different radius spacing, in the order of
%preference. ; we use here power peaks ; but power density or aspect ratio
%or multiple sorting methods- any can be used.
xarray = powerout; xTI = tI ; yarray = xarray; x1 = length(xarray);
dx = xarray(1:x1-1)-xarray(2:x1); % first derivative of the array;
xmm=find(sign(dx(1:x1-2).*dx(2:x1-1))<0)+1; % find min and max of the array
peak_ind = xmm(find(dx(xmm)>0)); % select peaks ( max) in the array;

```

```

if isempty(peak_ind); peak_ind=1; end; % use the recommended index ad one.
peaks = flipud(sortrows([ peak_ind' xarray(peak_ind)'],2)); % sort the peaks

% if recommended turbine index is not in the peaks , add it to the peaks
numpeak= min(3,size(peaks,1)); four_peaks= peaks(1:numpeak,:) ;
if(find(four_peaks(:,1)==xtI));
else; four_peaks = [ xtI xarray(xtI); four_peaks ]; numpeak = numpeak+1;
end
% if 4 peaks are not found ; pick the extra equally spaced in the array
if(numpeak<4) numinc = floor((x1-numpeak)/(4-numpeak));
yarray(four_peaks(:,1))=0;
pwsort = flipud(sortrows([[1:length(yarray)]' yarray'],2));
for i = 1:(4-numpeak);
four_peaks = [four_peaks; pwsort(1 + (i-1)*numinc,:)];
end
end

recommended_turbine = turbine{four_peaks(1,1)}; tI = four_peaks(1,1);

[sensitivity] = Sensitivity_turbine(recommended_turbine)

turbinespec.turbines = turbine;
turbinespec.sortMatrix = sortMatrix;
turbinespec.fourIndex = four_peaks(:,1)'; % 4 selected turbines - 1st one
recommended
turbinespec.sensitivity = sensitivity;
turbinespec.recommended = recommended_turbine;

save(savefile, 'turbinespec');

[table] = Output_turbine(turbinespec,tI, plots, savetable);
turbinespec.table = table;

end

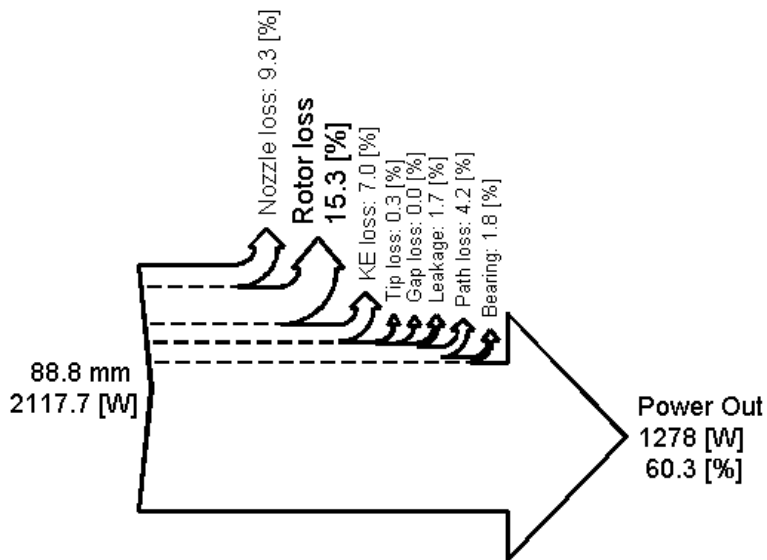
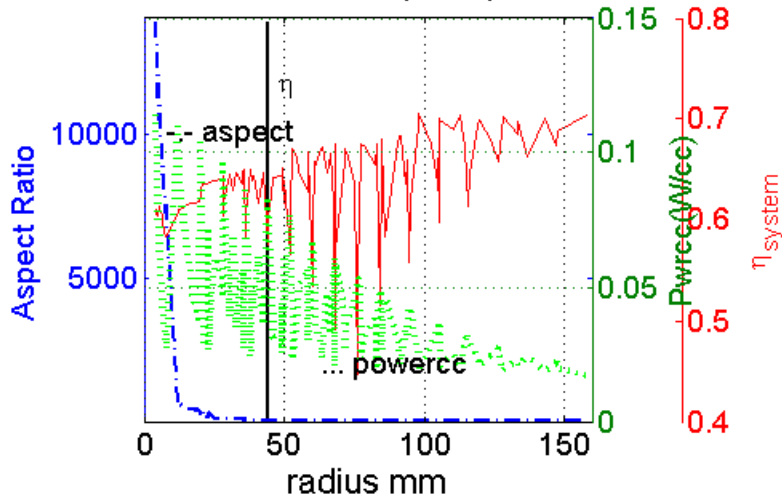
```

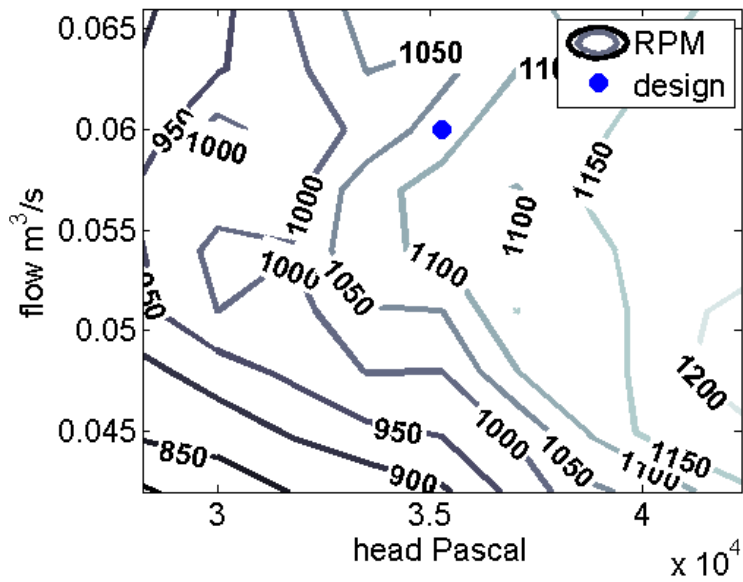
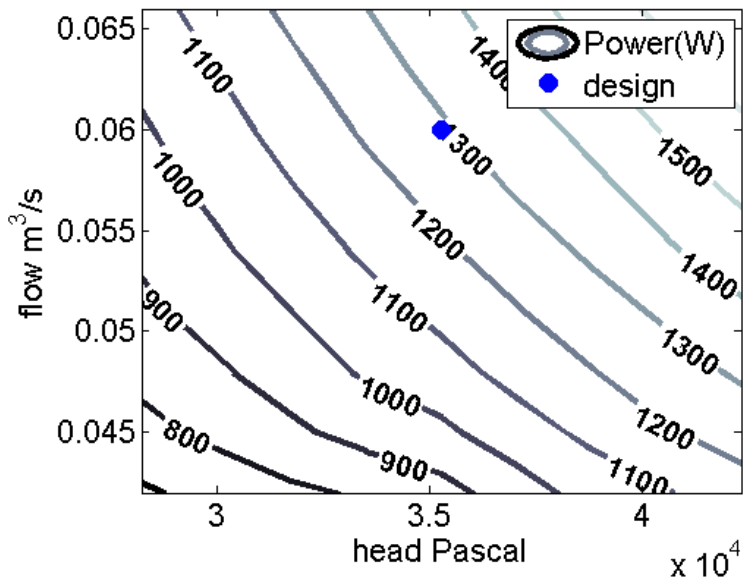
```

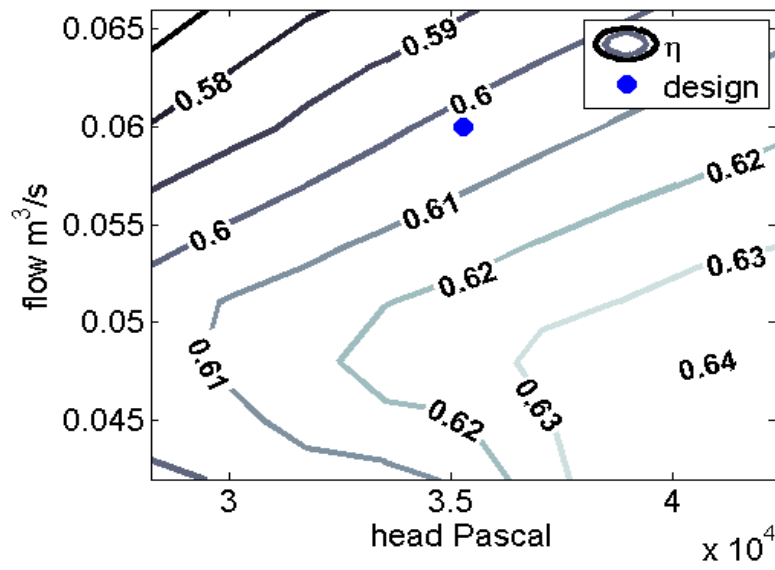
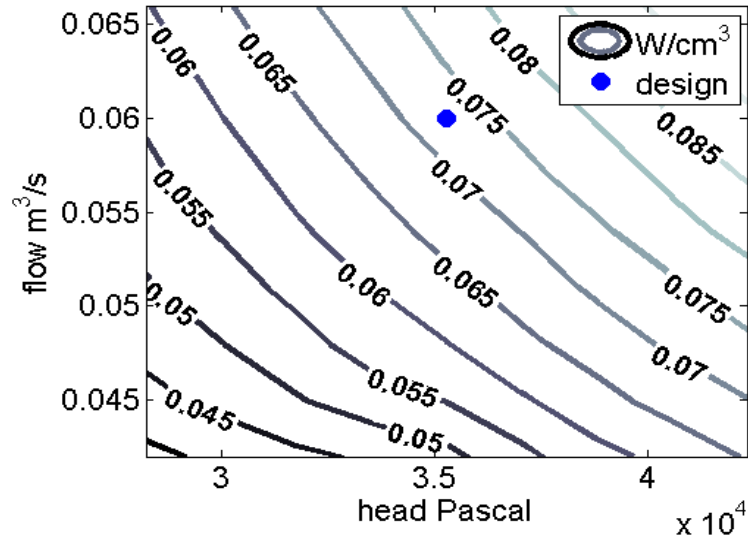
turbines: {1x120 cell}
sortMatrix: [120x8 double]
fourIndex: [45 110 113 103]
sensitivity: [1x1 struct]
recommended: [1x1 struct]
table: [1x1 struct]

```

radius mm = 44.4, space  $\mu\text{m}$  = 220







### A.3.14 Table of Design Specification

#### Turbine Input Specifications:

|                         |                                 |           |              |
|-------------------------|---------------------------------|-----------|--------------|
| <b>head input (m)</b>   | flow input (cm <sup>3</sup> /s) | dust (μm) | medium       |
| <b>3.6</b>              | 60000                           | 20        | water        |
| <b>power input ( W)</b> | Volume loss                     | Path loss | bearing loss |
| <b>2117</b>             | 2 %                             | 5 %       | 3 %          |

#### Turbine Output Specification:

|                                    |                                     |                 |                   |
|------------------------------------|-------------------------------------|-----------------|-------------------|
| <b>power out (W)</b>               | power density (mw/cm <sup>3</sup> ) | eta             | RPM               |
| <b>1277</b>                        | 72                                  | 0.6             | 1066              |
| <b>rotor aspect (height/width)</b> | Rotor Volume (liter)                | Head efficiency | Torque efficiency |
| <b>16.1</b>                        | 8.9                                 | 0.63            | 0.96              |

#### Sankey Loss fractions:

|                    |            |           |              |
|--------------------|------------|-----------|--------------|
| <b>Nozzle loss</b> | Rotor loss | Gap loss  | Tip loss     |
| <b>9.3%</b>        | 15.3%      | 0.04%     | 0.35%        |
| <b>KE loss</b>     | Leak loss  | Path loss | Bearing loss |
| <b>7%</b>          | 1.7%       | 4.2%      | 1.9%         |

#### Rotor Hardware:

|                    |            |                |                 |
|--------------------|------------|----------------|-----------------|
| <b>radius (mm)</b> | space (μm) | thickness (mm) | Xii             |
| <b>44</b>          | 220        | 110            | 0.35            |
| <b>Ndisks</b>      | gap (mm)   | clearance (μm) | Flow profile, n |
| <b>4345</b>        | 4.44       | 440            | 3.6             |

#### Nozzle Hardware:

|                   |             |               |               |
|-------------------|-------------|---------------|---------------|
| <b>Width (mm)</b> | Height (m)  | ARC width     | Tangent angle |
| <b>8</b>          | 1.43        | 10.4°         | 2.5°          |
| <b>Number</b>     | Length (mm) | Diameter (mm) | rough ratio   |
| <b>1</b>          | 100         | 16            | 0.01          |

#### Operating parameter:

|             |       |           |             |
|-------------|-------|-----------|-------------|
| <b>REm</b>  | Vro   | Vto       | reaction    |
| <b>0.98</b> | 0.045 | 1.05      | 0.49        |
| <b>Pt</b>   | T1    | eta rotor | eta turbine |
| <b>1.44</b> | 0.247 | 0.80      | 0.74        |

Table A-1: Design specification for a Tesla turbine (input spec. from Williamson's Turgo turbine)

## A.4 GUI

Two example user interfaces created using MATLAB GUIDE.

### A.4.1 GUI –Interface -1: Low Head and high flow

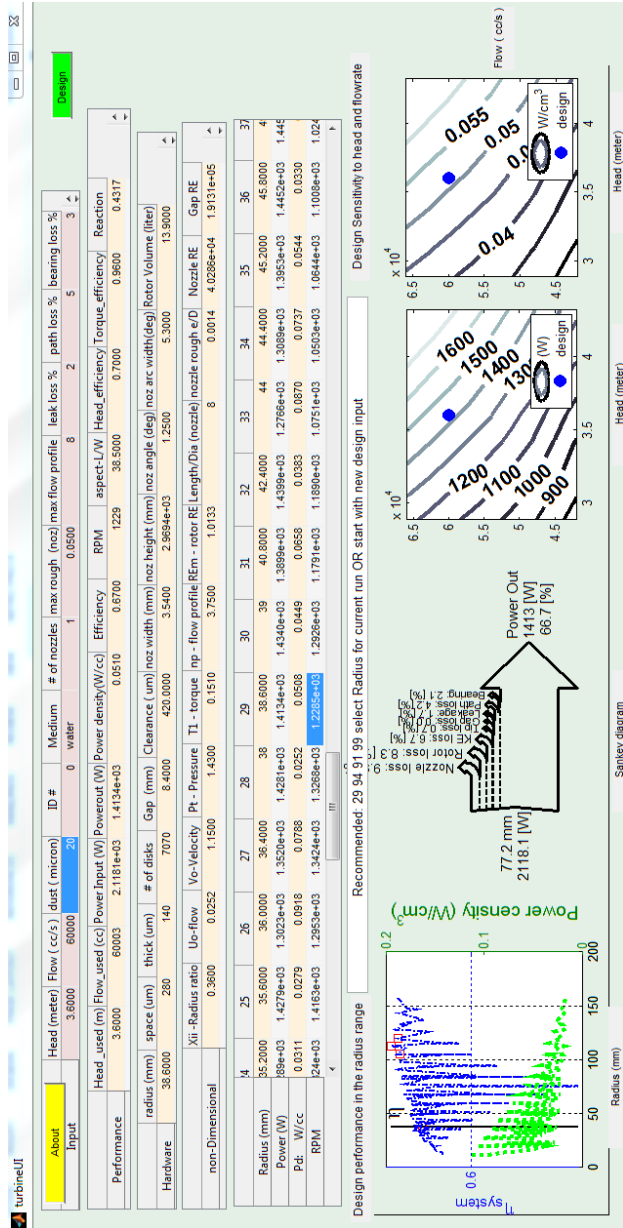


Figure A-2: Williamson turbine input-specification is used in this Tesla turbine based redesign

## A.4.2 GUI -Interface -2: High Head and Low Flow

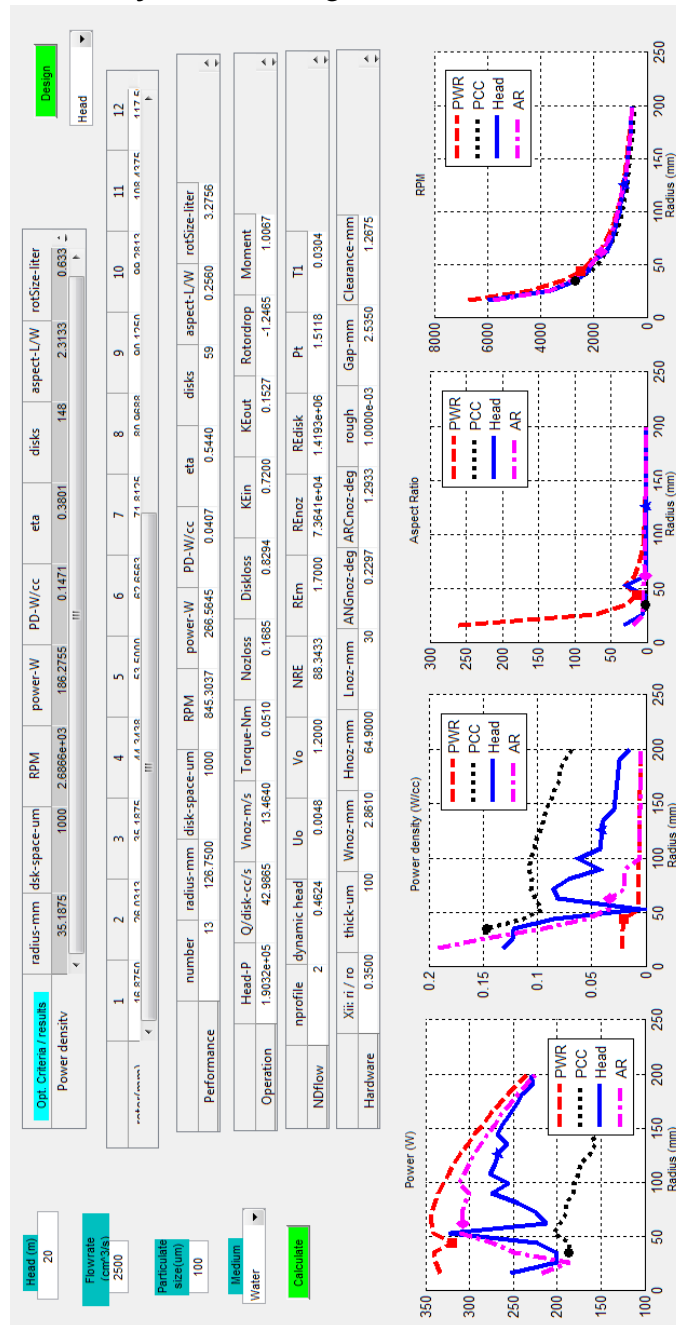


Figure A-3: Ho-Yan's turbine redesign with 126 mm radius and 1 mm interdisk space

GUI displays the performance curves over a desired radius range corresponding to the input specifications. In Figure A-2, Williamson's Turgo turbine input specification is used for the Tesla turbine design. All valid designs are displayed and recommended turbine indices displayed. Here the recommendation is based on power peaks spread over the

valid radius region. In Figure A-3, an alternate scheme is used and it displays the 4 recommended designs based on Power, Power density, Aspect Ratio and Closest to Head criteria. It also provides the radius list of all the valid turbine designs. When one radius is selected, the details of the turbine design with that radius is displayed. Ho-Yan's turbine is redesigned for 1 mm interdisk space and the GUI shows the possible turbine designs with recommended turbine at 126 mm radius operating at 54% efficiency and 41mW/cm<sup>3</sup> power density. I do not have the complete specifications of the example turbines from their designers. Only the input specifications of head, and flow are used to design the equivalent Tesla turbines.

The GUI interface helps in understanding the turbine behavior with the visual aid and was used in optimizing the design tool. User interface and optimality criteria will depend on practical applications, which is the purpose of this tool. All MATLAB code is based on the equations described in the body of this dissertation.